LOCAL MODES IN $Al_{10}V$

Thesis submitted for the degree of

Doctor of Philosophy

by

L. K. Nicholson

The Blackett Laboratory
Imperial College of Science and Technology
London, S.W.7.

July 1976.

ACKNOWLEDGEMENTS

To my supervisor, Dr. A.D. Caplin, I wish to express my deep gratitude for his invaluable encouragement, guidance and help throughout the course of this work. My thanks also go to Professor B.R. Coles, for his unfailing interest and enthusiasm, and to Professor J.E. Gordon whose practical help and enthusiastic approach in the early stages of this work, is greatly valued.

I wish also to express my deep gratitude to;Dr. H.E.N. Stone for making the samples and for many helpful discussions; Mr. I. Coole for his great technical assistance with the construction of the apparatus; and to all members of the Solid State Group for providing such a pleasant working atmosphere.

My special thanks go to Dr. C.N. Guy for so patiently reading this thesis and for many helpful suggestions and enlightening discussions. I also greatly appreciate the assistance given by Mr. M.H. Bennett with the electrical resistivity measurements.

My thanks go to Dr. M.W. Finnis of A.E.R.E. Harwell and Dr. P. Lanchester of Southampton University for giving permission to quote their unpublished results.

The majority of this work was carried out during the tenure of an S.R.C. Studentship, for which I am most grateful.

I wish to thank Mrs. T. Wright for typing this thesis so quickly and efficiently.

To my fiancé, Brian, I express my deep gratitude for his patience and understanding throughout this work, and also for his assistance with the data analysis and proof reading of this thesis.

Finally, my deepest thanks go to my parents whose encouragement has been unfailing -- to them I dedicate this thesis.

ABSTRACT

The Einstein like behaviour of the specific heat and electrical resistivity of the compound $Al_{10}V$, reported by earlier workers, has been investigated by low temperature measurements.

A well defined Einstein like contribution is observed in the specific heat of all $Al_{10}V$ samples measured, suggesting the existance of a single well defined mode having an Einstein temperature of about 23 K. Electrical resistivity data obtained on the same samples substantiates this evidence for a low frequency oscillator, as do the results of low temperature inelastic neutron scattering experiments. Data on the low temperature thermal expansion of one sample is also presented.

Earlier structural evidence suggests that the cubic unit cell (16 x $Al_{10}V$) contains one Al site, with very large coordination and spacing, to every two formula units of $Al_{10}V$. The low frequency oscillator is identified with a loosely bound Al atom on this site. Occupancy of the site is apparently not essential to the structure, and varied from 10 to 25% for the samples measured.

Results of calculations of the atom-atom pseudopotential for an Al atom on this site suggest a central maximum on which the loosely bound atom moves.

One sample of $Al_{10}V$ doped with 0.8% gallium has also been measured and results suggest strongly preferential occupancy of the loose sites by gallium atoms.

To our knowledge this local mode is unique in metallic systems.

INTRODUCTION

The anomalous behaviour of $Al_{10}V$, as reported by Dunlop, Grüner and Caplin (7) has prompted the investigations carried out in this work. Some low temperature specific heat and electrical resistivity data on $Al_{10}V$ reported in another publication (38) indicates the presence of a well defined local mode of Einstein character at an energy of about 2 meV.

The low frequency oscillators are identified with very loosely bound aluminium atcms in anomalous vacant sites in the crystal structure. Occupation of these sites is apparently not essential to the structure, and the composition is taken to vary from $Al_{10}V$ to $Al_{10.5}V$ across the phase.

A more detailed study of the low temperature specific heat of $Al_{10}V$ has been carried out, and some low temperature electrical resistivity, thermal expansion and neutron data has been obtained. The results of calculations of the interatomic pseudopotential for the loose atom are presented and the experimental data is considered in the light of this and earlier crystallographic investigations (40, 41).

A major part of this work comprised the design and construction of a specific heat cryostat to measure samples of a few grammes mass to about five percent accuracy.

The first chapter outlines some of the major aspects of the low temperature heat capacity of metals. A brief historical review of methods of low temperature specific heat measurement is then given. The design of the apparatus and methods of measurement are reported in Chapters II and III, with particular attention being given to frequency restraints in the A.C. method.

CONTENTS

		Page No.
ACKNOWLEDGEMENTS		1
ABSTRACT		2
INTRODUCTION		3
CHAPTER I.	The specific heat of metals at low temperatures.	8
	Introduction.	8
1.1(i)	Lattice heat capacity.	11
1.1(ii)	Recent work on lattice dynamics theory.	12
1.1(iii)	The Einstein theory.	13
1.1(iv)	The Debye theory.	14
1.1(v)	Modifications to the Debye theory.	16
1.1(vi)	Localised phonon modes.	18
1.2(i)	Electronic heat capacity.	20
1.2(ii)	Electronic heat capacity and the band structure.	21
1.2(iii)	The Schottky effect.	23
CHAPTER II.	Methods of measuring low temperature heat capacity.	25
2.1	Traditional method of measurement.	25
2.2	Measurements on small samples at low temperatures.	28
2.2(i)	Pulse techniques.	28
	(a) Morin and Maita.	28
	(b) Dunlop.	29
2.2(ii)	Step techniques.	30
2.2(iii)	A. C. method.	31
2.2(iv)	Sweep method.	33
2.3	Methods of measurement used in this work.	36
2.3(i)	Theory of step method.	36
2.3(ii)	Theory of A.C. method and frequency limitations.	39
	(a) Low frequency limit.	39
	(b) High frequency limit.	42

		Page No.
CHAPTER III.	Apparatus and experimental procedure.	44
3.1	Design of calorimeter.	44
3.1(i)	He_4 cryostat.	44
3.1(ii)	The sample chamber.	44
3.1(iii)	The sample mounting.	47
3.1(iv)	Heat sinking of wires.	48
3.2	Circuitry.	51
3.2(i)	Heater power supply and measuring circuit.	51
3.2(ii)	Germanium thermometer circuitry.	55
3.2(iii)	Carbon thermometer circuitry.	55
3.3	Thermometry.	58
3.4	Experimental procedure.	62
3.4(i)	Step method.	62
3.4(ii)	A. C. method.	64
3.5	Calibration of apparatus and heat capacity of the addenda.	68
3.5(i)	Heat capacity of the addenda.	68
3.5(ii)	Calibration of apparatus.	68
CHAPTER IV.	Previous work on $Al_{10}V$.	73
4.1	Introduction.	73
4.1(i)	Charge transfer and bonding in the aluminium-rich aluminium (3-d) transition metal compounds.	73
4.1(ii)	The Aluminium-Vanadium compounds.	75
4.2(i)	The structure of $Al_{10}V$.	76
4.2(ii)	Previous work on $Al_{10}V$.	80
	(a) Specific heat.	80
	(b) Electrical resistivity.	81
CHAPTER V.	Sample preparation and experimental results.	84
5.1(i)	Metallurgy.	84
5.1(ii)	Sample preparation.	84
5.2	The specific heat data.	88
	Introduction	88

		Page No.
CHAPTER V	Continued.	
5.2(i)	Presentation of results.	89
	(i) Electronic contribution.	89
	(ii) Lattice contribution.	89
	(iii) Excess contribution.	90
5.2(ii)	Results for the Gallium doped sample.	92
5.3	Electrical resistivity.	114
	Introduction.	114
5.3(i)	Method of measurement.	114
5.3(ii)	Analysis of data.	116
5.3(iii)	Estimated accuracy of resistivity data.	116
5.4	Inelastic neutron scattering from $Al_{10}V$.	122
	Introduction.	122
5.4(i)	Rotating crystal time of flight spectrometer IN4.	123
5.4(ii)	Results.	125
5.5	Thermal expansion.	127
CHAPTER VI.	Discussion and conclusions.	130
	Introduction.	130
6.1	Discussion of experimental results.	130
6.1(i)	Specific heat data.	130
6.1(ii)	Electrical resistivity.	132
6.1(iii)	Neutron data.	133
6.1(iv)	Thermal expansion.	135
6.1(v)	Discussion of results on doped samples of $Al_{10}V$.	136
6.2	Interatomic pseudopotential for the loose Al atom in $Al_{10}V$.	137
6.3	Other local mode systems.	140
	Introduction.	140
6.3(i)	Tunneling modes.	140
6.3(ii)	Compounds of the cubic β -Tungsten structure.	143
6.3(iii)	Other examples of Einstein modes.	145
	(a) Hexagonal Tungsten bronzes.	145
	(b) Inert gas clathrates.	147
CONCLUSION		147

		Page No.
APPENDIX I.	Derivation of the temperature response of the sample for the four possible input heater signals.	150
APPENDIX II.	Tabulation of the specific heat data.	153
REFERENCES.		160

CHAPTER I

THE SPECIFIC HEAT OF METALS AT LOW TEMPERATURES

INTRODUCTION

The specific heat of a material under constraint x is defined by the relationship;

$$C_x = \lim_{T \to 0} \left(\frac{\delta Q}{\delta T}\right)_x$$

where δT is the change in temperature for a change in heat input δQ. Provided that no external work is done, δQ is equal to the change in internal energy, U , of the system, and then;

$$C_x = \left.\frac{\partial U}{\partial T}\right|_x$$

The measurement of specific heat therefore entails measuring the resultant temperature change after the application of a known amount of heat to an isolated system.

Experimental determinations of specific heat are normally carried out at constant pressure, C_p, (especially for metals) whereas thermodynamic calculations generally yield the specific heat at constant volume, C_v. C_p and C_v are related by the thermodynamic identity;

$$C_p - C_v = \beta^2 \eta V T \qquad \text{(see Ref.1)}$$

where β is the volume compressibility and η the Bulk modulus. $C_p - C_v$ is quite small at low temperatures but becomes progressively more important at higher temperatures, when a correction must be made. E.g. for copper, $\frac{C_p - C_v}{C_p}$ has the following values :- 11% at 1,000K, 2.6% at 300K, 0.6% at 100K and falls even more rapidly as T is further decreased.

If the total energy, U , of an assembly varies with temperature, T, over the entire range of temperatures, there will be a specific heat at all values of T, as is the case with the crystal lattice and conduction electrons. However, if U varies only over a limited temperature range a specific heat contribution is

only observable over a restricted temperature range. This occurs when there is only a finite number of energy levels in the system. No further change in U with T will be observable once all the levels have been occupied. If the spacing of the energy levels is kT', a contribution to the specific heat will be observed only for temperatures of the order of T'. This behaviour is normally detected as a pronounced hump superimposed on the ordinary specific heat. One example of such an anomaly is the Schottky anomaly, which is important in the study of paramagnetic crystals at low temperatures.

The first measurements at low temperature were made by Nernst's school (see Chapter II, Section 1) in order to derive "chemical constants" used in the determination of equilibrium conditions for chemical reactions. Work carried out at that time was important in the development and acceptance of the third law of thermodynamics. Nowadays measurements of specific heat are often used to check ideas on the energy states of a system. The spectrum of lattice vibrations and its variation with temperature may be studied and to a certain extent the spectrum of electron energies may be investigated. Although the free electron picture is known to be unrealistic for real metals it is useful to describe their behaviour in terms of deviations from this simple model. In metals some information about the distribution of the electrons at the Fermi surface may be obtained from the specific heat. Recent theoretical advances, in general, many-body corrections to the single particle density of states, have proved important in the understanding of low temperature heat capacities.

A knowledge of the structure of electron energy bands is fundamental to an understanding of electronic heat capacity and a number of relevent band structure calculations have been made. The B.C.S. theory of superconductivity (2) provides a basis for the understanding of the superconducting state heat capacity

and shows superconductivity to be a consequence of the indirect attraction between electrons produced by electron-phonon coupling. From the realisation of the existance of a relation between electron phonon interaction and the critical temperature, McMillan (3) has derived information concerning the enhancement of normal state heat capacity.

The concept of the virtual bound state (VBS), (references 4 and 5), has been of great importance in the understanding of dilute alloys of transition metals in simple metal solvents. The hybridization of d states with the conduction band forms a virtual bound state, which has the nature of a resonance at the Fermi level (since it is expected to be narrow ($\simeq$ 1eV) compared to the width of the conduction band ($\simeq$ 10 eV)). The relative populations of spin-up and spin-down d states depends critically on the coulomb interaction between localised d electrons, U, the s-d admixture matrix element V_{sd}, and the density of states of the conduction electrons n_s. The width of the d state Δ is given by :-

$$\Delta = \pi V_{sd}^2 n_s$$

The condition that the impurity be magnetic is approximately $\Delta \ll U$. In the non-magnetic limit, $U < \Delta$, the spin-up and spin-down states are equally populated but there is an additional contribution to the density of states from the d states that enhances the heat capacity.

The additional states per atom at the Fermi level is given by :-

$$n_d(E_F) = \frac{10}{\pi\Delta} \sin^2\left(\frac{\pi N_d}{10}\right) \qquad (1.1)$$

for a Lorentzian V.B.S. of width Δ containing N_d d electrons.

The contribution to the molar specific heat is then given by :-

$$C_{V.B.S.} = \frac{1}{3} N\pi^2 k^2 n_d(E_F) T = \gamma_{V.B.S.} T \qquad (1.2)$$

where N is Avogadro's number.

Equations (1.1) and (1.2) ignore any many-body corrections and have not allowed for any splitting of the spin degeneracy of the V.B.S., but for small splittings the density of states is little affected. Caplin et al. have applied the V.B.S. description of the transition metal atom, (developed for dilute alloy systems), to the case of "dilute" compounds in their work on the Zinc transition metal ξ phases (Zn_{13} Mn; Zn_{13} Fe and Zn_{13} Co, reference 6) and also the aluminium rich aluminium-transition metal phases (reference 7).

Theoretical work on the Kondo effect (reviewed by Kondo (8) and Heeger (9)) shows the existence of a magnetic impurity-conduction electron quasibound state. The related heat capacity associated with single magnetic impurities seems to be the additional contribution needed to understand the heat capacity of certain magnetic alloys.

The basic theories of the lattice and electronic contributions to the heat capacity of metals will be outlined in this chapter; detailed discussion of the variety of contributions found in metals and their alloys is outside the scope of this work.

The low temperature heat capacities of transition metals and their alloys has been reviewed by Heiniger, Bucher and Muller (10); and nuclear contributions to heat capacities by Lounasamaa (11); N.E. Phillips' (12) review "Low Temperature Heat Capacities of Metals" provides an excellent picture of recent work and deals with contributions of magnetic origin in alloys in some detail.

1.1.(i) LATTICE HEAT CAPACITY

Classically each atom in a crystal may be considered as an independent harmonic oscillator which will have an energy 3 kT on the equipartition theorem. The total internal energy of one mole of material is therefore, $3N_0kT$ or $3RT$, where N_0 is Avogadro's number, and R is the gas constant per mole.

The lattice specific heat on this model is then given by $C_v = \left.\frac{\partial U}{\partial T}\right|_V$ = 3R = 24.94 Joules mole^{-1} K^{-1} . This value of 3R is only observed at high temperatures and it was found that C_v is less than 3R for some substances at room temperature and, for all substances, tended towards zero as T approached zero. This behaviour of specific heat on lowering temperature could only be explained at the beginning of this century with the advent of quantum theory.

1.1.(ii) RECENT WORK ON LATTICE DYNAMICS THEORY

The results of recent work on lattice dynamics theory have been summarized in N. E. Phillips review article (reference 12), and references are given to many comprchensive reviews on the subject.

The lattice heat capacity, C_L, is obtained by summing the heat capacities of N harmonic oscillators over the frequency spectrum of the lattice. If $g(\omega)$ is the number of modes with angular frequency between ω and $\omega + d\omega$ then :-

$$C_L = k \int \frac{d\omega\, g(\omega) (\hbar\omega/kT)^2 \exp(\hbar\omega/kT)}{(\exp(\hbar\omega/kT)-1)^2} \qquad (1.3)$$

where k is Boltzman's constant, and $\hbar$ is Planck's constant divided by 2π.

Although in a real lattice $g(\omega)$ is a complicated function of ω , at low temperatures C_L is dependent only on the low frequency part of the spectrum and important results may be obtained from quite simple and general considerations. It may be shown that $g(\omega)$ may be expressed as a power series in ω^2 ,

$$g(\omega) = b_2\omega^2 + b_4\omega^4 + \ldots . \qquad (1.4)$$

where $$b_2 = \frac{V}{(2\pi)^3} \sum_{i=1}^{3} \int_0^{2\pi}\int_0^{2\pi} \frac{\sin\theta\, d\theta\, d\phi}{v_i^5(\theta,\phi)}$$

where Θ and ϕ are the usual angular coordinates, $\frac{V}{(2\pi)^3}$ represents the normal mode density per unit volume in k space for a macroscopic crystal of volume V and the subscript i corresponds to the three possible directions in the lattice.

The resultant expression for C_L is then;

$$C_L = A_3T^3 + A_5T^5 + A_7T^7 + \cdots \tag{1.5}$$

where $$A_{2n+1} = \pi k \left(\frac{2\pi k}{h}\right)^{2n+1} B_{n+1} b_{2n}$$

and B_n are the Bernoulli numbers $B_1 = 1/6$, $B_2 = 1/30$, etc. The first term gives the Debye T^3 law; terms beyond T^3 for C_L are a consequence of dispersion in the ω - k relation for phonons. In general dispersion causes ω to decrease from linearity for a given k value and hence $g(\omega)$ rises faster than ω^2, giving a T dependence of C_L greater than T^3.

The information on dispersion available from C_L is limited by the accuracy to which A_5 and higher order terms can be evaluated. However a useful qualitative picture of the effects of phonon dispersion may be obtained from C_L in the region above that accessible by sound velocity measurements and at which inelastic neutron scattering data is not very accurate.

1.1.(iii) THE EINSTEIN THEORY

Einstein put forward a simple theory based on the assumption that all atoms within a crystal vibrate at the same frequency, ω_E, totally independent of each other. The vibrational energy levels of such an atom are given by; $$\varepsilon_n = \left(n + \frac{1}{2}\right)\hbar\omega_E$$

where h is Planck's constant and n is zero or an integer, $\frac{1}{2}\hbar\omega_E$ gives the zero point energy.

On applying Maxwell Boltzman statistics to evaluate the average energy

of such atoms, one obtains,

$$\bar{\varepsilon} = \frac{\sum_n \varepsilon_n \exp(-\varepsilon_n/kT)}{\sum_n \exp(-\varepsilon_n/kT)} = \frac{1}{2}\hbar\omega_E + \frac{\hbar\omega_E}{\exp(\hbar\omega_E/kT-1)}$$

The specific heat per mole of substance is then;

$$C = \frac{\partial[\bar{\varepsilon}]}{\partial T} = 3R\left(\frac{\hbar\omega_E}{kT}\right)^2 \frac{\exp(\hbar\omega_E/kT)}{(\exp(\hbar\omega_E/kT)-1)^2} \qquad (1.6)$$

where the characteristic temperature, $(\hbar\omega_E/k)$, of such a system is called the Einstein temperature, Θ_E. Considering this expression for the specific heat one finds that in the limit of high temperature the classical limit 3R is obtained, whereas at low T, $(T \ll \Theta_E)$, the expression becomes :-

$$C \simeq 3R\left(\frac{\Theta_E}{T}\right)^2 \exp(-\Theta_E/T) \qquad (1.7)$$

This expression does not give the experimentally observed dependence of $C \propto T^3$ as T approaches zero, but is proportional to $\exp(-\Theta_E/T)$. That is, the Einstein specific heat falls off too rapidly. The reason for this discrepancy is found in the oversimplified model of Einstein since the vibrational spectrum of a solid in fact covers a wide range of frequencies due to the strong coupling between atomic vibrations.

1.1.(iv) THE DEBYE THEORY

In Debye's theory for low temperature heat capacity the atomic system is assumed to be an elastic continuum, since only long wavelengths are excited and so far as these modes are concerned the material is essentially continuous. ($\lambda \gg$ lattice spacing, a; and as for elastic waves $\omega \propto$ wavevector).

For each allowed frequency there will be two transverse and one longitudinal mode, and in general the velocity of propagation of these (c_l and and c_t respectively) will not be the same.

The number of allowed modes of vibration in the frequency interval

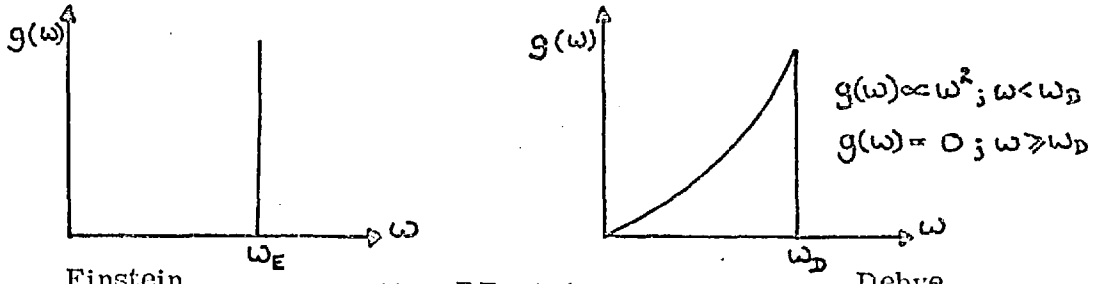
ω to $\omega + d\omega$ will be given by :-

$$g(\omega)d\omega = 4\pi V\left(\frac{1}{c_l^3} + \frac{2}{c_t^3}\right)\omega^2 d\omega \qquad (1.8)$$

(c_l and c_t are assumed to be independent of wavelength). To limit the number of allowed modes to 3N a cut off frequency, ω_D, is introduced which is defined by;

$$\int_0^{\omega_D} g(\omega)\, d\omega = 3N$$

The frequency spectra for the Debye and Einstein models are shown in Fig.(1.1) below;



Einstein FIGURE (1.1) Debye

Associated with each vibrational mode is a harmonic oscillator of the same frequency and so the total energy is given by :-

$$E = \int_0^{\omega_D} g(\omega)\langle\varepsilon\rangle\, d\omega = \int_0^{\omega_D} \frac{\hbar\omega\, g(\omega)\, d\omega}{(\exp(\hbar\omega/kT)-1)}$$

where $\langle\varepsilon\rangle$ = the average energy of an oscillator at temperature T.

Putting, $x = \hbar\omega/kT$ and $x_m = \hbar\omega_D/kT$, and defining the Debye temperature, $\Theta_D = \hbar\omega_D/k$

one has :- $$E = 9N\left(\frac{T}{\Theta_D}\right)^3 kT\int_0^{x_m} \frac{x^3}{(e^x-1)}\, dx$$

In the high temperature limit $T \gg \Theta_D$,

$$C_v = \frac{dE}{dT} = 3Nk$$ giving the classical limit for C_v.

In the low temperature limit $T \ll \Theta_D$, the upper limit of integration may be taken as infinity and since ;

$$\int_0^{\infty} \frac{x^3}{e^x-1}\, dx = \frac{\pi^4}{15}$$

one obtains :-

$$C_v = \frac{12}{5}\pi^4 Nk\left(\frac{T}{\Theta_D}\right)^3 = 1944\left(\frac{T}{\Theta_D}\right)^3 J.mole^{-1}K^{-1} \qquad (1.9)$$

which gives the well known T^3 dependence observed at low temperatures.

The coefficient of T^3 is related to sound velocities and elastic constants; comparisons of $\Theta_{el.}$ and $\Theta_{cal.}$ made on the basis of $\Theta_D(T = 0)$ usually agree within the combined probable experimental error. (The frequency at which $\Theta_{el.}$ is measured, say 10 MHz, corresponds to a temperature of $\simeq 5\times10^{-7}K$.

[Θ_{el} denotes Θ_D derived from elastic constant measurements,
Θ_{cal} denotes Θ_D derived from calorimetric measurements .]

According to the Debye theory this T^3 dependence should hold for $T \lesssim \Theta_D/10$ but is found in general to hold only for $\Theta_D/50$. This is because Θ_D should be temperature independent, but is however found to be constant for temperatures up to approximately $\Theta_D/50$ when it falls and passes through a minimum rising again to a constant value above $\Theta_D/2$. This deviation is due to the departure from the true density of states curve for the lattice vibrational modes from the simple quadratic form of the Debye model.

1.1.(v) MODIFICATIONS TO DEBYE THEORY

Born proposed a different cut-off procedure having a common minimum wavelength, λ_m, in the transverse and longitudinal modes, which leads to two distinct values of ω_D, as $\lambda_m = (4\pi V/3N)^{1/3}$ and hence:

$$\omega_{D_l} = 2\pi c_l \lambda_m \qquad \text{and} \qquad \omega_{D_t} = 2\pi c_t \lambda_m$$

This gives an expression for the specific heat :

$$C_v = R[F_D(\Theta_l/T) + 2F_D(\Theta_t/T)] \qquad (1.10)$$

where Θ_l and Θ_t are the Debye temperatures corresponding to the longitudinal and transverse modes respectively.

Born, von Karman and Blackman were the first workers to attempt to

eliminate the weakest point of Debye's theory, i.e. the assumption that the continuum representation of a lattice holds for all possible elastic waves. The minimum allowed wavelength is of the same order of magnitude as the interatomic distances, and hence a more rigorous treatment should give different results, especially in the high frequency region. Calculations were therefore carried out to determine the possible modes of vibration of atomic lattices.

Vibrational mode calculations for one dimensional lattices may be extended to two and three dimensions; Blackman first calculated the spectrum for the two dimensional and also the cubic lattice (13) and thus evaluated the specific heat. In the low temperature region the specific heat thus obtained may be equated with the Debye formula (1.9), and Θ_D calculated for different temperatures. Figure (1.2) shows Θ_D as a function of T for a simple cubic lattice (after Blackman, Ref.13). It is apparent that Θ_D is by no means constant, indicating the possibility of appreciable deviations from the Debye theory in actual crystals.

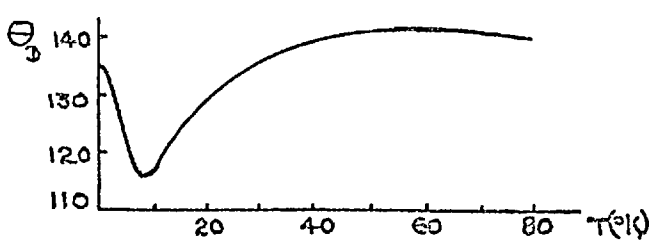


FIGURE (1.2)

Kellerman (14) investigated Na Cl , using ionic and repulsive forces between particles. Figure (1.3a) shows Kellerman's result for the frequency spectrum which is vastly different to the continuum spectrum used in the Debye theory; Fig.(1.3b) shows the behaviour of Θ_D with T, as calculated by Kellerman, and compared with experimental results .

FIGURE (1.3a)

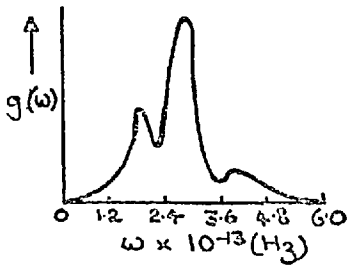
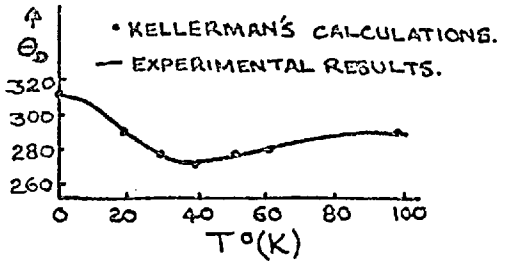


FIGURE (1.3b)



1.1.(vi) LOCALISED PHONON MODES

The presence of heavy impurity atoms in a lattice has been shown to establish low frequency modes in the vicinity of the impurity atom (15). These modes may make a considerable contribution to C_L, as shown in calculations by Kagan and Iosilevskii (16) based on the use of a Debye spectrum for the host metal and neglecting effects associated with the modification of force constants. The maximum in the frequency distribution of localized modes occurs at :-

$$\omega_o = \omega_D (3\delta)^{-\frac{1}{2}} \qquad (1.11)$$

where $\delta = M'/(M-1)$

and, M and M' are the masses of host and impurity atoms respectively. For $T \ll T_o ; (T_o \equiv \hbar\omega_o/k)$, the lattice heat capacity of the host C_L is increased by an amount proportional to C_L, such that $\Delta C_L/C_L = 3c\delta$ where c = fractional concentration of the impurity. δ can be fairly large, for example 7.5 for Pb in Mg, and hence the effect should be readily observable.

At higher temperatures, $\Delta C_L/C_L$, increases to a maximum about three times as great as the low temperature value and then drops. Cape et al.(17) report results on 1% Pb and 1% Cd in Mg which are in good qualitative agreement with the above theory, and using a more realistic frequency spectrum for Magnesium (but still ignoring changes in the force constants) the data is in good quantitative agreement. However, for Ag Al alloys, Hartman et al.(18) report that a discrepancy between theory and experiment is still apparent on the

latter treatment, which may be accounted for by considering the changes in force constants. Hence, the role of force constants is not clear, as it appears they may be neglected in Pb Mg and Cd Mg but not in Ag Al.

The excess contribution to the lattice specific heat due to a low concentration of Ag in Al is well pronounced but small in comparison to the excess observed in $Al_{10}V$, the compound investigated in this work. For example, for 0.95 atomic percent Ag in Al ΔC_L is 4% of C_L at 10 K and 8% at 20 K; whereas in $Al_{10}V$ the excess contribution is approximately 350% of C_L at 10 K and 60% at 20 K.

The subject of local phonon modes will be discussed in further detail in Chapter VI.

1.2.(i) THE ELECTRONIC HEAT CAPACITY, (C_e)

Clasically electrons would be considered as small particles moving freely and hence contributing a specific heat of $\frac{3}{2}$ k which would mean that at high temperatures the electronic heat capacity should be of the same order as the lattice contribution. However, the conduction electrons in a metal consist of a highly degenerate Fermi gas. On heating from absolute zero not every electron gains an energy $\simeq$ kT as expected classically, but only those electrons within an energy range kT of the Fermi level (E_F) are excited thermally. For N electrons only a fraction $\cong T/T_F$ can be excited thermally at temperature T as only these lie within kT of E_F.

At temperatures much less than the Fermi temperature T_F, (where $T_F = E_F/k$, and for a typical metal is $\simeq$ 10^4 to 10^5 K) the heat capacity can be expanded in a power series in T (see Ref.(19)):-

$$C_e = \frac{1}{3}\pi^2 k^2 N(\varepsilon_F) T - \frac{1}{6}\pi^4 k^4 \left\{ \frac{[N'(\varepsilon_F)]^2}{N(\varepsilon_F)} - \frac{1}{5} N''(\varepsilon_F) \right\} T^3 + \ldots\ldots \qquad (1.12)$$

where $N(\varepsilon)$ is the total electron density of states (including spin degeneracy) and the primes denote derivatives with respect to ε evaluated at E_F.

The derivation outlined below will deal only with the lowest order terms as experimental data are usually analysed using only the first term.

The calculation of the specific heat of electrons in a metal does not require a complete knowledge of energy levels. Only electrons within approximately kT of the Fermi surface are excited at room temperature, and consequently a knowledge of the number of states in the vicinity of the Fermi surface is sufficient to evaluate, C_e .

The energy per mole of the electronic system is given by :-

$$E = \int_0^\infty \varepsilon f(\varepsilon) N(\varepsilon)\, d\varepsilon = (kT)^2 \int_0^\infty \frac{N(kTx)\, x\, dx}{(\exp(x-u)+1)}$$

where $f(\varepsilon)$ is the Fermi Dirac distribution function;

$$f(\varepsilon) = \frac{1}{\exp(\varepsilon - \varepsilon_F/kT)+1}, \quad x = \frac{\varepsilon}{kT} \quad \text{and} \quad u = \frac{\varepsilon_F}{kT}.$$

It may be shown that the energy per mole is then given by :-

$$E = E_o + \frac{1}{6}\pi^2 (kT)^2 N(\varepsilon_F)$$

where E_o gives the zero point energy, and hence:-

$$C_e = \frac{1}{3}\pi^2 k^2 N(\varepsilon_F) T = \gamma T. \tag{1.13}$$

The electronic specific heat at temperature T, is thus determined solely by the density of states at the Fermi surface.

1.2.(ii) ELECTRONIC HEAT CAPACITY AND THE BAND STRUCTURE

In the absence of the periodic potential of the lattice and all interactions,

$$N(\varepsilon_F) = \frac{3mzN}{\hbar^2}\left(\frac{V}{3\pi^2 zN}\right)^{2/3} \tag{1.14}$$

$$C_e = \gamma_o T$$

where z = conduction electron per atom ratio

m = free electron mass

The differences between γ and γ_o (the free electron value), which arises from the periodic potential of the lattice and from direct and indirect electron-electron interactions, is represented by the effective mass ratio:-

$$\frac{m^*}{m} = \frac{\gamma}{\gamma_o}$$

The density of states is given by the integral over a constant energy surface in k space: $N(\varepsilon) = \frac{2V}{(2\pi)^3}\int \frac{dS}{|\text{grad}_k \varepsilon|}$ where dS is the element of area. The density of states of electrons moving in the periodic potential of the lattice but without interacting with each other is called the band structure (or single particle) density of states, $N(\varepsilon)_{BS}$. Several different methods of calculation have been used to evaluate the band structure which is basic to finding $N(\varepsilon)_{BS}$, (e.g.Ref.20).

Electronic heat capacities of alloys are occasionally discussed in

terms of the "rigid band" approximation, where it is assumed that changing z by alloying changes $\mathcal{E}_F$ but not the form of $N_{b.s.}(\mathcal{E})$. In this approximation variations of γ with z reflects the structure of $N_{b.s.}(\mathcal{E})$. The transition metal series has been interpreted in terms of this model using a single universal band structure for the whole series. The Fermi level is then moved within this rigid band according to the changing electron to atom ratio. Calculations of the b.c.c. metal band structures of the series Ti to Cu were made by Snow and Waber (21) using the APW method and their results show the widths and shapes of the bands to change considerably from metal to metal. In the case of alloys of simple metals with transition metals one would expect the Fermi levels of the alloy to shift to progressively higher energies, but Snow and Waber showed the Fermi levels of all the T3 b.c.c. metals to lie within one electron volt of each other. However, it was also found that the bottom of the 3d (4s) band dropped in energy at approximately the same rate as the Fermi level rose, and thus the relationship between $N(\mathcal{E}_F)$ and z was found to be in good qualitative agreement with the calculated band structure. Hence, although the rigid band model is not adequate for a complete discription of the alloy series, specific heat results interpreted within this framework do give an important guide to the form of the band.

$N(\mathcal{E}_F)$ differs from $N_{b.s.}(\mathcal{E}_F)$ because interactions modify the spectrum of single particle excitations at $\mathcal{E}_F$. For example interactions with spin waves and spin fluctuations in nearly magnetic materials. The effects of direct coulomb interactions and indirect phonon interactions are customarily included in C_e and assumed to be additive, such that

$$N(\mathcal{E}_F) = (1 + \lambda_c + \lambda)\, N_{b.s.}(\mathcal{E}_F) \qquad (1.15)$$

where λ_c and λ respectively are the coulomb and phonon enhancement factors.

Calculations suggest that λ_c is small for non-transition metals

and a comparison of theory and experiment suggests it to be smaller than or of the same order as the uncertainties in λ ; hence the expression may be reduced to:

$$N(\mathcal{E}_F) = (1+\lambda)\, N_{b.s}(\mathcal{E}_F) \tag{1.16}$$

λ may be obtained in a number of ways, for example by calculating $N_{b.s.}(\mathcal{E}_F)$ and using Equations 1.13 and 1.16 to evaluate λ from γ which is determined experimentally; or, by integration of the electron phonon matrix elements over the Fermi surface. It has however been recognised for some time that the electron-phonon interaction may be more complicated than is described by a constant λ (12). Results suggest effects of the order of 0.1 to 1% of the lattice heat capacity might be common.

1.2.(iii) THE SCHOTTKY EFFECT

In a system consisting of m discrete energy levels the spacing of these quantized levels is reflected in the specific heat. If we consider a two level system Δ apart then at temperatures $T \approx \Delta/k$ transitions from one level to the other occur. This gives rise to a large specific heat contribution which tends to zero at both high and low temperatures.

If we consider m levels, separated from the ground state by energies $\mathcal{E}_1, \mathcal{E}_2 \cdots \mathcal{E}_m$ and with degeneracies $g_1, g_2 \cdots g_m$ then the probability of a particle occupying the r^{th} level is: $g_r \exp(-\mathcal{E}_r/kT) / \sum_n g_r \exp(-\mathcal{E}_r/kT)$ and for N independent particles the mean energy at temperature T is;

$$E = N \frac{\sum_{r=0}^{m} \mathcal{E}_r g_r \exp(-\mathcal{E}_r/kT)}{\sum_{r=0} g_r \exp(-\mathcal{E}_r/kT)}$$

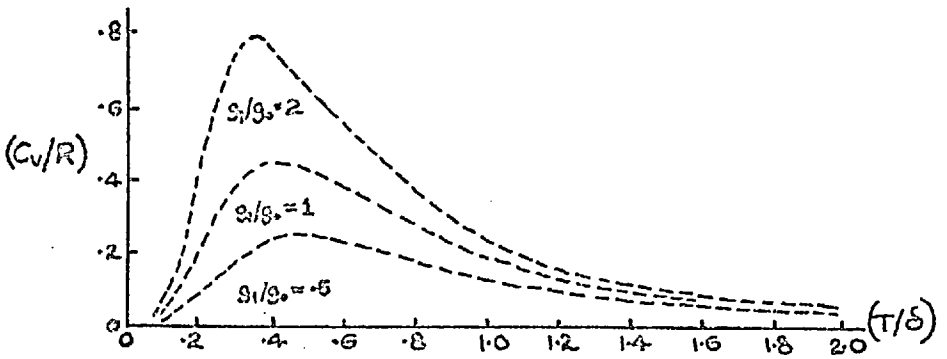
For the simple case of a two level system then;

$$C_{Sch.} = \frac{dE}{dT} = R\left(\frac{\delta}{T}\right)^2 \frac{g_0}{g_1} \frac{\exp(\delta/T)}{[1+(g_0/g_1)\exp(\delta/T)]^2} \tag{1.18}$$

where $\delta = \mathcal{E}/k$ is the energy separation in degrees Kelvin.

FIGURE (1.4)

The Schottky heat capacity of a two-level system for several values of g_1/g_0



It may be seen that for $T \ll \delta$; $C_{Sch} = R \frac{g_1}{g_0}\left(\frac{\delta}{T}\right)^2 \exp(-\delta/T)$

$T \gg \delta$; $C_{Sch} = R\, g_0 g_1 (g_0+g_1)^{-2} (\delta/T)^2$

Paramagnetic salts, in which magnetic dipoles have energy levels with spacings of approximately 1 to 10^{o}K form the natural examples of simple systems exhibiting Schottky peaks. Nuclear Schottky effects may also arise where the nucleus of an ion has a spin and hence a magnetic moment. Then, due to the mutual interaction of the nuclear and electron dipoles there will be an extra splitting of the ionic levels, (above that caused by the crystalline electric field), the hyperfine splitting. The energy spread of these levels is between 10^{-3} and 10^{-1} K. If the nucleus has a quadrupole moment its interaction with the field gradients produced by neighbouring atoms will cause small level splittings. Nuclear anomalies usually occur well below 1^{o}K.

CHAPTER II

METHODS OF MEASURING HEAT CAPACITY AT LOW TEMPERATURES

2.1. TRADITIONAL METHODS OF MEASUREMENT

In 1910, Nernst (23) devised the original vacuum calorimeter for use at liquid air or hydrogen temperatures, a similar arrangement was later used by Keesom at liquid helium temperatures.

A cylindrical block of the sample itself, or a silvered canister containing the sample, is provided with a heating coil of platinum wire, which also serves as a temperature sensor. The block or canister is suspended by fine wires inside a glass vessel. Whilst the sample is initially being cooled a small amount of exchange gas is used and once the sample has reached its lowest temperature the vessel is evacuated in order to minimise stray heat leaks.

Measurements are made by applying a known quantity of heat, ΔQ, and measuring the resulting temperature rise, ΔT. The heat capacity, C, of the sample plus addenda is then given by;

$$C = \frac{\Delta Q}{\Delta T}$$

An accuracy of .5 to 1% has been reported using the above arrangement, after making corrections for stray heat inputs via lead wires.

In 1930 the adiabatic calorimeter was improved by the incorporation of an adiabatic shield with a heating coil, outside the sample chamber. The temperature of the shield may be varied so that it follows that of the inner container. Keesom further improved the design by attaching the sample heating coil to a separate metal core onto which the specimen is screwed.

In present day adiabatic calorimetry the specimen is usually suspended in the inner container by some thermally insulating material (e.g. nylon thread)

such that it is thermally isolated from the container.

It is not possible to achieve absolute adiabatic conditions and so corrections must be made to account for stray heat inputs. To minimise these corrections the temperature of the enclosure must be kept as close as possible to that of the specimen, and care must be taken in the choice of materials to reduce stray heat leaks by conduction, radiation and Joule heating.

The use of helium as an exchange gas during the initial cooling of the sample has proved to have two major disadvantages. It can take several hours to pump the gas out to a sufficiently low pressure, and a film of helium may be adsorbed onto the surface of the sample at low temperatures. Although this film cannot be removed by pumping, helium gas boils off on warming the specimen and this leads to anomalously high specific heats due to the heat required for the desorption of the helium. These problems have led to the use of mechanical heat switches (24). A mechanical connection is made between the specimen and shield during cooling and then the connection is broken to give thermal isolation whilst measurements are made. However, with the usual methods of sample suspension in adiabatic calorimeters, the system is very sensitive to vibrational heating and so any mechanical action on the sample is undesirable.

C. Luengo (25) describes a system where the mechanical switch is jaw shaped and makes thermal contact on a metallic contact attached to the sample (see Fig.2.1.a.). Luengo also describes an alternative arrangement where the sample is rigidly suspended by a thermally insulating material (see Fig.2.1.b.). This semi-adiabatic system is less sensitive to vibrational heating and a more simple design of heat switch may be used as the force required for effective thermal contact may

be directly applied to the sample.

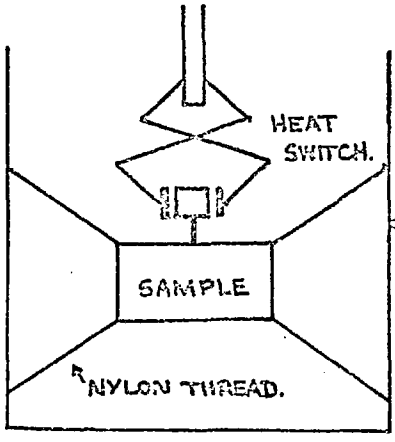


FIGURE (2.1.a)

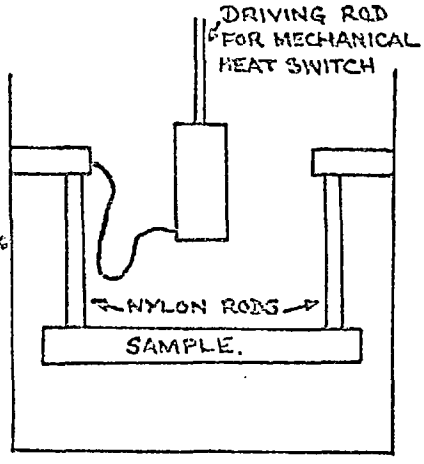


FIGURE (2.1.b)

The major disadvantages of this semi-adiabatic arrangement are drifts in temperature, which Luengo reports to be of the order of 10% of ΔT per minute at 5K and 1% of ΔT per minute at .5K.

2.2 METHODS OF SPECIFIC HEAT MEASUREMENT ON SMALL SAMPLES AT LOW TEMPERATURES

In the previous section some traditional calorimetric methods have been discussed. These required large samples (of the order of hundreds of grammes) in order to minimise the effects of stray heat leaks. Exchange gas or complicated mechanical devices were required to obtain sufficient isolation during the measurement and yet allow the sample to initially cool down in a reasonable length of time.

There have been many recent advances which have increased the reliability of calorimetric data, for example, the use of superconducting switches, the development of stable germanium thermometers, the availability of cryostats enabling measurements below one degree Kelvin, and improvements in sample purity and analytical techniques.

During recent years a number of methods of measurement have been devised which allow the measurement of small samples (from a few grammes down to as little as one milligramme in some cases) to a few percent. All the methods to be described use a deliberate "heat leak" from the cold bath to the sample. The time constant for thermal relaxation to the constant temperature heat reservoir (To) is given by,

$$\tau_1 = \frac{C}{k} \qquad (2.1)$$

where C is the heat capacity of the sample plus addenda and k is the thermal conductance of the weak thermal link. Hence for a given system a suitable value for τ_1 may be obtained by the use of an appropriate heat link.

2.2.(i) PULSE TECHNIQUES

(a) MORIN AND MAITA

A pulse technique was used by Morin and Maita (26) on small samples (of mass down to 200 milligrammes). The sample is contained in an evacuated

can filled with aluminium oxide powder following the procedure of Kunzler (27). This arrangement minimises radiation losses and vibration heating, whilst the powder provides a thermal link with the cold bath. The time constant for thermal relaxation to the bath temperature, τ_1, may be adjusted by variation of the powder composition. τ_1 must be greater than the internal time constant of the sample, but short enough to allow cooling from 20K to 1.5K in a few hours.

The measurements are made by applying square current pulses of about two seconds in length to a wire wound heater in order to give a rise in temperature, ΔT, of the sample of approximately a few tenths of a percent of the ambient temperature. The heat capacity is evaluated using the basic equation $C = \frac{\Delta Q}{\Delta T}$

The heater and silicon chip thermometer are attached to the sample using Ge 7301 varnish as shown in Fig.(2.2.) below.

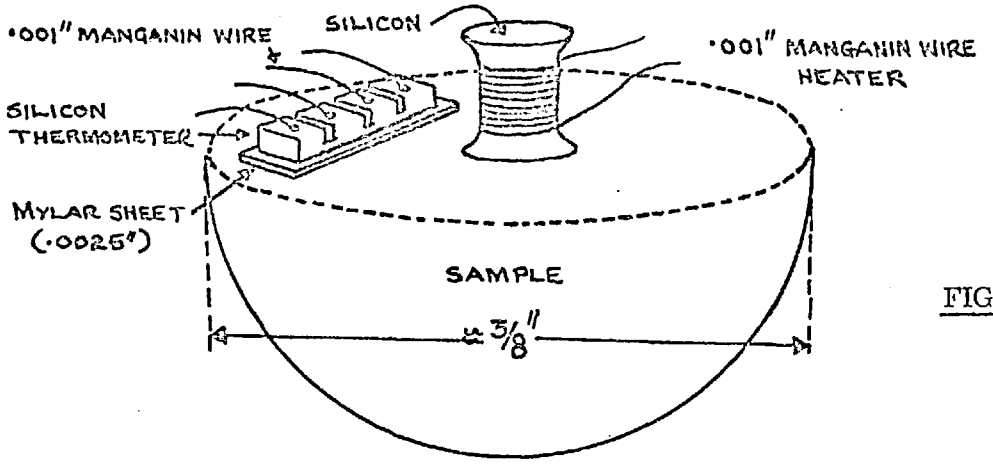


FIGURE (2.2)

(b) DUNLOP

An alternative pulse technique is described by Dunlop (28) for measurements on samples of about 2 gms. The specimen is mounted on Mylar sheet using Ge 7301 varnish, and the heater, a thin film of nichrome, is evaporated onto the underside of the Mylar sheet which is suspended in the

sample chamber by nylon thread.

A small amount of exchange gas is admitted to the inner chamber and the pressure adjusted until τ_1 is of the order of thirty seconds. Corrections must be made to the observed temperature rise depending on the ratio between the length of the heat pulse (Δt) and τ_1 ; since from Dunlop's calculations, $C = \frac{\Delta Q}{\Delta T}\left(1 - \frac{\Delta t}{\tau_1}\right)$. This correction factor is reported as being of the order of 7%.

2.2.(ii) STEP TECHNIQUE

One of the methods described by Bachmann et al (29) is based on the measurement of the thermal relaxation time constant, τ_1 , defined earlier, by stepping the heater voltage either up or down and measuring the time constant of the resulting exponential change in temperature.

Using the arrangement described by Bachmann measurements may be made on samples of mass 1 to 100 mgm. The sample holder consists of a silicon chip bolometer which is insulating at low temperatures. An active layer of silicon is doped onto one side of the bolometer, and this layer is divided into two providing a resistance thermometer and Joule heater. The sample is secured to the opposite side of the bolometer using grease or indium solder. Lead wires from the heater and thermometer provide the mechanical support and thermal connection to the constant temperature heat reservoir, which in this arrangement is a copper block, the temperature of which may be varied using a bifilar wound manganin heater driven by a Zener regulated voltage supply. When the sample temperature, T_1 , is raised above the block temperature, T_0 , it is important to keep T_0 fixed. (The change in T_0 upon heating is given by,

$$\Delta T_0 = (T_1 - T_0) \times \frac{\text{bolometer to block thermal conductance}}{\text{block to bath thermal conductance}})$$

This arrangement takes advantage of the adjustability of k, the thermal conductance linking the sample and heat reservoir. It is reported that with this system it is possible to control the heat link over several decades of k, by a suitable choice of lead wires. (The other methods of measurement described in this section may all be employed using a similar arrangement).

As shown in section 3 of this chapter, if the power input to the sample is switched to zero at time $t = 0$, the resultant change in temperature is given by :

$$\Delta T(t) = \Delta T(t=0) \exp(-t/\tau_1)$$

and

$$\tau_1 = \frac{C}{k}$$

Hence measuring k and τ_1 constitutes a measurement of C. Details of the theory of this method will be included in the next section.

The major advantage of this method over the A.C. method to be described below is that internal thermal relaxation effects are more easily recognised and accounted for.

2.2.(iii) A. C. METHOD

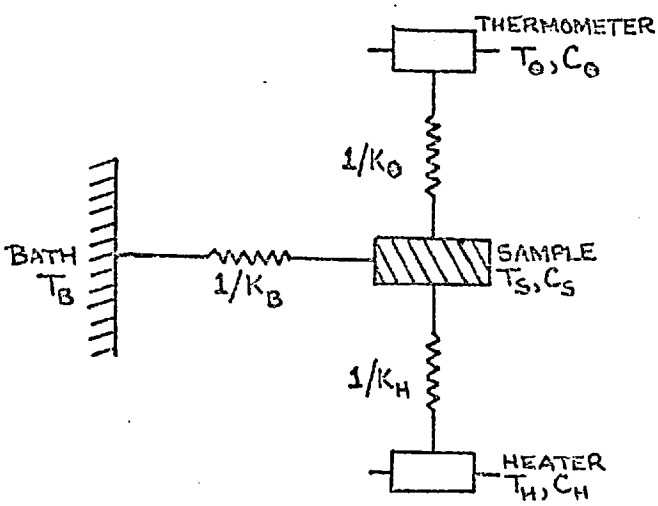
A steady state method of measurement is described by Sullivan and Siedel (30) for samples of mass greater than 1 mgm, to an accuracy of one percent. The sample is coupled thermally to the cold bath using a fairly rigid suspension system, and schematically the arrangement may be represented by Figure (2.3) below.

If heat is generated at a rate $\dot{Q} = \dot{Q}_0 (\cos \omega t)^2$, and provided the heater and thermometer are coupled to the sample with very short relaxation times (i.e. $\omega^2(\tau_\theta^2 + \tau_H^2) \ll 1$) then the resultant a.c. temperature variation, T_2, (which will be at a frequency 2ω ,) of a sample of finite thermal

diffusivity is given by ;

$$T_2 = \left(\frac{\dot{Q}_0}{4\omega C}\right)\left[1 + \frac{1}{4\omega^2\tau_1^2} + 4\omega^2\tau_2^2 + \frac{2K_B}{3K_S}\right]^{-\frac{1}{2}} \qquad (2.2)$$

where C represents the heat capacity of the sample plus addenda, τ_1 is the sample to bath time constant for thermal relaxation, and τ_2 represents the internal thermal time constants such that, $\tau_2^2 = \tau_\theta^2 + \tau_H^2 + \tau_S^2$



K_θ , K_B , K_H refer respectively to the sample to thermometer, bath, and heater thermal conductances. The same subscripts are used to denote the heat capacities, temperatures and thermal relaxation times of the various components. K_S is the internal thermal conductance of the sample.

If the sample thermal conductance (K_S) is low, (i.e. τ_S large), there will be a temperature gradient in the sample and the measured signal will not give an accurate measurement of the heat capacity. Provided the applied heater voltage frequency, ω , lies within the limitations set by the time constants τ_1 and τ_2 (see section 3.(ii)(a) and (b)), i.e. $\frac{\omega\tau_1}{7} > 1 > 15\tau_2\omega$, the heat capacity may be evaluated to one percent from the expression :

$$|T_2| = \left(\frac{\dot{Q}_0}{4\omega C}\right) \qquad (2.3)$$

Using this technique small changes in heat capacity with some experimentally variable parameter may be recorded directly. A continuous

readout of heat capacity may be obtained whereas the pulse technique gives strictly point to point measurements.

A detailed explanation of the theory may be found in Ref.(30) and section 3 of this chapter gives further information on frequency limitations.

2.2.(iv) SWEEP METHOD

This method gives a continuous readout of heat capacity which is especially advantageous for the examination of sharp structures in heat capacity, e.g. order-disorder phenomena and other cooperative effects. Considering a system where $T_2 \ll T_1$, so that a one dimensional model for heat flow in the system may be employed (see section 3.1 of this chapter), the heat balance equation for the system may be written as :

$$\text{Power into sample} = \text{power out} + \frac{\partial}{\partial t}(\text{heat in sample})$$

$$P = AK\frac{\partial T}{\partial Z} + C(T)\frac{\partial T}{\partial t} \qquad (2.4)$$

where P is the power put into the sample, A is the cross-sectional area of the thermal link between the sample and constant temperature heat reservoir, K is its thermal conductivity, and heat flows along the Z axis.

In the steady state i.e. sample temperature $T = T_1 =$ constant then we have:

$$P(T_1) = \int_{T_0}^{T_1} k(T')\,dT'$$

where T_0 is the temperature of the heat reservoir.

If the power is measured as a function of T_1 a smooth curve is obtained (which is parabolic if k(T) is linear in T). If at T_1 the power is suddenly reduced to zero, then measuring dT/dt enables the heat capacity to be obtained from the expression :-

$$C(T) = \left(\frac{dT}{dt}\right)^{-1}\int_{T_0}^{T_1} k\,dT' = \left(\frac{dT}{dt}\right)^{-1} P(T_1). \qquad (2.5)$$

The thermal time constants τ_1 and τ_2 are again of vital importance in this method. τ_1 must be long enough to facilitate accurate measurement of (dT/dt) and τ_2 must be short. τ_2 effects can distort the data especially when measuring a peak in the heat capacity with this method. A rise in C causes a corresponding rise in τ_2 and if;

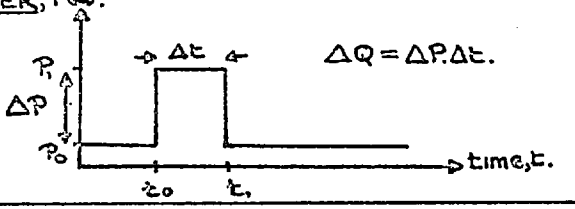
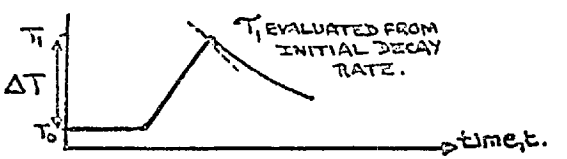
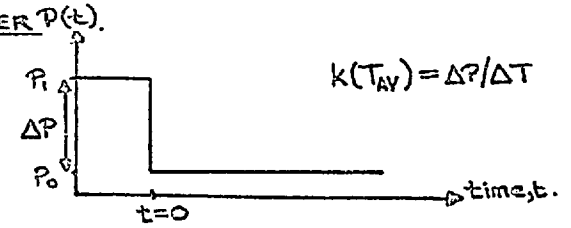
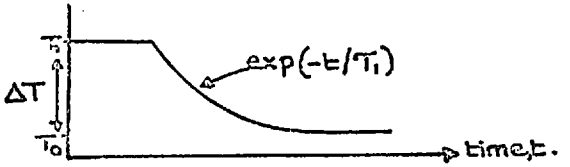
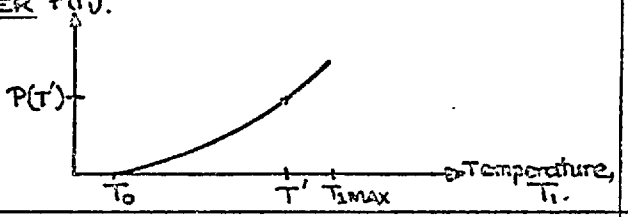
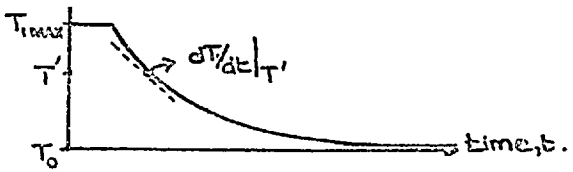
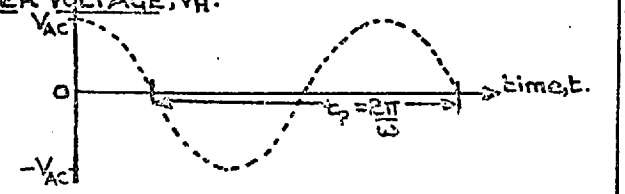
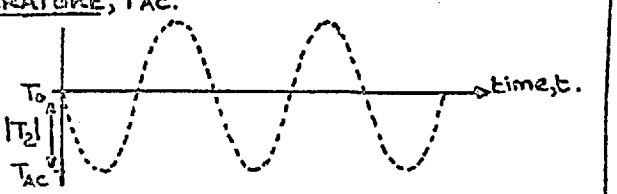
$$\frac{dT}{dt} \simeq \frac{\text{PEAKWIDTH}}{\tau_{2(MAX)}}$$

then the sample temperature will significantly lag behind the bolometer temperature. The application of brief heat pulses throughout the peak region enables easy detection of this effect, an overshoot in the bolometer temperature implies a lag in the sample temperature. To avoid such effects the following condition must be satisfied ;

$$\frac{(T_1 - T_0)}{\tau_{2(MAX)}} \gg \frac{dT}{dt}$$

(A comparison of the methods described in this section is given in Table 2.1).

TABLE 2.1 - COMPARISON OF METHODS

METHOD	DEFINING RELATION	GRAPHICAL REPRESENTATION	
PULSE (After Ref. 28)	$C = \Delta Q / \Delta T.$ * Correction factor:- $(1 - \Delta t/\tau_1)$	POWER, P(t).  	TEMPERATURE, T. 
STEP (After Ref.30, and this work)	$C = k\tau_1$ (To 1% provided:- $\tau_1 \gg \tau_2$)	POWER P(t).  	TEMPERATURE, T. 
SWEEP (After Ref.30)	$C(T') = \left.\frac{dT}{dt}\right|^{-1}_{T'} P(T')$ (To 1% provided:- $\frac{(T_1 - T_0)}{\tau_{2max}} \gg \frac{dT}{dt}$)	POWER P(T').  	TEMPERATURE, T. 
A. C.	$C = \dot{Q}/(4\omega\|T_2\|)$ (To 1% provided:- $\frac{\omega\tau_1}{7} > 1 > 15\omega\tau_2$)	HEATER VOLTAGE, VH.  	TEMPERATURE, TAC. 

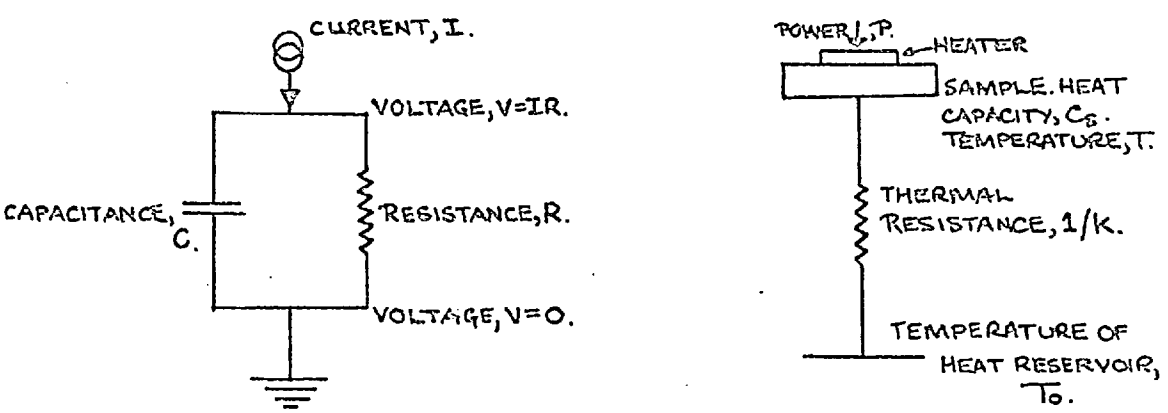
2.3 METHODS OF MEASUREMENT USED IN THIS WORK

A system was required for this work that would enable the measurement of the heat capacity of samples of a few grammes mass to about five percent accuracy. Details of the apparatus and experimental procedure are given in the next chapter; in this section the theory of the methods of measurement chosen will be given.

Both the step and a.c. techniques have been used, although the a.c. method was found to be preferable in terms of ease of data analysis. Problems were encountered with the accurate evaluation of τ_1 using the step technique due to drifts in the base line. The initial use of the step technique proved invaluable however in terms of rigorously investigating the system for τ_2 effects which, as stated previously, are readily recognisable in this method.

2.3.(i) THEORY OF STEP METHOD

The basic system may be illustrated by the use of a simple electrical analogue :-



(a) (b)

In the steady state in (a) current, I, and in (b) power, P, flows through the system. When in (a) the current, and in (b) the power is switched off the voltage in (a) decays to V = 0 with time constant $\tau = RC$ and in

(b) the temperature decays to $T = T_0$ with time constant $\tau_1 = C_s/k$

Provided τ_2 effects are negligible (and this includes the assumption that all lateral diffusion times are much shorter than the longitudinal diffusion down the thermal link), then we may consider a very simple one dimensional model for heat flow in the system.

The heat balance equation for heat flowing along the z axis may be expressed as :-

Power into sample = Power out of sample + $\frac{\partial}{\partial t}$ (heat in sample)

$$P = AK(T)\frac{\partial T}{\partial z} + C(T)\frac{\partial T}{\partial t} \qquad (2.6)$$

where A = Cross sectional area of the thermal link

K = Thermal conductivity of the link.

Integrating over the length, ℓ, of the thermal link;

$$\int_0^{\ell} P\, dz = \int_0^{\ell} AK(T)\frac{dT}{dz}\, dz + \int_0^{\ell} C(T)\frac{dT}{dt}\, dz.$$

and hence :

$$P.\ell. = \int_{T_0}^{T} AK(T)\, dT + C(T).\ell.\frac{dT}{dt}$$

$$C(T) = \left(\frac{dT}{dt}\right)^{-1}\left[P - \int_{T_0}^{T} k(T')\, dT'\right]$$

where $k(T') = \frac{AK(T')}{\ell}$ = Thermal conductance of the link. The assumption is made that the link has no thermal capacity, a more detailed analysis (see Ref.29) shows that one third the heat capacity of the link should be included in the addenda.

Provided the temperature change $T_1 - T_0 = \Delta T$ is small enough, (and for 1% accuracy ΔT must be such that τ_1 changes by less than 1%), then

$$\int_{T_0}^{T} k\, dT' = k(T_{Av})\Delta T$$

where $T_{AV} = \frac{1}{2}(T + T_o)$

and provided the reservoir temperature, T_o, is stablized so that $dT_o/dt \ll dT/dt$ we may say;

$$\frac{dT}{dt} = \frac{d(\Delta T)}{dt}$$

therefore

$$C(T) = \left(\frac{d(\Delta T)}{dt}\right)^{-1}\left[P - k(T_{AV})\Delta T\right]$$

if at $t = 0$ the power is switched off, and assuming $C(T)$ to be constant over the temperature change $(T - T_o)$:-

$$C\,\frac{1}{\Delta T}\,\frac{d(\Delta T)}{dt} = -k(T_{AV})$$

$$C = -k\left[\frac{d(\ln(\Delta T))}{dt}\right]^{-1}$$

$$\Delta T(t) = \Delta T_{t=0}\exp\left(-\frac{t}{\tau_1}\right) \qquad (2.7)$$

Since $\tau_1 = \frac{C}{K}$, measurement of the heat capacity involves measuring k and τ_1. If the internal time constants are not negligible compared to τ_1 the decay curve shows non exponential behaviour as depicted in Fig. (2.5)

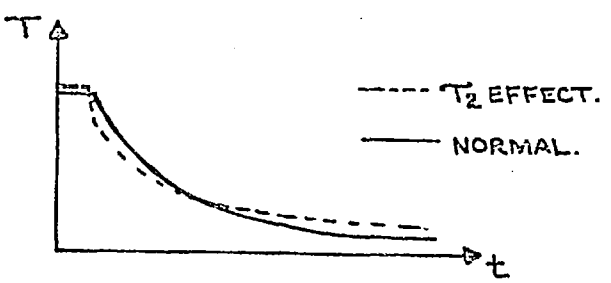


FIGURE 2.5

2.3.(ii) A.C. METHOD AND FREQUENCY LIMITATIONS

As stated in section 2(iii) of this chapter if heat is supplied to a sample, thermally coupled to the bath, heater and thermometer as shown in Fig.(2.3), at a rate $\dot{Q} = \dot{Q}_0(\cos\omega t)^2 = (\dot{Q}_0/2)(1+\cos 2\omega t)$ then the a.c. temperature variation, at frequency 2ω, is given by equation (2.2), i.e.

$$|T_2| = \frac{\dot{Q}_0}{4\omega C}\left[1 + \frac{1}{4\omega^2\tau_1^2} + 4\omega^2\tau_2^2 + \frac{2K_B}{3K_S}\right]^{-1/2}$$

The last term in this expression is a geometric term, in the sense that its magnitude depends on the position at which the temperature is measured. In Sullivan and Seidel's calculation the thermometer position is such that this correction is a maximum (i.e. thermometer and heater at opposite ends of the sample). Considering a typical copper sample and brass heat link at 10K then $2K_B/3K_S \simeq 10^{-4}$ and hence this term may be safely ignored.

The heat capacity may be evaluated to 1% from equation (2.3),

i.e. $$|T_2| = \frac{\dot{Q}_0}{4\omega C}$$

provided the applied heater frequency, ω, lies within the limits set by τ_1 and τ_2. For 1% accuracy we require,

$$0.99 \leq (1 + 1/4\omega^2\tau_1^2 + 4\omega^2\tau_2^2)^{-1/2} \leq 1.01$$

if this condition is not satisfied equation (2.3) becomes invalid, i.e. $|T_2|$ will not be proportional to $(\omega)^{-1}$. The upper and lower frequency limitations are evaluated in the following sections.

(a) LOW FREQUENCY LIMIT

If the applied heater signal is at too low a frequency, compared to τ_1, then the sample temperature will not follow a sinusoidal response, i.e. linearity (eqn.2.3) will be lost.

Assuming the thermometer and heater to be coupled by infinite thermal conductances to the sample also of infinite thermal conductance (i.e. $\tau_2 = 0$),

and supplying the heater (resistance R_H) with a voltage $V = V_{A.C.}(\cos \omega t)$, then the thermal equation for the system is given by :-

$$\frac{V_{AC}^2}{2R_H}(1+\cos 2\omega t) = P(T) + C_S \frac{dT}{dt} \tag{2.8}$$

where P(T) represents the rate of heat lost via the thermal link.

Letting the temperature variation be of the form,

$$T = T_o + T_2 e^{i2\omega t} \tag{2.9}$$

then P(T) may be expressed in a Taylor expansion as :-

$$P(T) = P(T_o) + \frac{dP}{dT}\Big|_{T_o}(T-T_o) = P(T_o) + T_2 e^{i2\omega t}\frac{dP}{dT}\Big|_{T_o}$$

for :- $|T_2| \ll T_o$.

This gives for the steady state,

$$\frac{V_{AC}^2}{2R_H} = P(T_o) \tag{2.10}$$

and for the transient state,

$$P(T_o)\cos 2\omega t = T_2 e^{i2\omega t}\left[\frac{dP}{dT}\Big|_{T_o} + i2\omega C_S\right]$$

Defining the thermal resistance at T_o as

$$R(T_o) = \frac{dP}{dT}\Big|_{T_o}^{-1} = \frac{1}{K_B(T_o)}$$

then we have :-

$$|T_2| = P(T_o)R(T_o)[1+4\omega^2\tau_1^2]^{-1/2}$$

$$= \frac{P(T_o)}{2\omega C_S}\left[1 + \frac{1}{4\omega^2\tau_1^2}\right]^{-1/2} \tag{2.11}$$

as; $\tau_1(T_o) = \frac{C_S}{K_B(T_o)} = C_S R(T_o)$

which is identical to Sullivan and Seidel's expression assuming infinite, K_Θ , K_H

and K_s ; and where $P(T_o) = \dot{Q}_o/2$ in their expression.

If we assume that at low temperatures the thermal conductance of the link is proportional to T; that is,

$$K_B(T) = \chi T$$

then:-

$$P(T_o) = \int_{T_b}^{T_o} \chi T dT = \frac{1}{2}\chi(T_o^2 - T_b^2)$$

where T_b is the bath temperature

and

$$R(T_o) = (\chi T_o)^{-1}$$

Then provided $2\omega\tau_1 \gtrsim 7$, i. e. $t_p \lesssim 2\tau_1$, to 1% we have :

$$\frac{|T_2|}{T_o} = \frac{1}{2}\left(1 - \frac{T_b^2}{T_o^2}\right)\left(\frac{t_p}{4\pi\tau_1}\right) \qquad (2.12)$$

where $t_p = 2\pi/\omega$ = time period of the heater voltage.

Considering sample temperatures much greater than the bath temperature Equation (2.12) further simplifies to give :

$$\frac{|T_2|}{T_o} \simeq \frac{t_p}{8\pi\tau_1} \qquad (2.13)$$

However, to ensure that the assumption of constant C_s over $|T_2|$ is valid we must have $|T_2|/T_o \lesssim 0{\cdot}05$ which gives the following conditions for t_p :-

For $T_b \simeq 4K$:-

$t_p \lesssim 1{\cdot}25\tau_1$ down to $T_o = 8K$.

$t_p \lesssim 2{\cdot}00\tau_1$ down to $T_o = 4K$.

and for $T_b \simeq 2K$:-

$t_p \lesssim 1{\cdot}50\tau_1$ down to $T_o = 4K$.

$t_p \lesssim 2{\cdot}00\tau_1$ down to $T_o = 2K$.

(b) HIGH FREQUENCY LIMIT

Now considering the situation where K_H , K_θ and K_s are finite, at "high" frequencies one must take care that the internal time constants of the system are short enough compared to the frequency of the heater voltage in order to avoid thermal gradients in the system. Measurement of the internal time constants (embodied in τ_2) must therefore be made in order to establish the upper frequency limit for a given sample and thermal link.

In order to measure $\tau_2(T)$ a d.c. heater voltage is used to stablise the sample temperature at T^oK. A small "low" frequency a.c. signal, capacitively coupled to the operational amplifier in the heater supply circuit (see chapter 3, section 2) is then superimposed on the D.C. signal. As may be seen from equations A.1.3 and A.1.4 in Appendix 1, if the a.c. signal is small, so that $V_{AC} \ll V_{DC}$ the temperature response is at the applied frequency, ω ; the second harmonic term being negligible.

Provided the condition from the previous section is obeyed so that the term in τ_1 may be neglected, then the amplitude of the temperature response $|T_1|$, as explained in Appendix 1 is given by :-

$$|T_1| = \frac{2R_o^2 c V_{DC} V_{AC}}{R_H R_2 C_s} \left[1 + \omega^2 \tau_2^2\right]^{-1/2} \qquad (2.14)$$

(the terms are defined in the appendix).

To evaluate τ_2 , the frequency of the a.c. signal is increased until the amplitude, $|T_1|$, has been reduced by a factor of two.

If $\omega_{1/2}$ is the frequency for half amplitude response we have :-

$$(1 + \omega_{1/2}^2 \tau_2^2)^{1/2} = 2$$

$$\omega_{1/2} \tau_2 = \sqrt{3}$$

If $t_{p1/2} = 2\pi/\omega_{1/2}$, then $t_{p1/2} = 3{\cdot}6\,\tau_2$

To obtain 1% accuracy we require that:-

$$\omega^2 \tau_2^2 \leq 0{\cdot}02$$

i.e. $$t_p \geq 12{\cdot}5 t_{p_{1/2}}$$

Since this effectively measures the fastest response time of the system for equation (2.3) to be valid, we must use the condition

$$t_p \geq 25 t_{p_{1/2}} \tag{2.15}$$

since when making measurements with the resistively coupled pure A.C. signal, the temperature responds at twice the frequency of the input signal.

(N.B. t_p must always be greater than 2secs as the response time of the circuitry restricts the time period of the temperature response to $>$ 1 sec. for good linearity).

CHAPTER III

APPARATUS AND EXPERIMENTAL PROCEDURE

3.1 DESIGN OF CALORIMETER

The calorimeter is designed to measure the heat capacity of small samples (approximately a few grammes) in the temperature range 2 to 40 K to about 5%.

In the choice of materials to be used the main considerations are those of avoiding stray heat inputs to the helium bath and sample chamber, and minimising the heat capacity of the addenda.

In the methods of measurements used in this work it is necessary to have a single well defined time constant for thermal relaxation from sample to cold bath. In order to avoid spurious thermal time constants care must be taken to ensure that the thermal diffusivity (D cm^2 sec^{-1}) of materials used in the sample chamber are sufficiently large.

3.1.(i) He_4 CRYOSTAT

The helium dewar is a standard metal double dewar in which the calorimeter is suspended. The helium level detector consists of an Allen Bradley carbon resistor supported on a steel tube of adjustable height. The resistor is supplied with a constant voltage and resistance changes are monitored by variations in the current registered on a milli-ammeter.

Fig.(3.1.1) shows an overall picture of the specific heat cryostat.

3.1.(ii) THE SAMPLE CHAMBER

The sample chamber shown in Figs.(3.1.1. and 3.1.2) is suspended in the helium space by the pumping tube, which is secured to the top flange of the cryostat using Genevac couplings. The pumping tube is thin walled (0.02") stainless steel tubing (O.D. 0.5"), stainless steel being used to reduce heat

FIG.(3.1.1) SCHEMATIC DIAGRAM OF SPECIFIC HEAT CRYOSTAT.

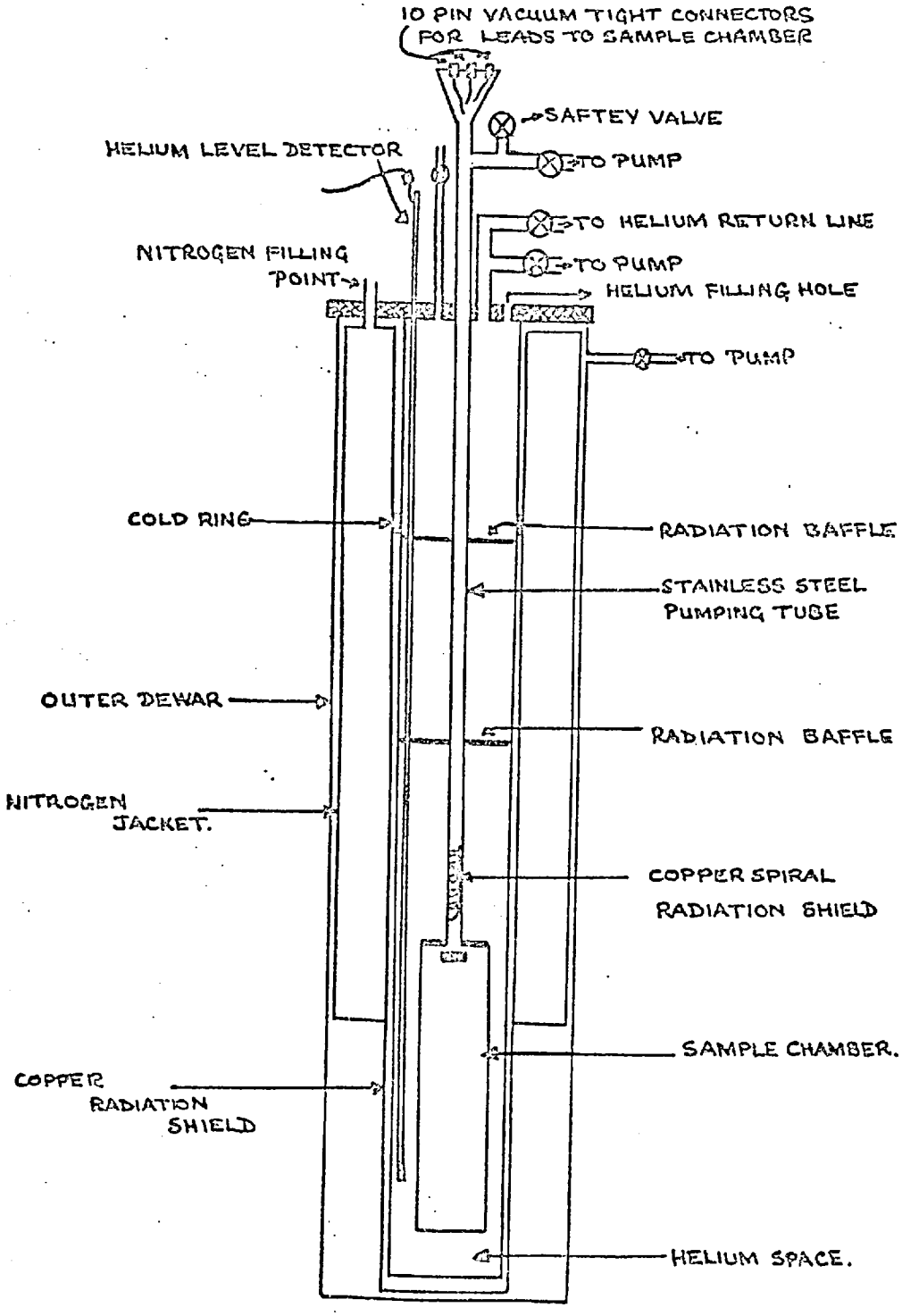
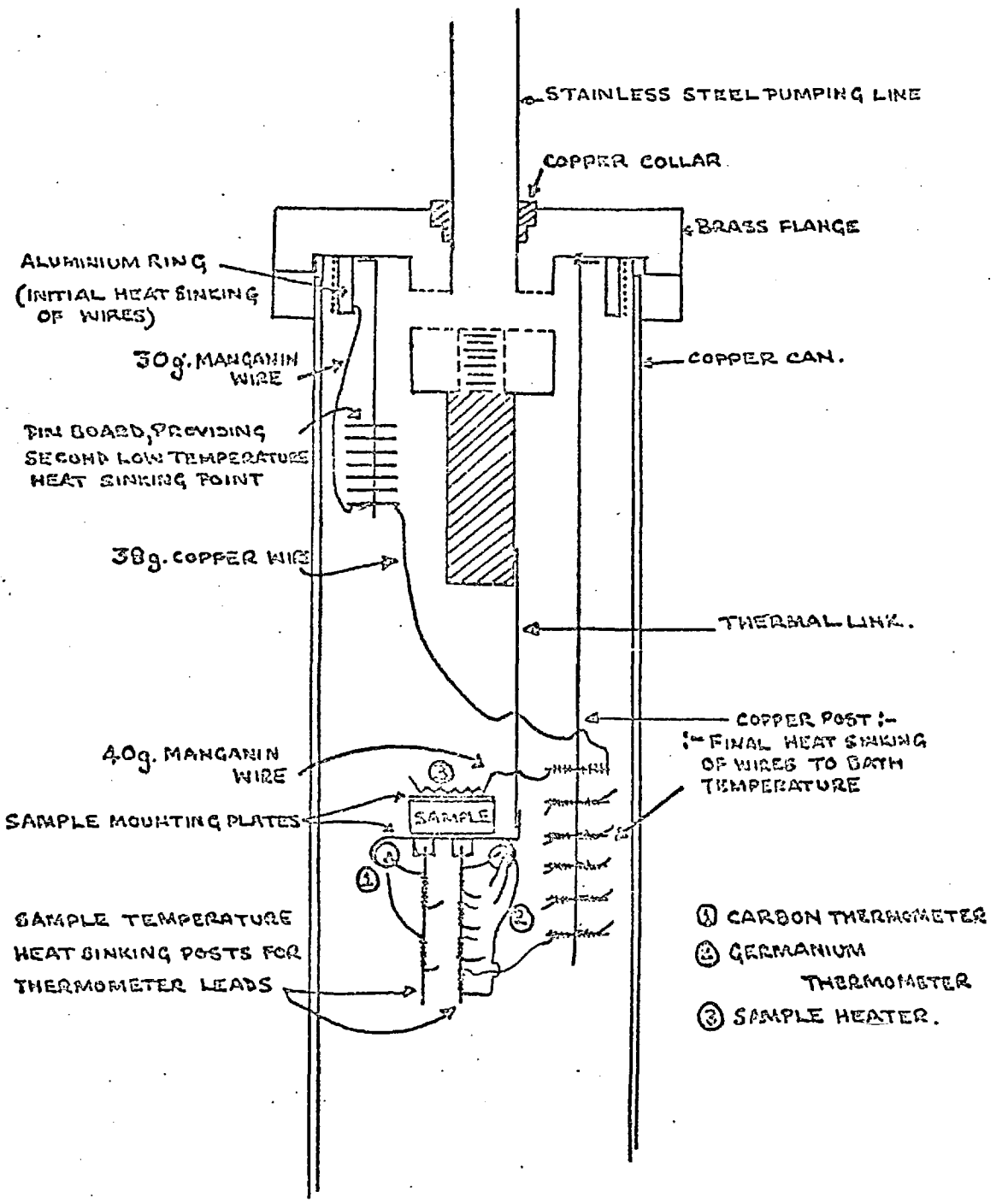


FIG. 3.1.2. SCHEMATIC DIAGRAM OF SAMPLE CHAMBER, INDICATING SAMPLE MOUNTING AND HEAT SINKING OF WIRES.



leaks by conduction down the tube. In order to reduce radiation leaks from room temperature to the helium bath two radiation baffles are secured to the pumping tube. A radiation shield in the form of a spiral of copper foil is incorporated in the pumping tube and a radiation baffle is formed at the base of the pumping tube by means of a "T" hole.

The lower end of the pumping tube is connected to the brass flange of the sample chamber by means of a counter sunk copper collar. The stainless steel to copper, and copper to brass joints are all soft soldered. The brass flange is secured to the inner can by means of an indium 'O'-ring, providing a demountable vacuum tight seal.

In order to achieve good temperature uniformity of the sample chamber thin walled copper tubing (O. D. 2 3/8") is used. A .5" diameter Cu rod is threaded into the flange of the sample chamber using a little vacuum grease to provide good thermal contact and a copper tab is soldered to the bottom of this rod to provide a suitable soldering point for the weak thermal link.

The heat link from the sample mounting to the constant temperature bath is provided by a strip of brass (or other metal) of appropriate dimensions to give the required τ_1 for a given sample and method of measurement;

where $\tau_1 \approx C/k$ = Time constant for thermal relaxation to bath

and C = Heat capacity of sample plus addenda

$$k = \frac{\text{Thermal conductance of link} \times \text{cross sectional area}}{\text{Length}}$$

3.1.(iii) THE SAMPLE MOUNTING

The sample mounting is designed to have low thermal mass and to facilitate the ease with which the sample and the weak thermal link can be changed.

The mounting consists of two copper plates of 0.01" foil, one of

which is supported horizontally by soldering to the lower end of the heat link. This plate, on which the sample rests, is cut to provide two coils (which house the thermometers) and soldering tabs, - for the heat link and heat sinking rods for the thermometer leads.

The thermometers used are a nominal 100Ω , 1/10.Watt. Allen Bradley carbon resistance thermometer and a calibrated germanium thermometer from Cryocal. These are tightly enclosed in the copper coils with a small amount of vacuum grease to provide good thermal contact. Leads from the two thermometers are heat sunk to the sample temperature. The sample mounting is shown in Fig.(3.1.2.).

The sample heater, a thin film 1 KΩ heater is attached to a copper tab using Ge 7031 varnish and soldered to the second, upper,plate of the mounting. Radio Spares heat sink compound is used to provide the thermal contact between the sample and its mounting. To ensure that the same quantity of grease is used for each measurement a small quantity is measured from the nozzle of a syringe ($\approx$ 25 mgms) and then spread evenly over the mating surfaces. Firm pressure is applied to remove any trapped air and ensure good contact.

The total thermal mass of the addenda is found to be approximately equivalent to 3 gms of copper (see section 5 of this chapter).

3.1.(iv) HEAT SINKING OF WIRES

The wires taken from room temperature to the sample chamber are soldered to three ten-pin vacuum-tight connectors at the top of the pumping tube, and are taken down the pumping tube to the sample chamber. 30 gauge manganin wire is used, as a material with low thermal conductivity is required.

On reaching the sample chamber these wires are varnished to an

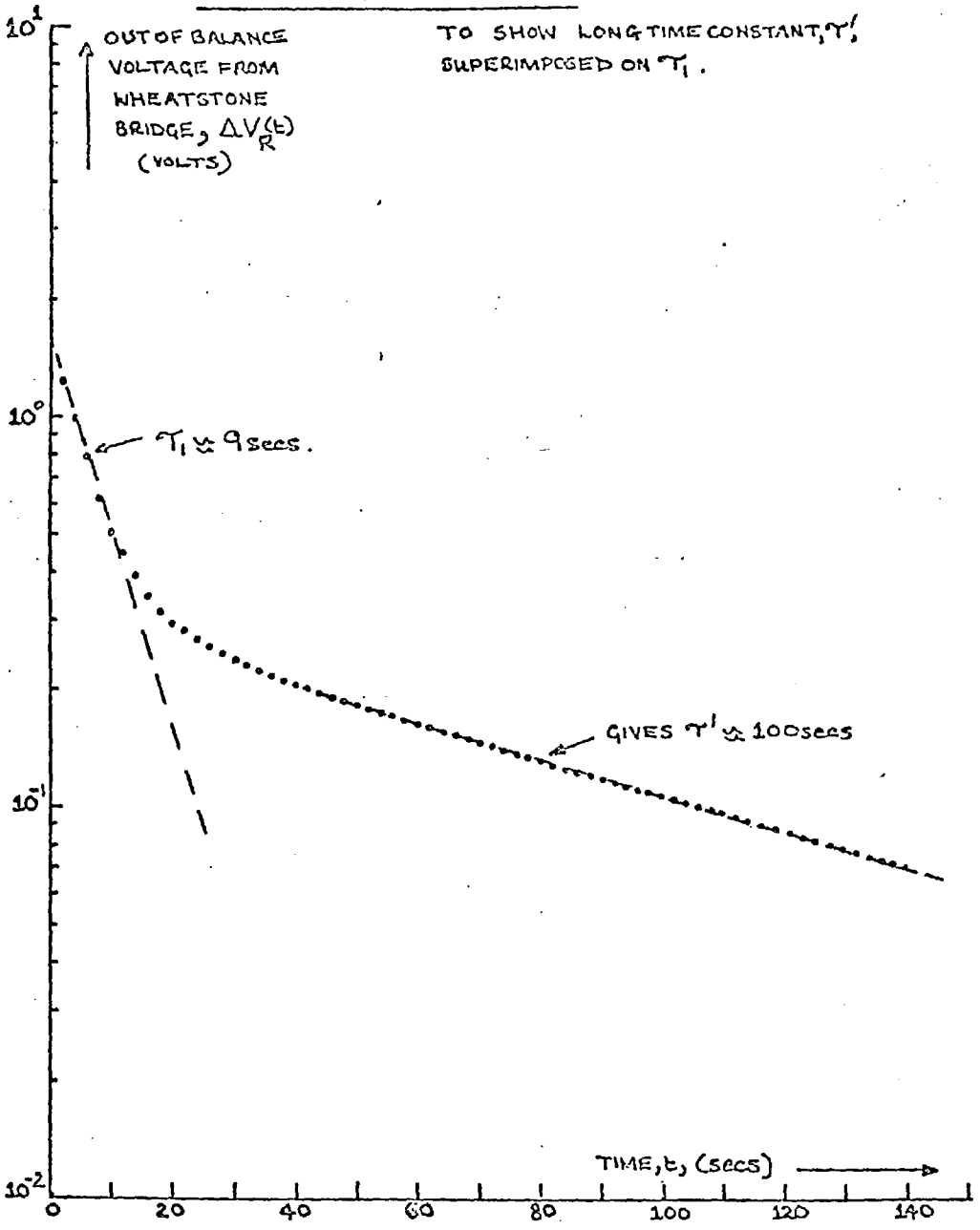
aluminium ring which is securely bolted and greased to the brass flange of the inner can to provide the initial low temperature heat sinking point. The same wires are further heat sunk by soldering to a pin board which is also bolted to the flange of the sample chamber.

In the initial form of this rig, 40 gauge manganin wires were taken from this pin board, directly to the thermometers and heater on the sample mounting. Problems were encountered with this arrangement in the form of an excessively long cool down time (approximately 4 hours from 77 K to 4.2 K after transferring liquid helium) and an additional very long time constant (of the order of 100 secs at 10 K) was found, superimposed on τ_1 ($\lesssim$ 10 secs) (see Fig.(3.1.3)) when analysing data using the step method.

Calculations showed the thermal diffusion times for these leads, which were about 10 cms. length, to be very long; and further calculations on the Joule heating effect in the current carrying leads showed that, at 10 K the centre of such a lead carrying 1 mA could heat up by as much as 20 K. The time to reach thermal equilibrium in this case would be of the order of 10^2 to 10^3 seconds.

To eliminate this problem it was decided that the length of unheat sunk wire should be reduced to about 1 cm. A further heat sinking post (see Fig.3.1.2) was therefore incorporated. Copper leads (38 g) are taken from the pin-board mentioned above to the second low temperature heat sinking post lying close to the sample mounting. 40 gauge manganin wires are then similarly heat sunk to this post before being taken to yet more heat sinking points on the actual sample mounting.

FIG(3.1.3) $\log \Delta V_R(t)$ VERSUS t



3.2 CIRCUITRY

(Block diagrams of the circuitry for both the step and a.c. methods are shown in Fig.3.2.1).

3.2.(i) HEATER POWER SUPPLY AND MEASURING CURCUIT

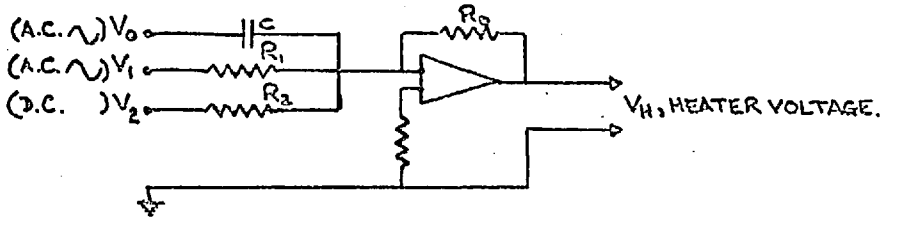
To facilitate the use of either the step or a.c. methods of measurement a heater power supply was designed which would allow either an a.c. and/or d.c. signal to be applied to the sample heater. (See Fig.(3.2.2)).

The 130K Dekastat incorporated in the circuit as a potential divider, is used to step the d.c. heater voltage up or down as required.

For the a.c. signal a Brookdeal signal source type 9471 is used to provide a sine wave of frequencies from approximately 1 Hz to .005 Hz and of r.m.s. amplitude 1 mV to 3.2 V. The signal may be a.c. only, or an a.c. signal superimposed on a d.c. signal. The a.c. component may be coupled capacitively or resistively to the operational amplifier.

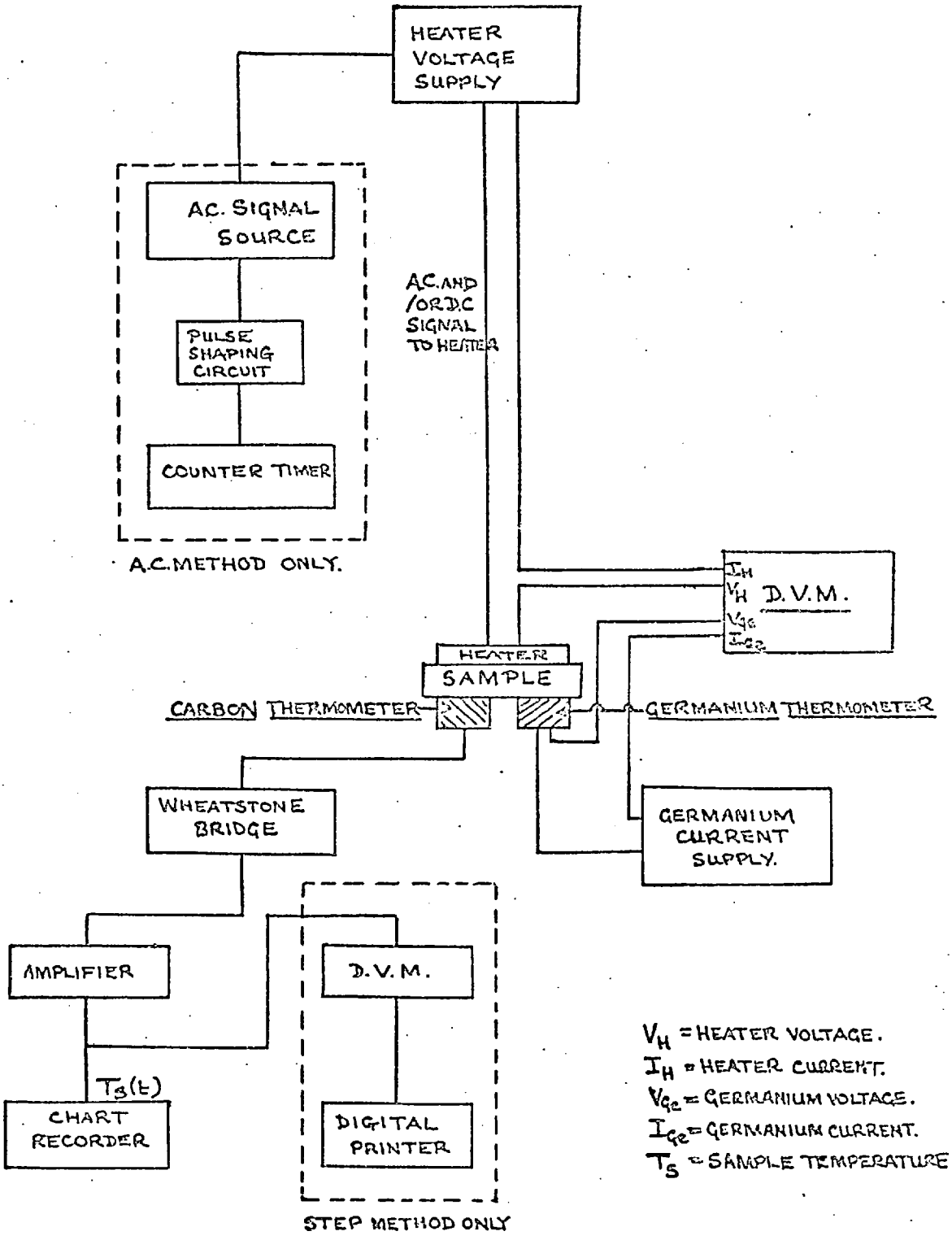
Appendix 1 explains the derivation of the output voltages and resulting temperature responses listed in Table (3.1) for the four possible singals input to the simplified form of the heater circuit shown below, and supplying heat to an isolated system,

FIGURE (3.2.3)



To determine the power dissipated by the heater a standard four terminal measurement technique is used, reading the voltage drop across the heater and across the standard 1K Ω resistor in the supply circuit, on a six figure D.V.M.

FIG(3.2.1) BLOCK DIAGRAM OF CIRCUITRY FOR SPECIFIC HEAT MEASUREMENT.



FIG(3.2.2) HEATER POWER SUPPLY.

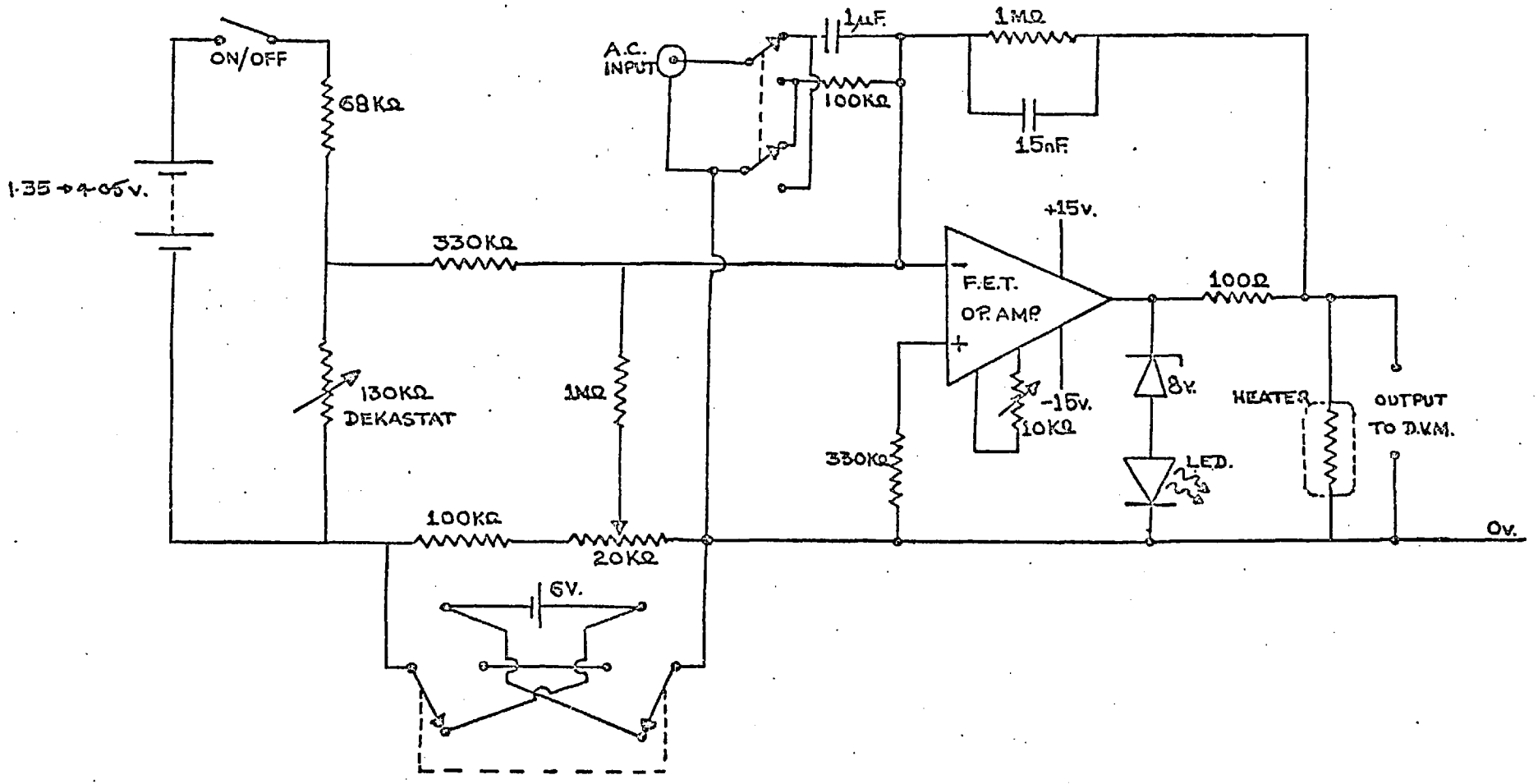


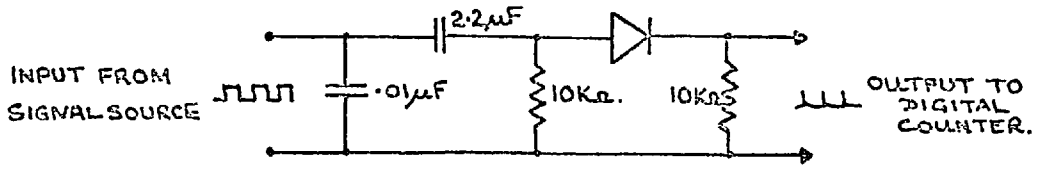
TABLE 3.1

Table to show the form of the temperature response in an isolated system for heater voltages V_H as obtained for four different signal inputs to the heater supply circuit shown in Fig.(3.2.3.)

Input Signal	Output Signal (V_H)	Resultant Temperature Response of Sample		
		D.C. Component	1st Harmonic component	2nd Harmonic component
A.C. Only Capacitively coupled $V_{AC} \cos \omega t$	$-\omega R_o C V_{AC} \sin \omega t$	$\frac{(R_o.C.\omega.V_{AC})^2 t}{2 C_s R_H}$		$\frac{(R_o.C.V_{AC})^2 \omega}{4 C_s R_H} \sin 2\omega t$
A.C. Only Resistively coupled $V_{AC} \cos \omega t$	$\frac{R_o}{R_1} V_{AC} \cos \omega t$	$\frac{(R_o.V_{AC})^2 t}{2.R_1^2.R_H C_s}$		$\frac{(R_o.V_{AC})^2}{4.R_1^2 R_H C_s \omega} \sin 2\omega t$
A.C. + D.C. A.C. Capacitively coupled. D.C. Resistively coupled. $V_{DC} + V_{AC} \cos \omega t$	$\frac{R_o}{R_2} V_{DC} - \omega R_o.C.V_{AC} \sin \omega t$	$\frac{(R_o.V_{DC})^2 t}{R_2^2 R_H C_s} + \frac{(R_o.C.\omega.V_{AC})^2 t}{2 R_H C_s}$	$\frac{2R_o^2.C.V_{DC} V_{AC}}{R_2 R_H C_s} \cos \omega t$	$-\frac{(R_o.C.V_{AC})^2 \omega}{4 R_H C_s} \sin 2\omega t$
A.C. + D.C. Both Resistively coupled. $V_{DC} + V_{AC} \cos \omega t$	$\frac{R_o}{R_2} V_{DC} + \frac{R_o}{R_1} V_{AC} \cos \omega t$	$\frac{(R_o V_{DC})^2 t}{R_2^2 R_H C_s} + \frac{(R_o V_{AC})^2 t}{2 R_1^2 R_H C_s}$	$\frac{2R_o^2 V_{DC} V_{AC}}{\omega R_1 R_2 R_H C_s} \sin \omega t$	$\frac{(R_o V_{AC})^2}{4 R_1^2 \omega R_H C_s} \sin 2\omega t$

The terms used are as defined in Appendix 1.

The time period of the applied a.c. signal is measured using an AMF Venner, digital counter, which is triggered by a pulse generated from a square wave output on the signal source via the pulse shaping circuit shown below.



3.2.(ii) GERMANIUM THERMOMETER CIRCUITRY

A standard d.c. constant current power supply is used for the germanium thermometer. To prevent Joule heating effects the currents given in Table 3.2 below are used in the quoted temperature ranges.

TABLE 3.2

Temp. Range (K)	Current (μA)	Approx. Ge. Resistance (Ω)
40 — 30	230	18 — 26
30 — 20	70	26 — 45
20 — 13	28	45 — 88
13 — 8	9	88 — 245
8 — 5	3	245 — 581
5 — 4.2	1	581 — 1010

The germanium resistance is determined by a standard four terminal measurement using a six figure D.V.M., the current being reversed for each measurement to eliminate thermal e.m.f's.

3.2.(iii) CARBON THERMOMETER CIRCUITRY

The resistance of the carbon thermometer is measured using a standard wheatstone bridge arrangement. The output from the bridge is then fed to a Bryan's 2700 chart recorder, via a high gain d.c. amplifier, which traces out the temperature response of the sample.

Fig. (3.2.4) shows the circuit diagram for the wheatstone bridge; the dummy leads in arm 2 of the bridge (which are leads taken down to the sample chamber of the same length and materials as those to the carbon thermometer) may be shorted out when initially zeroing the bridge using the same resistance settings on the variable resistances in each arm of the bridge.

The thermometer resistance may be read to $0.1\,\Omega$. using the variable resistance box (Dekastat D.S.1463, $12\,k\Omega$) in arm 2 of the bridge.

The d.c. amplifier consists of an Ancom 15C-3 with an intrinsic gain of 10^4 (but arranged to give variable gain). Since the response is linear only for output voltages of less than 5 V care must be taken to ensure that the input voltages from the wheatstone bridge are always less than $500\,\mu V$

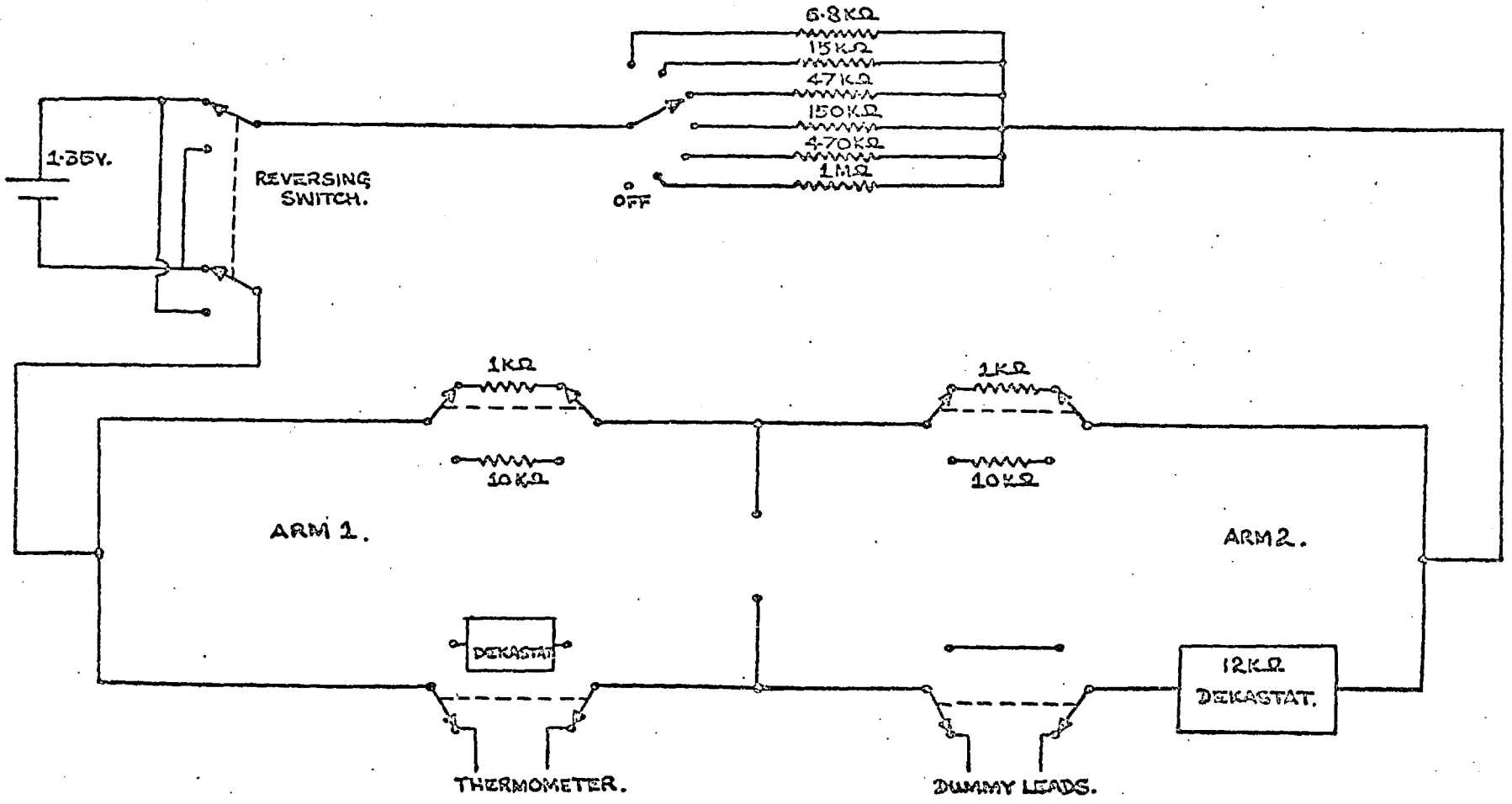
The gain adjustment is a potential divider on the output of the amplifier. The zero offset adjustment on the amplifier is time and temperature dependent and must be checked from time to time during use.

A variable time constant facility is incorporated in the amplifier circuit to reduce noise, the bandwidth is hence also variable. For the a.c. method we require that $2\omega RC < \cdot 1$ where $\omega = 2\pi/t_p$ and

t_p = time period of the applied heater voltage.

When using the step method the out of balance signal from the wheatstone bridge is printed out at suitable time intervals (compared to T_1) by an A.M.F. digital printer connected to the BCD output of a DVM. The time constant of the exponential temperature rise or fall may then be more accurately determined (from the out of balance voltage readings) than by measuring from the chart trace.

FIG (3.2.4.) WHEATSTONE BRIDGE CIRCUIT DIAGRAM.



3.3 THERMOMETRY

Germanium Thermometer

The thermometer was calibrated by Cryocal between 4.2 and 100 K at 46 points to a quoted accuracy of .1%. Interpolation of the calibration data was carried out by computer using a cubic spline routine. The difference between the calibration values and fitted values was found to be good to .1% throughout the calibration range.

This thermometer is used as a standard against which the carbon thermometer is calibrated (above 4.2 K) during each run.

Carbon Thermometer

(1/8th watt, nominal 100Ω , Allen Bradley).

It was not found possible to fit the behaviour of this thermometer over the complete range of temperature used (2 K to 35 K) using the usual three parameter equation due to Clement and Quinnell (31);-

$$\log_{10} R + \frac{K}{\log_{10} R} = A + \frac{B}{T} \qquad (3.1)$$

where R = Resistance of thermometer (Ω)

T = Temperature (^{o}K)

and A, B and K are constants.

With the A.C. method of measurement for heat capacity it is necessary to not only know the temperature accurately but also the sensitivity. In order to achieve 1% reproducibility in the sensitivity it is necessary to achieve .5% in the absolute temperature.

The carbon thermometer is calibrated during each experiment, below 4.2 K against the vapour pressure of He_4 , and above 4.2 against the calibrated germanium thermometer.

From 2 K to 4.2 K the thermometer is calibrated during the pump down.

The pressure, which is controlled by a manostat, is measured to 0.5 mm Hg.

Measuring the vapour pressure to 0.5 mm should give an accuracy of $\pm$ .5% in temperature at 2 K and of at least $\pm$ .1% at 3 K. However with the arrangement used (see Fig.(3.1.1)) temperature inhomogeneities in the liquid may make the recorded vapour pressure a poor indication of the true liquid temperature. From calibration data obtained on a copper sample, however, it appears that any uncertainties in the temperature or thermometer sensitivity lie well within the overall experimental error of the system.

The calibration data is fitted to the three parameter equation (3.1) and the constants A, B and K evaluated.

From 4.2 K to approximately 16 K the thermometer is calibrated against the germanium thermometer and again fitted to the above equation.

Temperatures calculated from resistance values using the above equation were found to be within $\pm$ .2% of the measured temperatures. Both temperatures and sensitivities were evaluated for given resistance values using a programmable Hewlett Packard (9820A) desk calculator.

Above 16 K no reasonable fit could be obtained to the above equation and a different method of calibration was adopted.

It was found that approximately linear plots could be obtained, for both thermometers, of the form :-

$$\log_{10}(R+W) = X + \frac{Y}{T} \qquad (3.2)$$

where W, X and Y are constants, and R is the thermometer resistance.

By evaluating the constants for each thermometer, a smooth function, (Z), of the carbon resistance (R_c), and germanium resistance (R_{Ge}) against temperature was obtained :-

$$Z(R_c, R_{Ge}) = [5 + \log_{10}(R_{Ge}+40) - 2.6\log_{10}(R_c+200)]10^3 \qquad (3.3)$$

Fig.(3.3.1) shows a typical plot of Z versus T.

For a given value of R_c, and estimated temperature, T' (estimated from previous data), the value of R_{Ge} may be evaluated from :-

$$\log_{10}(R_{Ge}+40) = [2.6\log_{10}(R_c+200) - 5 + Z.10^{-3}] \qquad (3.4)$$

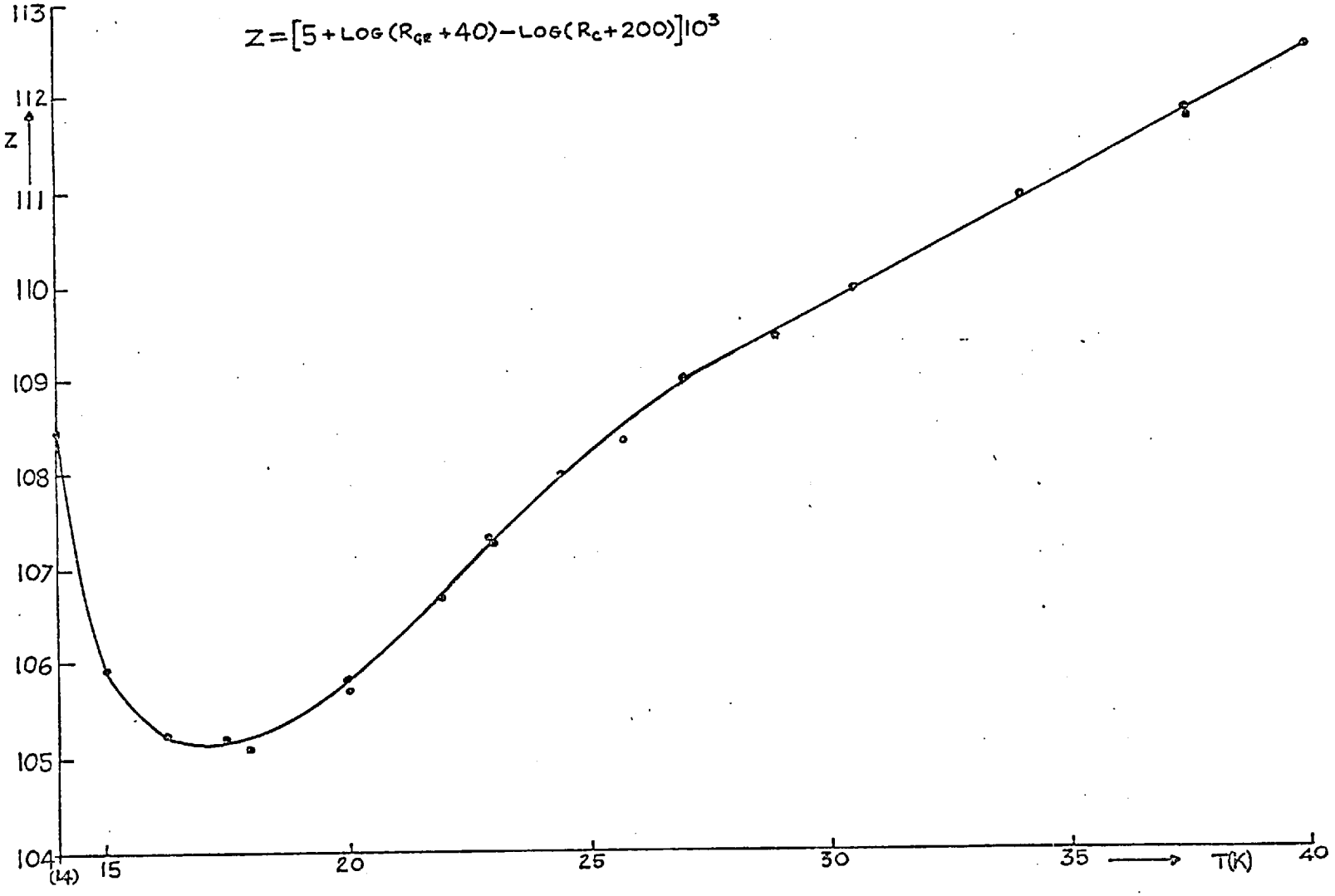
The temperature, T_{Ge}, may then be found from the germanium calibration and the sensitivity of the carbon thermometer at T_{Ge} is given by:-

$$\left(\frac{dT}{dR_c}\right)_{T_{Ge}} = -\left[\frac{1}{2.6}\left(\frac{dR_{Ge}}{dT}\right)\left(\frac{R_c+200}{R_{Ge}+40}\right) + \frac{2.303.10^{-3}(R_c+200)}{2.6}\left(\frac{dZ}{dT}\right)_{T_{Ge}}\right]^{-1} \qquad (3.5)$$

Using this technique for temperature evaluation at the higher temperatures one is relying on an estimation of temperature from the carbon resistance using a previous calibration. The maximum shift in the calibration data from any one run to the next was found to correspond to a change of $1\,\Omega$ in R_c. At 30 K this corresponds to a temperature change of approximately .5 K. It is found that an error of $\pm$ 0.5 K in the estimated temperature T' at 30 K gives a resultant error in temperature of less than .1% and in dT/dR_c of less than .2%.

A comparison of the overlap regions for the three different calibrations used for any given experiment shows the temperatures to agree to within $\pm$ .5% for extrapolated values up to 1^{o}K beyond the range of a given fit. Comparing the calibration data for a given temperature range for different runs shows the temperatures to agree to within $\pm$ 0.5 %.

FIG. (3.3.1)


Z=[5+LOG(R_GE+40)−LOG(R_C+200)]10^3
113
112
111
110
109
108
107
106
105
104
Z
15
20
25
30
35
40
T(K)

3.4 EXPERIMENTAL PROCEDURE

An estimate of the heat capacity of the sample plus addenda must be made in order to choose a suitable thermal link, to give appropriate values of τ_1 (the sample to bath thermal relaxation time) for the method to be used.

For the step method the minimum value of τ_1 that can be accurately measured is about 5 seconds, one therefore requires that at the minimum temperature of measurement, $T_{min} :- \tau_1(T_{min}) \simeq \frac{C(T_{min}).\ell}{K(T_{min})A} \geq 5secs.$ where K is the thermal conductance of the link, ℓ its length and A is cross-sectional area.

This also provides a suitable guideline for the a.c. method where at the lowest temperatures we have the condition $t_p \leq 2\tau_1$ (see Chap.II, section (3.(ii)). A lower limit is set on t_p (apart from the previously stipulated condition of $t_p > 25 t_{p_{1/2}}$ due to the internal thermal time constants of the system (Chapter II, Section (3)), by the response time of the circuitry . The shortest time period for the input singal that may be used is 2 secs., which gives a time period for the thermometer response of 1 sec.

The link and sample are mounted as described in section (1.3) of this chapter and the can sealed using an indium 'O'-ring. After checking the circuitry, evacuating and leak testing the system the nitrogen space is filled and the cryostat left to cool down to 77 K overnight, before transferring liquid helium (three and a half litres of liquid helium are adequate for at least twelve hours measurements).

3.4.(i) EXPERIMENTAL PROCEDURE FOR STEP METHOD

As shown in Chapter II, Section (3.1) the defining relation for the step method is, $C(T) = k(T)\tau_1$; for each data point therefore, accurate measurement is required of T, τ_1 , and $k(T) = \Delta P/\Delta T$, where ΔT is the temperature change for a change in heater power of ΔP.

The absolute temperature is measured at the beginning (temperature T_1) and end (temperature T_o) of each data point, by measuring the carbon resistance on the wheatstone bridge. The change in temperature is given by $\Delta T = T_1 - T_o$, and the mean temperature, $\bar{T} = (T_o + T_1)/2$, is defined as the absolute temperature of measurement.

When for a given heater voltage, V_1, the temperature, T_1, is seen from the trace on the chart recorder to be steady, then V_1 is reduced to V_o (let this be at time $t = 0$). The exponential response of the sample temperature is monitored on the chart recorder and the out of balance signal from the bridge ($V_R(t)$) is simultaneously printed out every (δt) secs. (where $\delta t \lesssim \tau_1/10$).

The change in power input, $\Delta P = (V_1^2 - V_o^2)/R_H$ must be such as to give a temperature change:- $\Delta T \lesssim .01\,\bar{T}$.

The condition used to ensure that the system has reached the steady state (i.e. that there is no further change in T with time) is that $T = T_o$ after time $t = 7 \times \tau_1$.

The time constant, τ_1, may then be evaluated from the expression derived in Chapter II, Section (3);

$$\Delta T(t) = \Delta T_{t=0} \exp(-t/\tau_1)$$

or in terms of the voltage readings from the printer :

$$\Delta V_R(t) = \Delta V_{R(t=0)} \exp(-t/\tau_1)$$

A graph of $\ln.(\Delta V_R(t))$ against time therefore gives a straight line of gradient $(-1/\tau_1)$.

The thermal conductivity of weak thermal link, (k), is read from the smoothed curve of $(\Delta P/\Delta T)$ versus T plotted from values taken at each data point.

The main problem encountered with this method was in the evaluation

of τ_1 . A drift in the baseline (i.e. of T_o) corresponding to only 1 mK/ minute at 7K was found to introduce a 6% uncertainty in τ_1 .

3.4.(ii) EXPERIMENTAL PROCEDURE FOR A.C. TECHNIQUE

For a sample heated at a rate $(V_1^2/R_H)(\cos\omega t)^2$ the heat capacity may be evaluated to 1% by the expression :-

$$C(T) = V_1^2 t_p / 8\pi R_H |T_2| \qquad \text{(See Chapter II, Sect.(3))}$$

provided the conditions stipulated in Chapter II, Sect.(3) are obeyed.

T, $|T_2|$, V_1 R_H and t_p must therefore all be accurately measured. V_1 and t_p are measured as described in section (2) of this chapter, and R_H is 1000Ω to .3% throughout the temperature range of measurement. The absolute temperature for each data point is evaluated from the null point carbon resistance reading on the wheatstone bridge.

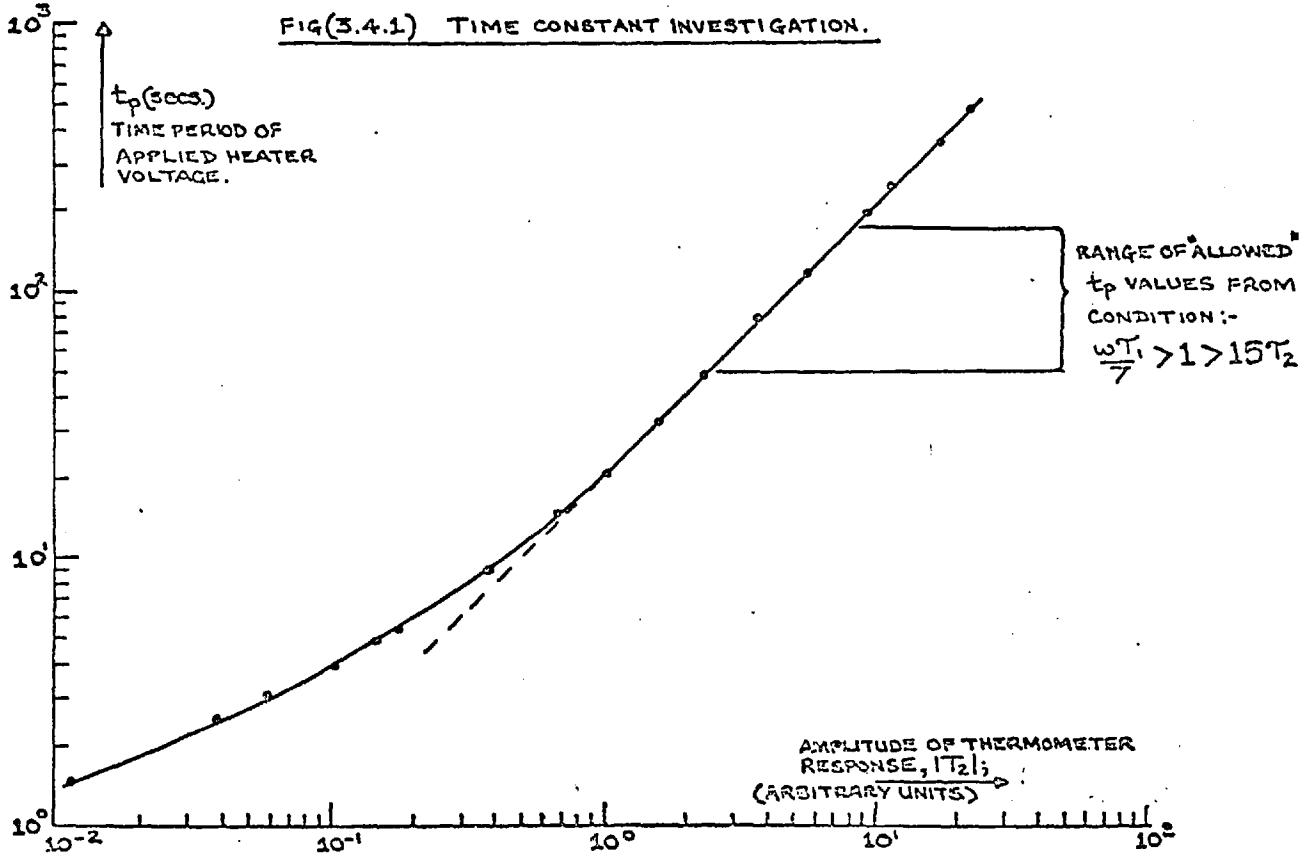
In order to ensure that "allowed" values of ω are used; τ_1 and τ_2, the internal time constant of the system, must be known.

Hence the initial stage of an experiment on a new sample involves an investigation of τ_1 and τ_2 . The step technique is used to evaluate τ_1 , and a capacitively coupled (AC + DC) voltage signal used to evaluate τ_2 (or rather $t_{p\,1/2} = 3.6\tau_2$) as described in Chapter II . By applying the conditions evaluated in Chapter II, Section (3) one thus has a definite guideline for the allowed values of ω .

Data is taken at three different frequencies for each temperature and provided the frequencies lie within the limitations stated, then (from Eqn.(2.3)) a plot of $|T_2|$ versus t_p gives a straight line with zero intercept.

Fig.(3.4.1) shows a plot of t_p versus $|T_2|$ for values of t_p from 500 secs. to 1.5 secs. The time constant investigation for the system

FIG(3.4.1) TIME CONSTANT INVESTIGATION.



gave the range of allowed time periods as 170 secs. to 45 secs. The graph shows that these frequencies do indeed lie well within the region of good linearity.

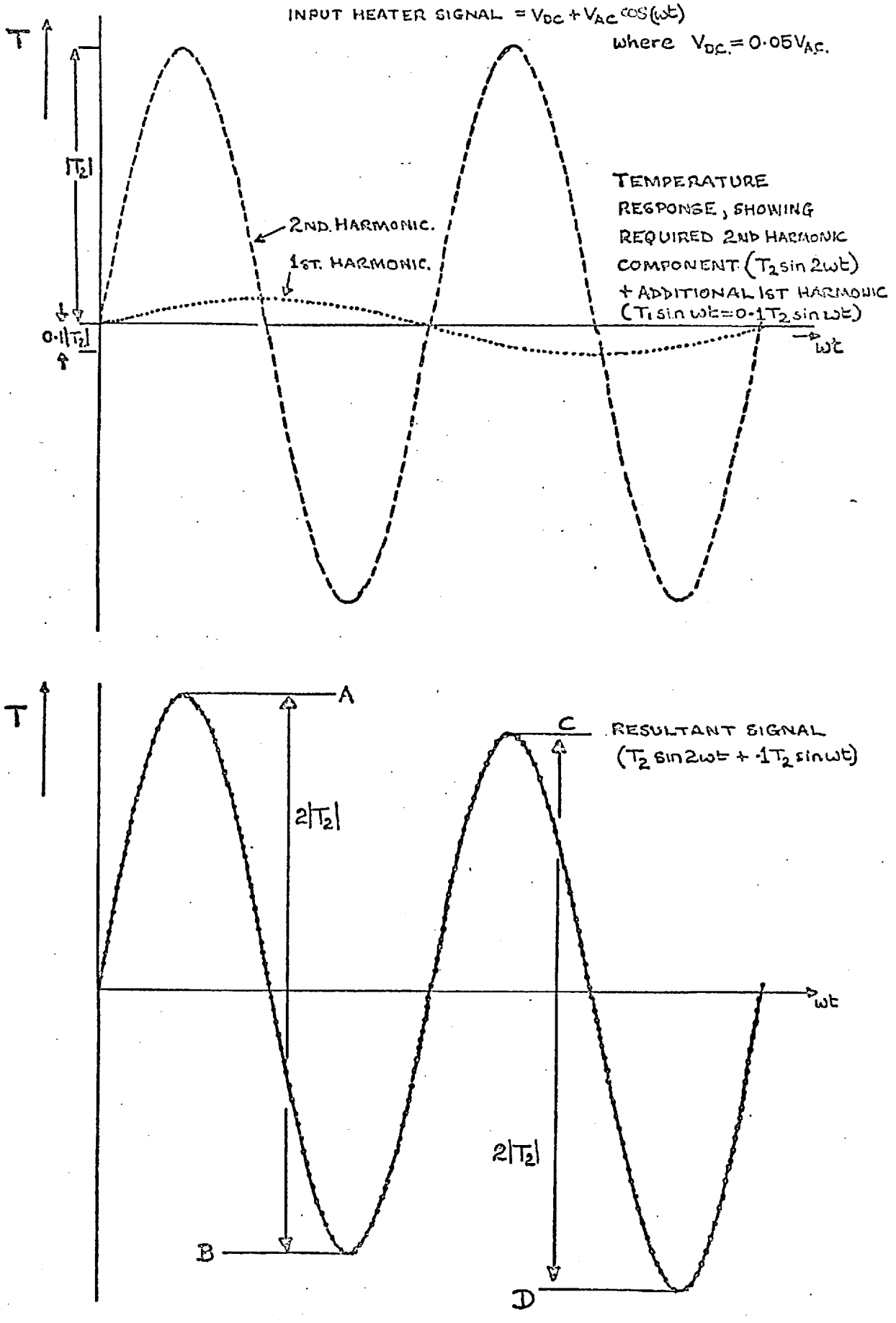
The sinusoidal form of the temperature response is traced by the chart recorder and the peak to peak amplitude (proportional to $2 \times |T_2|$) is measured from the chart paper. These traces of $|T_2|$ are found to be assymetric, due to a small d.c. level in the a.c. signal from the signal source. Hence, rather than the purely second harmonic response which would be expected from an a.c. signal only, resistively coupled to the operational amplifier (as given in Table (3.1)) there is an additional first harmonic component.

The presence of this first harmonic component results in a phase shift in the resultant compared to the second harmonic. For the maximum d.c. level observed, of $.05\ V_{AC}$ this phase shift is only of the order of 4^{o}. The resulting change in amplitude is found to be of the order of 4% and may be accounted for in the measuring procedure. Fig.(3.4.2) shows the two components and their resultant, in order to measure the true amplitude (i.e. the 2nd harmonic) peak to peak measurements are taken as shown in the diagram from A to B or C to D.

If the peak to peak amplitude as measured from the chart paper is Y cms, then a graph of Y versus t_p gives a straight line of gradient $\propto$ cms/sec.

By switching from the sample thermometer to the variable resistance box in arm (1) of the bridge and changing the resistance of one of the variable resistances by a known amount the chart paper may be calibrated to give $X\,\Omega$/cm. Then the heat capacity is evaluated from; $C(T) = V_{AC}^2 / (4\pi \propto X R_H \cdot dT/dR|_T)$ where $dT/dR\big|_T$ is evaluated as described in section 3 of this chapter.

FIG(3.4.2.) DIAGRAM TO SHOW RESULANT TEMPERATURE RESPONSE DUE TO A SMALL D.C. LEVEL SUPERIMPOSED ON, THE MAIN, A.C. INPUT HEATER VOLTAGE.



3.5.(i) THE HEAT CAPACITY OF THE ADDENDA

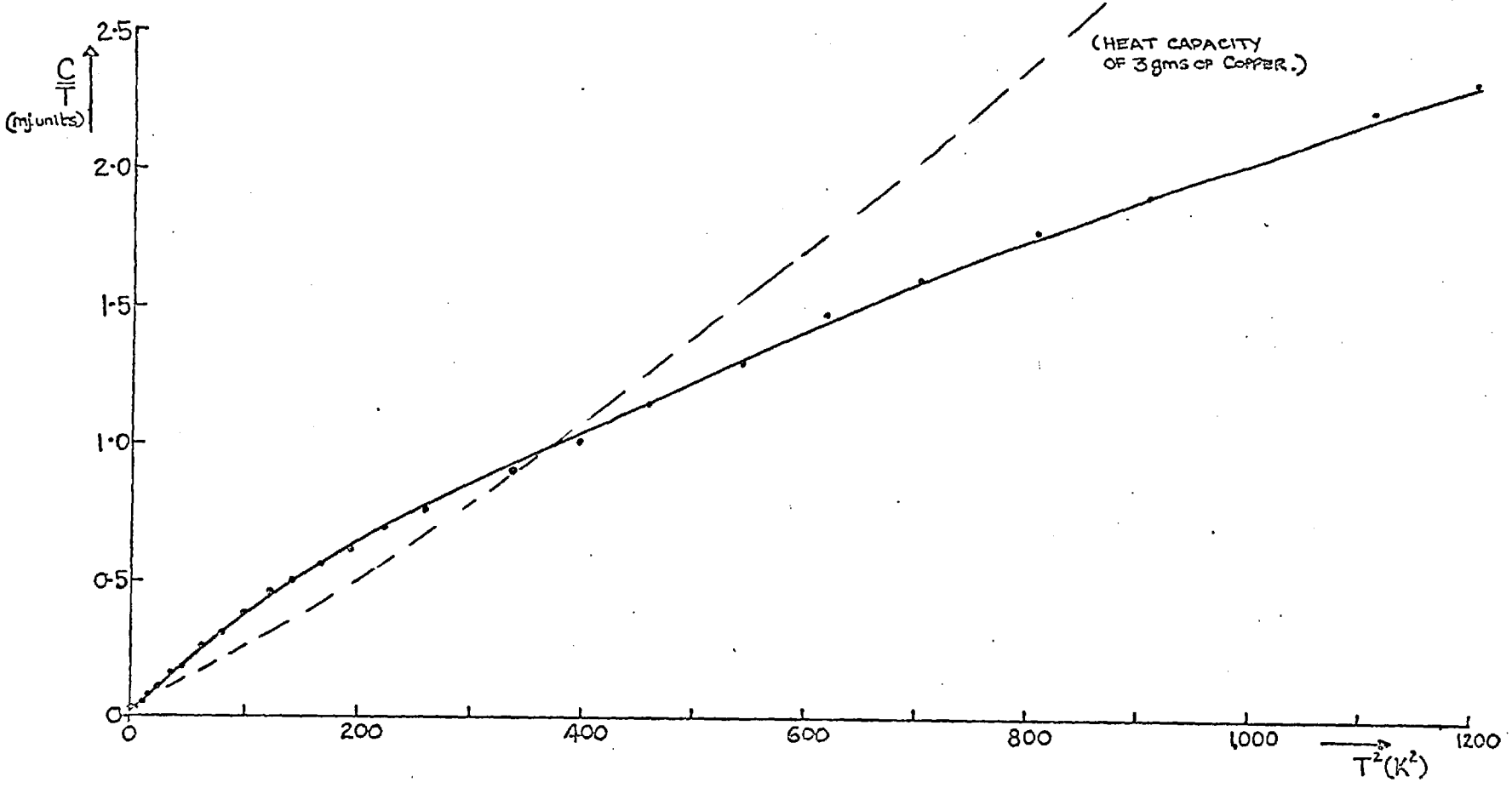
In measuring specific heat one necessarily measures the heat capacity of the sample plus addenda. The latter must therefore be measured in a separate experiment.

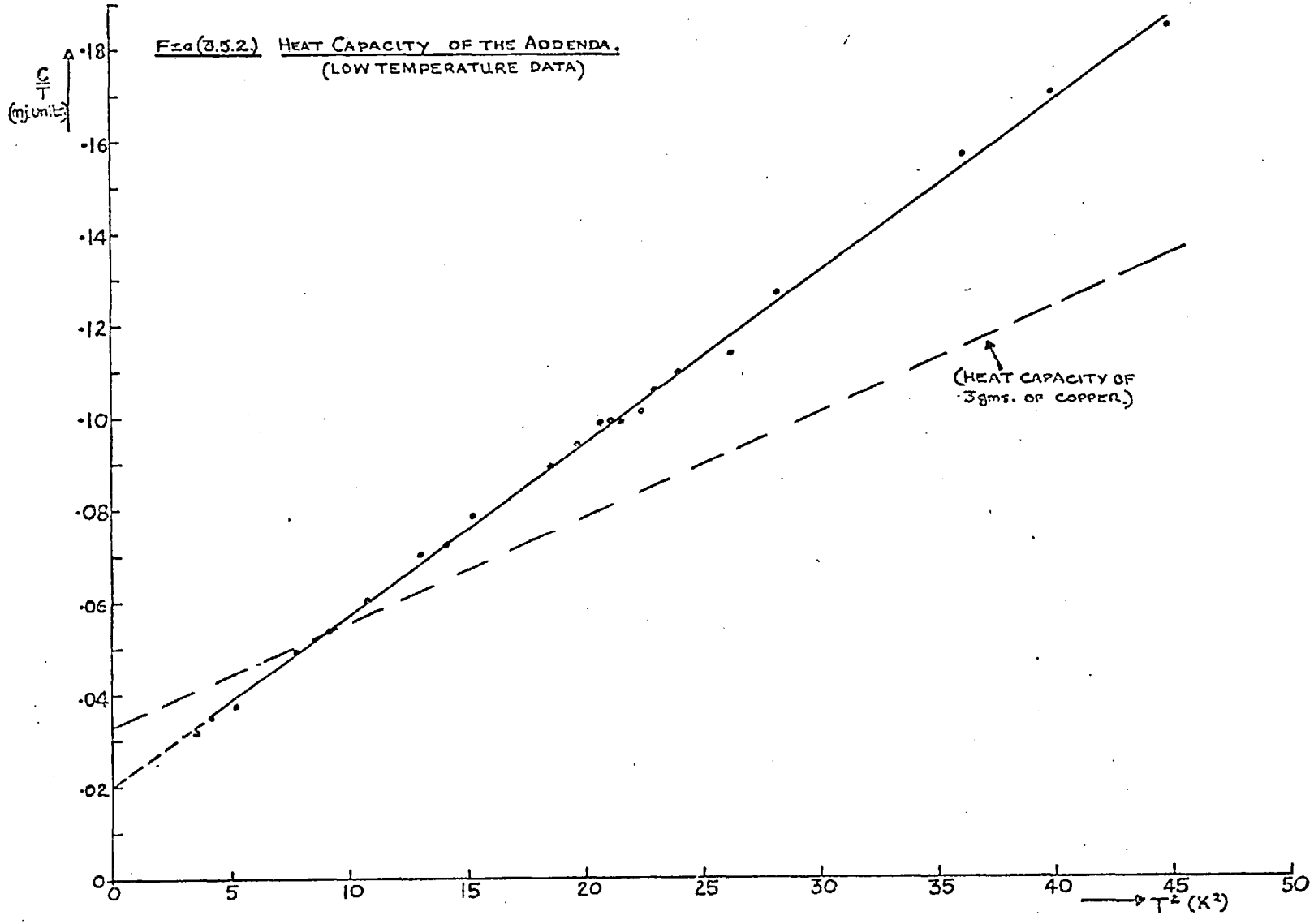
For the arrangement described the addenda consists of approximately one gram of copper, the heater, two thermometers, heat sink compound etc. and was estimated to have a thermal mass approximately equivalent to three grammes of copper. The results of the measurement of the addenda alone are presented in Figs. (3.5.1 and 3.5.2) and are compared to the heat capacity of three grammes of copper.

3.5.(ii) CALIBRATION OF THE APPARATUS

The error on the measurement of C(T) is estimated at $\pm$ 4% and to check the accuracy of the apparatus measurements were made on a sample of pure copper (mass 4 gms.). The uncertainty in measurement is increased at the high temperature end of the data due to the reduced sensitivity of the thermometry. The results on copper are presented in Figs.(3.5.3) and (3.5.4) compared to those of Holste (32). The value of the coefficient of the electronic term (γ) disagrees with Holste's value by 8% and the coefficient of the lattice term (β) disagrees by 6%.

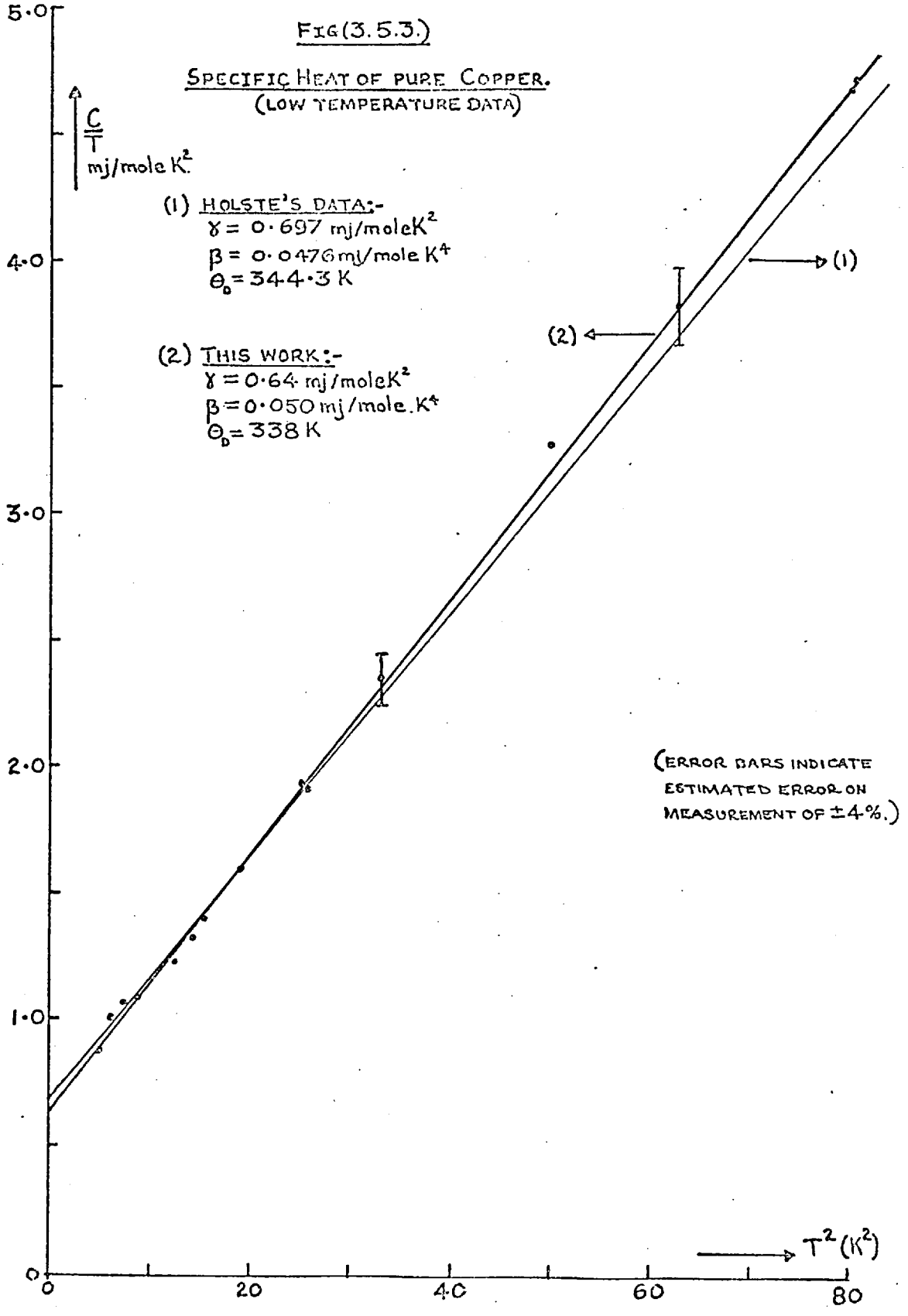
FIG(3.5.1) HEAT CAPACITY OF THE ADDENDA.

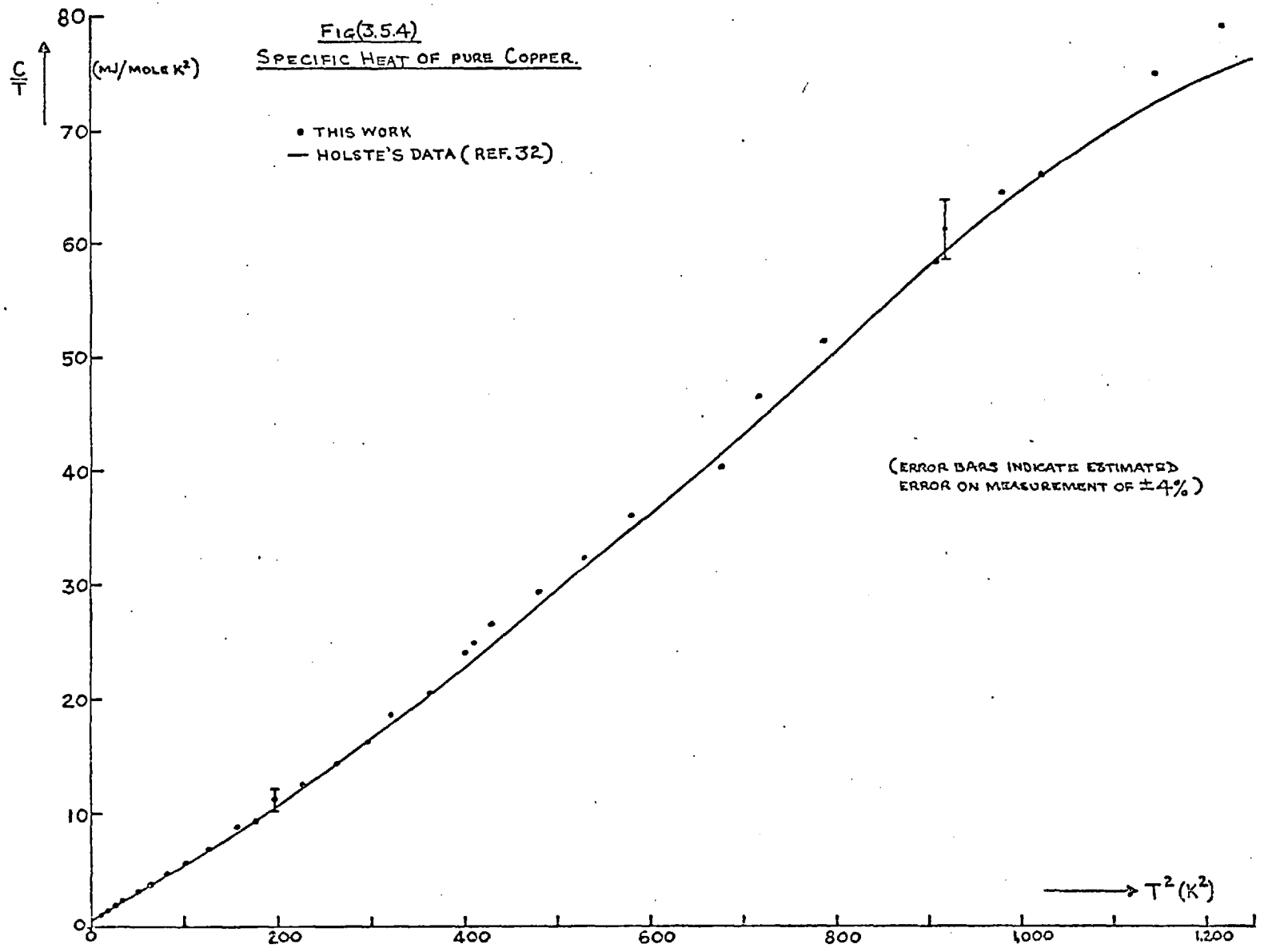



Fig (3.5.2.) HEAT CAPACITY OF THE ADDENDA.
(LOW TEMPERATURE DATA)
C/T (mj/unit)
·18
·16
·14
·12
·10
·08
·06
·04
·02
0
0
5
10
15
20
25
30
35
40
45
50
T² (K²)
(HEAT CAPACITY OF 3gms. OF COPPER.)

FIG(3.5.3.)

SPECIFIC HEAT OF PURE COPPER.
(LOW TEMPERATURE DATA)





FIG(3.5.4)
SPECIFIC HEAT OF PURE COPPER.

CHAPTER IV

PREVIOUS WORK ON $Al_{10}V$

4.1 INTRODUCTION

In their paper entitled "Properties of aluminium rich, aluminium transition metal phases" (7), Dunlop, Grüner and Caplin report the results of low temperature measurements of the specific heat and of some magnetic and transport properties of nine aluminium compounds involving the 3-d transition elements (T3). For all except the three Al-V compounds (Al_3V, Al_7V and $Al_{10}V$) the specific heat and electrical resistivity data suggest a V.B.S. model for the d electrons having a width of about 2 eV.

Previously (6) the same authors used the V.B.S. description in their work on the compounds $Zn_{13}Mn$, $Zn_{13}Fe$ and $Zn_{13}Co$. The experimental evidence on the Al-T3 compounds however, forces consideration of questions of charge transfer and bonding that were absent fromthe zinc based ξ phases. The Al-V compounds were found to be anomalous in every respect, perhaps because of the particular importance of bonding effects.

The crystal structures of the Al-T3 compounds are usually complex and based on large unit cells, and in most cases (except Al_7V and Al_7Cr) the T3 atoms are separated from each other by Al atoms. Many compounds have anomalously short Al-T3 distances in the first coordination shell of T3 atoms, whilst for all except the Al-V compounds the Al-Al distances are similar to those in metallic aluminium.

4.1.(i) CHARGE TRANSFER AND BONDING IN THE Al-T3 COMPOUNDS

Consideration has been given to the particular question of bonding in the Al-transition metal compounds for many years.

Raynor (1949 (33)) noted the steady decrease in aluminium content

down the series of Al-T3 compounds from vanadium to nickel and suggested the d-shells on the T3 atoms to be completely filled by charge transfer. This gives an approximately constant number of conduction electrons per atom for all the compounds. Hence, Raynor's view was one of electron compounds in which the overall electron to atom ratio is the controlling factor determining the crystal structure.

However, in contrast to this picture, the specific heat and electrical resistivity results of Dunlop et al (7), show a definite additional contribution to the density of states at the Fermi level consistant with a V.B.S. picture in which the number of d electrons rises steadily along the T3 series. Measurements by Taylor (34) show these compounds to have a small, weakly temperature dependent magnetic susceptibility, but no well defined magnetic moment on the T3 atoms. The absence of a well defined magnetic moment is consistant with non-magnetic part filled d shells rather than the full d shells suggested by Raynor.

Pauling (35) considered the anomalously short Al-T3 distances to be indicative of covalent bonding in these compounds. The absence of a magnetic moment would follow naturally from the pairing of spins on this model, where T3 d electrons would be involved in covalent bonding with the surrounding aluminium atoms. However, this would give no d-like contribution to the specific heat.

Neither viewpoint gives the whole truth, both charge transfer and bonding must be considered in dealing with these compounds.

Evidence from soft X-ray spectroscopy by Wenger, Bürri and Steinemann (36) indicates that charge transfers of the order of one electron or less do occur in the Al-T3 series of compounds. Figure (4.1.1) below shows $\Delta n_d = n_d - n_d'$ where n_d and n_d' are the number of

d electrons per T3 atom in the intermetallic compound and pure metal respectively. In the first half of the series the d shell tends to empty slightly and in the second half to fill slightly.

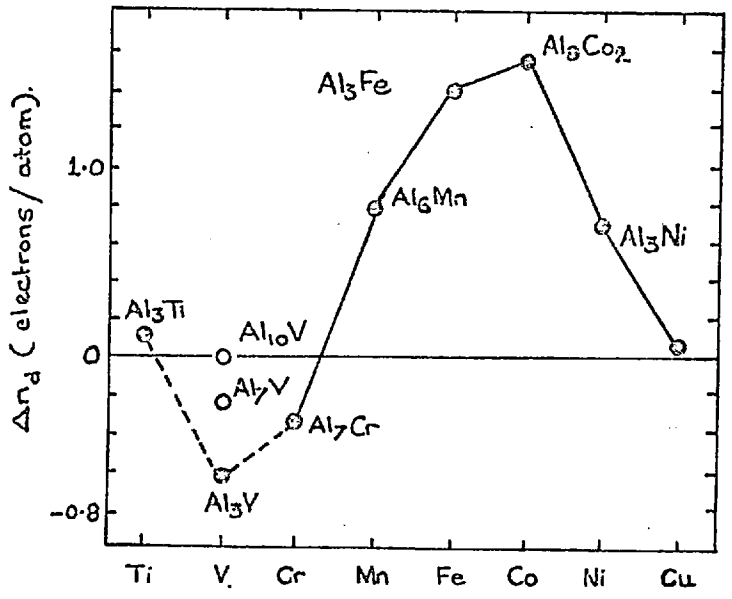


FIGURE (4.1.1)

Electron transfer onto the T3 atom in the most dilute Al-T3 compounds relative to the pure T3 metal (After Ref.(36)).

In every case except the Al-V compounds the magnitude of the charge transfer increases with increasing aluminium content.

4.1(ii) THE ALUMINIUM-VANADIUM COMPOUNDS

The V.B.S. approach used by Dunlop et al, which gave an adequate description of the electronic specific heat and electrical resistivity of the other Al-T3 compounds, is inappropriate for the Al-V compounds. The structural evidence shows that directional bonding must be important and the large specific heat indicates the V.B.S. model to be unsuitable. Not only are the Al-T3 distances unusually short in these compounds, but simultaneously there are anomalously long Al-Al distances elsewhere in the unit cell. In the particular case of $Al_{10}V$ there is one site where the aluminium atom, (if present), is virtually uncoupled from the rest of the structure.

The electronic specific heat of all the Al-V compounds lies

above the general trend across the T3 series, as shown in Fig.(4.1.2) below.

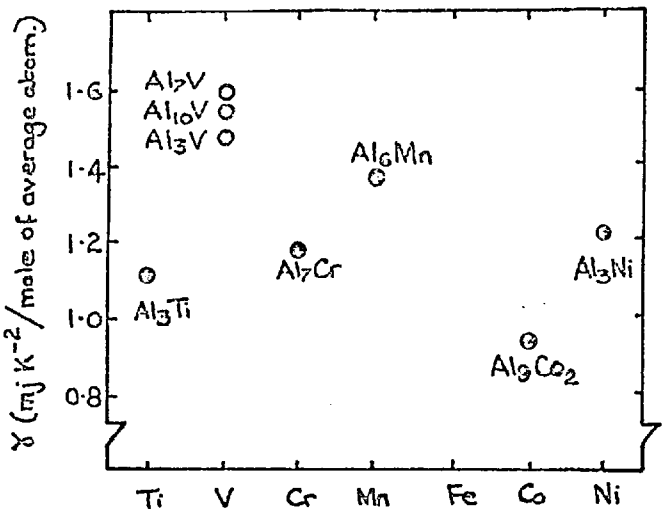


FIGURE (4.1.2)

The electronic specific heat coefficient (γ) for the most dilute Al-T3 compounds.

The electrical resistivities of the Al-V compounds also exemplifies their unusual behaviour. In Al_3V and Al_7V a well defined T^2 behaviour is observed below 20 K (probably indicative of an electron-electron scattering mechanism (see Baber scattering, Ref.(37)) rather than one involving phonons) as compared to the T^4 behaviour found in the other Al-T3 compounds. In $Al_{10}V$ however the low temperature resistivity is found to be dominated by scattering from the loose atom.

It is the extremely unusual behaviour of $Al_{10}V$, that has prompted the investigations described in this work. In section (2.2) of this chapter the specific heat and resistivity data of Caplin et al (38) are reported in further detail and it is seen that their results are reasonably well fitted by an Einstein model.

4.2.(i) THE STRUCTURE OF $Al_{10}V$

Early work by Carlson, Kenney and Wilhelm (39) on the V-Al system showed the existance of three peritectic phases α , β , and γ , on the

aluminium rich end of the phase (see phase diagram, Chapter V.1). The most Al-rich of these phases, α , was found to have space group Fd 3m and was given the formula V Al_{11}. The structure of this phase was determined by P.J. Brown (40) from single crystal X-ray data by a comparison of a complete rotation photograph about [001], with a similar photograph of the compound $Mg_3 Cr_2 Al_{18}$ (structure given by Samson (1954)). The two were found to be almost identical and the α (V Al) to have space group symmetry O_h^7 - Fd 3m. with vanadium atoms in the 16(c) positions and aluminium atoms in the 96(g), 48(f) and 16(d) positions. The most interesting feature of the structure is the large volume available at the 8(b) positions. Brown's investigations showed that 10% or less of the 8(b) sites were occupied by Al atoms, whereas later work by Ray and Smith (41) indicated that their crystals had approximately 50% occupancy of the 8(b) sites. It was inferred that the composition ranges from $Al_{10}V$ to $Al_{10.5}V$ across the phase.

The cubic unit cell of $Al_{10}V$ is found to contain sixteen formula units (160 Al, and 16 V atoms) and the lattice parameter, a, was found to be 14.492 Å for Brown's sample and 14.516 Å for Ray and Smith's, the difference being due to the difference in the Al occupancy of the 8(b) positions.

Each vanadium atom is surrounded by six Al_1 and six Al_2 neighbours in nearly regular icosahedra (where Al_1 and Al_2 indicate the lattice sites as given in Table (4.1) below). The icosahedra are linked in the [110] direction sharing Al_2 atoms. Fig.(4.2.1) below shows four icosahedra linked in this way.

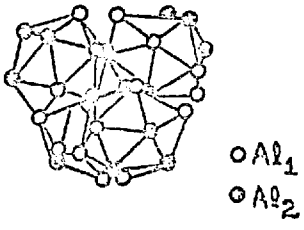


FIGURE (4.2.1)

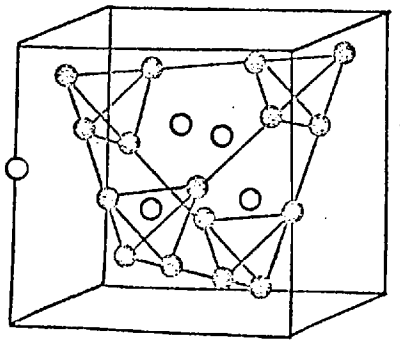
The Vanadium atoms are at the centre of the icosehedra which are drawn as though solid. (After Ref.(40)).

TABLE (4.1)

Atoms	Sites
Al_1	96 (g)
Al_2	48 (f)
Al_3	6 (d)
V	16 (c)
"Hole"	8 (b)

The next diagram (4.2.2) shows how four of these groupsare arranged in the unit cell to form a tetrahedral framework. The Al_3 atoms occupy the midpoints of the faces of the tetrahedra and the empty 8(b) position is at the centre. (Aluminium atoms in contact with vanadium atoms are omitted).

FIGURE (4.2.2)



The interatomic distances are listed below (in Table (4.2)); there it is seen that each vanadium atom has twelve neighbours, six of which are at a distance of 2.57 Å, this is considerably shorter than the sum of the twelve coordinated radii for vanadium and aluminium, of 2.77 Å.

TABLE (4.2)	Interatomic Distances (Å)
V . . . . . 6 Al_1	2.826
. . . . . 6 Al_2	2.572
Al_3 . . . .12 Al_1	3.083
Al_1 . . . . 2 Al_1	2.943
. . . . . 2 Al_1	2.740
. . . . . 1 Al_1	2.679
. . . . . 2 Al_2	2.880
. . . . . 1 Al_2	2.679
. . . . . 2 Al_3	3.083
. . . . . 1 V	2.826
Al_2 . . . . . 4 Al_2	2.882
. . . . . 2 Al_1	2.676
. . . . . 4 Al_1	2.880
. . . . . 2 V	2.572
"Hole" . . .12 Al_1	3.181
. . . . . 4 Al_3	3.137

Similar contractions have been found in other aluminium-rich transition metal compounds and are thought possibly to be due to electron transfer to the transition metal atom. There is no direct evidence for this in $Al_{10}V$. (see Fig.(4.1.1.)).

The mean distance between Al atoms in contact with vanadium is about 2.8 Å which is normal for this type of compound. The Al_3 atom which has no V neighbours has twelve aluminium neighbours at 3.08 Å, and for an aluminium atom at the 8(b) site there would be sixteen neighbours at unusually large distances, 12 Al_1 at 3.181 Å and 4 Al_3 at 3.137 Å.

Due to the loose packing of atoms which are not in contact with vanadium atoms the average atomic volume of this structure is very large; 17 $Å^3$ per atom, as compared to 15.1 $Å^3$ for Al_9Co_2, 15.5 $Å^3$ for Al_6Mn and 16.4 $Å^3$ for pure aluminium. Brown concludes that it is a strong Al-V interaction giving rise to the framework of linked icosahedra which is important in the formation of this structure.

Aluminium atoms in sites not in contact with vanadium atoms cannot take part in this interaction, and are either dropped out or show an abnormally large radius.

4.2.(ii) PREVIOUS WORK ON $Al_{10}V$

Low temperature measurements of the specific heat and electrical resistivity of $Al_{10}V$ reported by Caplin et al (38) indicate the existance of a local soft mode in $Al_{10}V$, with a characteristic temperature of about 22 K. They associate this local mode with the presence of loosely bound aluminium atoms on the 8(b) site described above. The results are well described by an Einstein model (42).

(a) SPECIFIC HEAT

Measurements on two different samples are reported, both show the same functional temperature dependence in their vibrational specific heats, but one is 15% smaller in magnitude.

The heat capacity was measured from 2 to 4.5 K and the results for one of the samples are shown in Fig.(4.2.3) below, compared to those for

$Al_9 Co_2$, a typical Al-T3 compound.

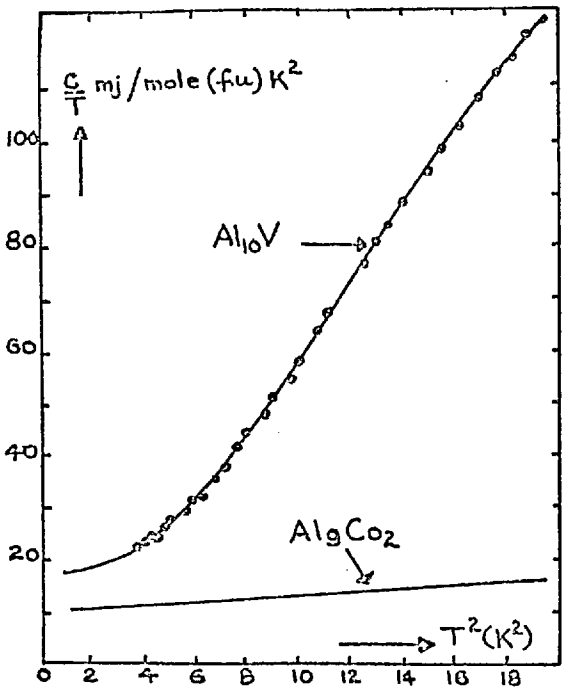


FIGURE (4.2.3)

The specific heat of $Al_{10}V$ as compared to that of Al_9Co_2 (After Ref. (38)).

The very rapid increase with temperature is indicative of a very low lying vibrational mode; and the data is reported to be well fitted by the Einstein formula for specific heat (C_{EIN}) (See Chapter I, section 1(iii)).

That is :- $C = C_{EIN} + \gamma T$

where $$C_{EIN} = 3 N_o N_\ell k_B \left(\frac{\Theta_E}{T}\right)^2 \left(\frac{\exp(\Theta_E/T)}{\exp(\Theta_E/T)-1}\right)^2 \qquad (4.1)$$

with an Einstein temperature $\Theta_E = 22 \pm 2K$ and a density of local (3-dimensional) oscillators N_ℓ, equivalent to $.11 \pm .03$ per $Al_{10}V$ formula unit.

(b) ELECTRICAL RESISTIVITY

In the same paper measurements of the electrical resistivity are also reported. The form of the resistivity is immediately seen to be unusual in both magnitude and shape when compared to that for $Al_9 Co_2$ (see Fig.(4.2.4) at

the end of this chapter).

The resistivity contributed by a set of Einstein oscillators to a free electron gas is given by :-

$$\rho(T) - \rho(0) = G \cdot \frac{1}{\Theta_E} \left(\frac{N a}{\exp(\Theta_E/T)-1} \right) \qquad (4.2)$$

where $G = 2.06\ (m^2/ne^2\hbar\ Mk_B)$ with n = conduction electron density and M the oscillator mass.

An attempt to fit this simple Einstein expression to the resistivity data proved successful in a very limited region only, clear deviations being apparent from 5K upwards.

In a later publication however, J.R. Cooper (43) calculates, using Ziman's variational method, an upper bound to the electrical resistivity (ρ_E) of an Einstein solid; ρ_E is shown to be proportional to the product of the local mode specific heat and the temperature. This theory gives a greatly improved fit to the data of Caplin et al.

In their calculation of the electrical resistivity Caplin and Dunlop used the formula for an Einstein solid : $\rho \propto (\exp(\Theta_E/T)-1)^{-1}$, that is, the resistivity is proportional to the mean square oscillation amplitude, or total energy of the oscillators (excluding the zero point energy). This formula, based on the treatment of Mott and Jones (44) should not be used at low temperatures as it does not properly account for the inelastic scattering of electrons from the aluminium atoms with an energy $k_B \Theta_E$ which may be greater than $k_B T$.

The expression for the resistivity is essentially a simplified form of the one given for electron-phonon resistivity in Ziman's book (45). The final expression is :

$$\rho_E(T) = KN\left[MT\left(\exp(\Theta_E/T)-1\right)\left(1-\exp(-\Theta_E/T)\right)\right]^{-1} \qquad (4.3)$$

where N is the number of oscillators / unit volume

and K is a constant, independent of the local mode parameters but dependent on the electron density of the metal, and the local mode coupling strength. In terms of the Einstein heat capacity for one-dimensional oscillators,

i.e. $C_E(T) = N_0 k_B \left(\frac{\Theta_E}{T}\right)^2 \frac{\exp(\Theta_E/T)}{(\exp(\Theta_E/T)-1)^2}$ Eqn.(4.3) becomes :-

$$\rho_E(T) = \frac{KT\,C_{EIN}N.}{M\Theta_E^2 k_B} \qquad (4.4)$$

which, as for the Mott and Jones formula, gives in the high temperature limit :-

$$\rho_E(T) = \frac{KNT}{M\Theta_E^2}$$

N.B. For the more realistic case of 3-dimensional oscillators, C_E and the inelastic part of the resistivity should be multiplied by 3.

As may be seen in the figure below, the above expression gives an excellent fit to the data of Caplin and Dunlop, using Θ_E and N_ℓ as evaluated from their specific heat data, and treating K as an adjustable parameter. The deviations which are seen to occur above 20 K are consistent with normal phonon resistivity as measured in other aluminium intermetallics.

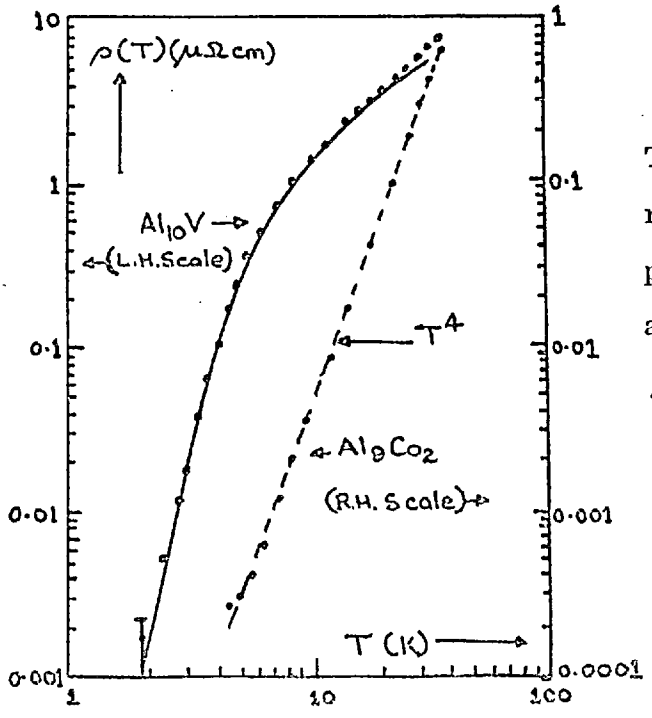


FIGURE (4.2.4)

The temperature dependent part of the resistivity of $Al_{10}V$. Experimental points from Ref.(38); solid line $\rho_E(T)$ as calculated from Eqn.(4.4). ρ (T) for Al_9Co_2 is also shown.

CHAPTER V

SAMPLE PREPARATION AND EXPERIMENTAL RESULTS

5.1.(i) METALLURGY

The phase diagram for the aluminium end of the Al-V system is shown in Fig.(5.1.1.). The work of Carlson, Kenney and Wilhelm (39) showed the existence of the three aluminium rich phases $Al_{11}V$, Al_6V and Al_3V; these are formed peritectically and decompose at 668°C, 735°C and 1360°C respectively. Evidence for the existence of another phase, Al_7V, having a peritectic horizontal very close to $Al_{11}V$ (at approximately 700°C) is reported by Elliot and Mondolfo (46) in the published discussion of Carlson et al's paper. As described in Chapter IV, the subsequent investigations of Brown (40) and of Ray and Smith (41) suggest that the composition of the compound richest in aluminium extends from $Al_{10}V$ to $Al_{10.5}V$.

5.1.(ii) SAMPLE PREPARATION

Five samples of $Al_{10}V$ were used in this work and they are labelled 3, 5, 6, 7 and 8 respectively. A sixth sample, No.9, was made, which is nominally $Al_{10.5}V$ doped with 0.8% gallium (0.8% by atomic replacement of aluminium). An attempt was made to form samples of different compositions across the phase field from $Al_{10}V$ to $Al_{10.5}V$, but this proved unsuccessful, as may be seen from Table (5.1.1), where the compositions are quoted for each sample, (a) as made up and (b) as evaluated from the specific heat data (see section 2 of this chapter). A possible explanation for this lack of success is divorcement of traces of residual aluminium solid solution and the other intermetallic compound (presumably Al_7V) in the course of the peritectic heat treatment.

TABLE 5.1.1

Sample No.	Desired Composition	Apparent Composition from Specific Heat Data
3	10.75 : 1	10.10 : 1
5	10.36 : 1	10.05 : 1
6	10.15 : 1	10.10 : 1
7	10.02 : 1	10.07 : 1
8	10.51 : 1	10.12 : 1

The samples were prepared by two different methods, the weights of the materials being checked before and after melting and annealing to check for any undue weight loss. The materials used were as given in Table (5.1.2) below.

TABLE 5.1.2

Sample No.	Metal	Source
3, 5, 6, 7.	Al	COMINCO.
	V	Goodfellow, 4N.
8, 9.	Al	Johnson-Mathey SPECPURE.
	V	Koch-Light, 3N.
9.	Ga	Koch-Light, 4N.

(1) SAMPLES 3, 5, 6 AND 7.

These samples were melted and solidified in a tapered graphite crucible lined with alumina (as the aluminium-transition metal (Al-T) preparations are reported to wet graphite more easily than alumina and Al-T carbides form easily). The aluminium, in the form of pellets, was placed in the crucible with vanadium foil on top. The crucible was then fired to 900^{o}C in vacuo, at which temperature the aluminium wets the vanadium and drags it down. After the admission of approximately 0.25 of an atmosphere of argon the temperature was raised and held above 1200^{o}C for about five minutes before cooling. To increase the rate of cooling an atmosphere of argon was admitted.

(2) SAMPLES 8 AND 9.

These were prepared by a standard arc-melting technique using a tungsten electrode and water cooled copper hearth. Due to the relatively high melting point of vanadium compared to that of aluminium care was taken to ensure macroscopically uniform samples by remelting at least four times and inverting the sample between melts. The loss of vanadium as vapour was minimised by placing this metal at the bottom of the hearth depression and covering with pieces of the aluminium charge; the vanadium was thus sheltered from direct arc heat during the initial melting together.

The heat treatment for all the samples followed the same basic procedure. The weighed samples were placed on an alumina boat in a silica tube which was sealed, under a vacuum of approximately 3×10^{-5} Torr, at about $300^{\circ}C$ (to drive off any water vapour and adsorbed gases). The samples were then placed in a resistance-type tube-furnace and the temperature gradually increased to about $660^{\circ}C$, care being taken to ensure that the temperature did not exceed $668^{\circ}C$, the decomposition point of $Al_{10}V$. The temperature was thermostatically controlled and checked periodically against a chromel/alumel reference thermocouple. The samples were annealed for not less than two and a half days at the end of which they were air-cooled, extracted from their capsules and small fragments taken for metallographic examination.

Microhardness determinations and electron-microprobe checks confirmed that in all cases the samples consisted of a matrix of the desired compound, $Al_{10}V$. A variable amount (from no trace up to about 20%) of a second phase (Al_7V), was present in each sample; this was identified by the techniques mentioned above. The Al_7V areas appeared as discrete rounded masses. In no case was a structure typical of incomplete peritectic solidification observed and this was substantiated by the fact that only traces of (bright)

aluminium solid solution were seen under the microscope.

The samples were prepared for use in the specific heat cryostat by planing two approximately parallel faces on the spark machine, which were subsequently polished to give good thermal contact with the copper mounting plates.

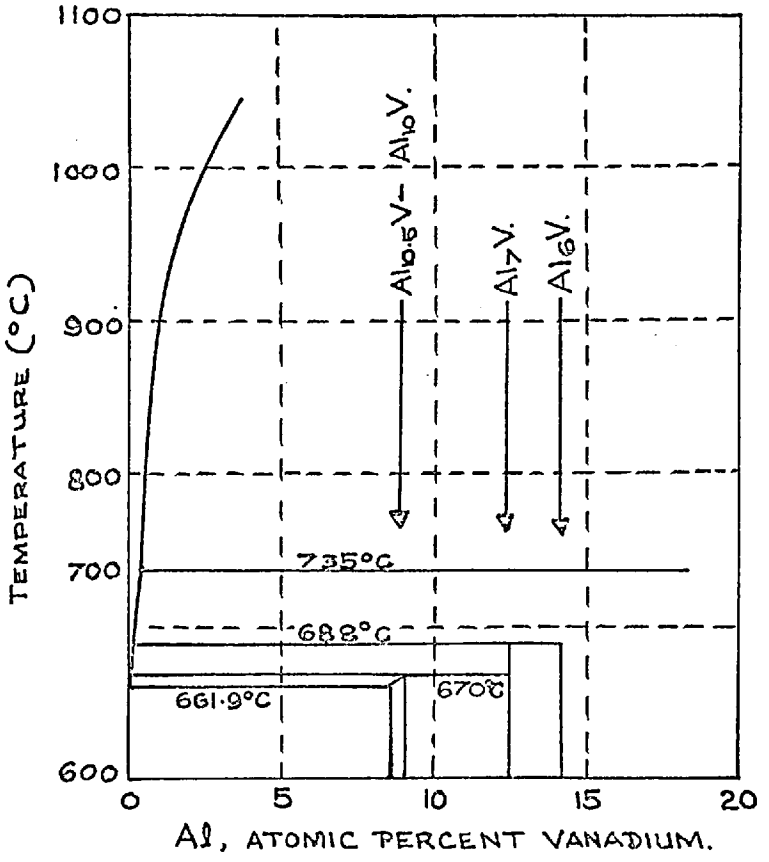


FIGURE (5.1.1)

Phase diagram for Aluminium rich end of the Al-V system

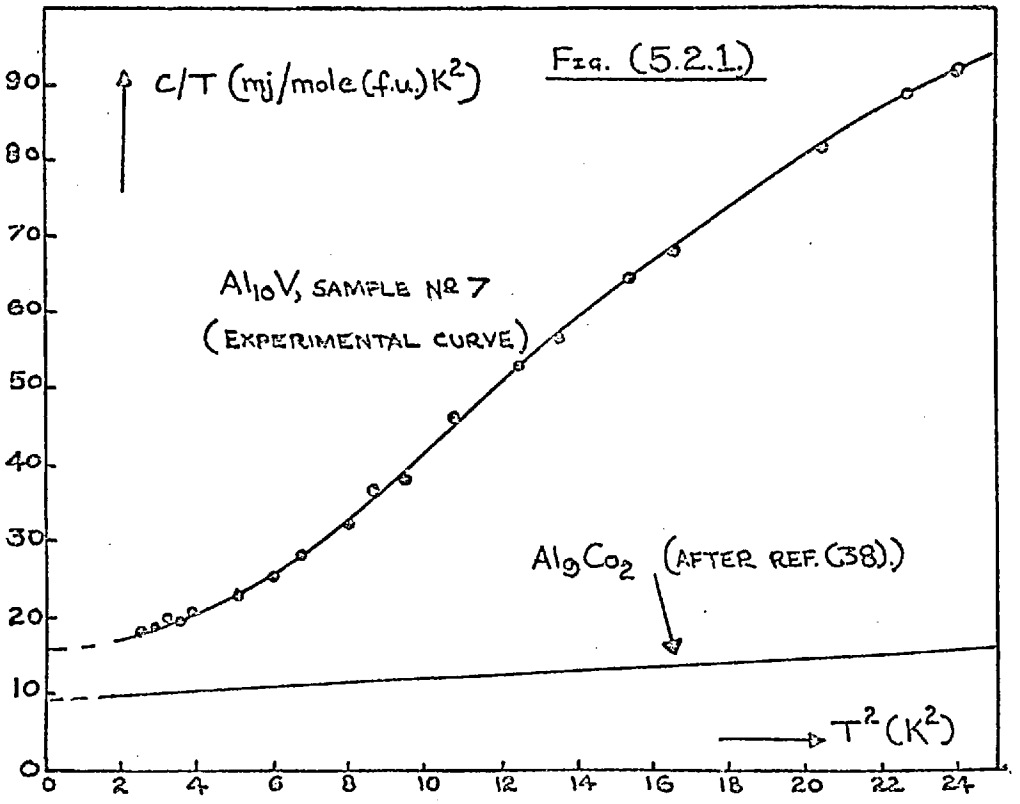
5.2 THE SPECIFIC HEAT DATA

INTRODUCTION

Specific heat measurements were made in the temperature range 1.8K to 35K on the five samples of $Al_{10}V$. The sample of $Al_{10}V$ doped with 0.8% gallium was also measured (sample No.9).

Measurements were made using the A.C. technique except in the case of sample No.3, for which results using both the A.C. and D.C. (step) methods are presented.

All the $Al_{10}V$ samples exhibit an anomalously large heat capacity corresponding in general shape and magnitude to that obtained by Caplin et al (38). Fig.(5.2.1) below shows the heat capacity for sample No.7 together with that for Al_9Co_2, a typical Al-T3 compound.



The excess heat capacity which is readily distinguishable above the electronic and lattice terms is found to be of Einstein form over the whole range of measurement.

The results are presented for each sample in the form of C/T versus T^2 plots :-

(i) for the low temperature data $1.8\,K < T < 10\,K$ from which the electronic term, $C_e = \gamma T$, is estimated;

(ii) for the overall range of measurement, to show the excess heat capacity over the electronic and lattice contributions;

(iii) for the excess heat capacity as compared with theoretical Einstein values.

The results for sample No.7 are shown in detail to explain the procedure used in the data analysis.

PRESENTATION OF RESULTS

Results for Sample No.7

(i) The Electronic Contribution

Figure (5.2.2) shows the low temperature data for sample No.7 extrapolated to $T = 0\,K$ to give the estimated value of γ, the coefficient of the electronic contribution to the heat capacity. For all the $Al_{10}V$ samples measured γ is found to be 17.0 ± 1.4 mj/mole(f.u)K^2.

(ii) The Lattice Contribution

The estimation of the lattice contribution involves a large uncertainty since the excess contribution is unknown. The assumption is made that at the high temperature end ($T > 20\,K$, where the excess contribution is small) the lattice contribution is proportional to T^3, i.e. $C_L = \beta T^3$. Plotting $(C - \gamma T)$ against T^3 for $T > 20\,K$ gives a straight line of gradient β and the intercept gives an indication of the number of oscillators contributing to the excess heat capacity. For large T the Einstein heat capacity gives the classical value of $C_{EIN} = 3R$, and in this case we have N_ℓ oscillators per

formula unit, hence $C_{EIN} = 3RN_\ell$. Figure (5.2.3) shows the plot of $(C - \gamma T)$ versus T^3 for sample No.7. For this sample $\beta = 0.404 \pm .044$ mj/mole(fu)K^4 which gives $\Theta_D = 381°K \pm 12.6°K$

The intercept (1.6 j/mole(fu)K) gives a rough estimate of .06/fu for N_ℓ, which is in good agreement with the value found from the more detailed analysis of the excess contribution (of 0.067/fu).

From the good fit obtained to the excess heat capacity at high temperatures (see for example Fig.(5.2.7)) the method used for estimating β is felt to be well justified.

(iii) The Excess Contribution

Figure (5.2.4) shows C/T versus T^2 together with the electronic and lattice terms which when subtracted off leave the excess heat capacity C'. C' is fitted to the Einstein expression for specific heat (for three dimensional oscillators):-

$$C_{EIN} = 3N_o N_\ell k_B \left(\frac{\Theta_E}{T}\right)^2 \frac{\exp(\Theta_E/T)}{(\exp(\Theta_E/T)-1)^2} \qquad (5.1)$$

by evaluating N_ℓ, the number of oscillators per formula unit, and the Einstein temperature, Θ_E, from the low temperature data, since for $T < \Theta_E/3$, to 1% Eqn.(5.1) becomes :-

$$C_{EIN} = 3N_o N_\ell k_B \left(\frac{\Theta_E}{T}\right)^2 \exp(-\Theta_E/T). \qquad (5.2)$$

Hence in this temperature region plotting $\ell n.(C_E T^2)$ against $1/T$ gives a straight line of gradient $-\Theta_E$, and N_ℓ may then be evaluated from Eqn.(5.1).

Figure (5.2.5) shows the graph of $\ell n.(C' T^2)$ against $1/T$ for sample No.7.

The dashed lines (1) and (2) on this graph show the lines of maximum and minimum slope fitted to the data points, which indicate an error of 11% in N_ℓ and 3% in Θ_E. Figure (5.2.6) shows the theoretical curves

(C_{EIN}/T versus T^2) evaluated for the extreme values of N_ℓ and Θ_E. These curves are seen to lie well within the estimated error on C' evaluated from the uncertainties in estimating γ, β and in the measurement of C.

Figure (5.2.7) shows the theoretical curve from the best fit to the data points in Fig.(5.2.5). The low temperature part of this fit is shown on an expanded scale in Fig.(5.2.8).

The low temperature data for samples 5, 6 and 7 are shown in Figure (5.2.9) and for samples 3, 8 and 9 in Fig.(5.2.10). The obvious difference in the low temperature heat capacities indicates how the Einstein contribution varies from sample to sample.

Plots of C/T versus T^2 and the excess heat capacity for the entire range of measurement are shown in diagrams (5.2.11) to (5.2.18) for samples 3, 5, 6 and 8. The electronic and lattice contributions, and the theoretical Einstein curves are also shown.

The results for the five $Al_{10}V$ samples are tabulated below, and it may be seen that for the samples measured the occupancy of the loose atom site varies from 10% to 25%, (assuming three dimensional harmonic motion).

TABLE 5.2.1.

Sample No.	γ mj/mole(fu)K^2 ± 8%	β mj/mole(fu)K^4 ± 10%	Θ_D (K) ± 3.3%	Θ_E (K) ± 3%	N_ℓ^{-1} (fu)$^{-1}$ ±11%
3	17.0	0.504	354	23.5	.103
5	17.0	0.386	386	22.7	.051
6	17.0	0.481	359	22.6	.103
7	17.0	0.404	381	22.7	.067
8	17.0	0.531	348	23.4	.119

5.2.(ii) RESULTS FOR GALLIUM DOPED SAMPLE No.9.

The low temperature data for the gallium doped sample is shown in Figure (5.2.10) together with that for samples 3 and 8. It is apparent from the greatly enhanced heat capacity at low temperatures, that there is an additional term in the excess heat capacity. This is consistent with an additional Einstein contribution of lower characteristic temperature than that for the aluminium atoms; suggesting the occupancy of some of the vacant sites by gallium, (whose atomic mass is 2.5 times greater than that of aluminium).

The assumption is made that the electronic contribution for this sample is the same as for 'pure' $Al_{10}V$ samples, i.e. γ = 17mj/mole(fu)K^2, and the lattice contribution was estimated from the high temperature data as described above for the other samples.

Figure (5.2.19) depicts the total heat capacity together with the electronic and lattice contributions. The excess contribution to the heat capacity, C', plotted as $\ell n\ (C'T^2)$ against $(1/T)$ for the low temperature data is shown in Figure (5.2.5). It is seen that rather than the linear behaviour of sample No.7, the data for this sample gives a curve, consistent in general form with the sum of two exponentials; i.e.

$$C'T^2 = 3k_B N_o \times (N_1\Theta_1^2 \exp(-\Theta_1/T) + N_2\Theta_2^2 \exp(-\Theta_2/T)) \qquad (5.3)$$

where subscript 1 refers to the contribution from aluminium atoms and 2 to that from gallium atoms.

Reliable analysis of this data is difficult since the characteristic temperature for the contribution from the gallium atoms is of the order of 10 K and data was only obtained down to 1.5 K. The low temperature approximation for C_{EIN} (Eqn.(5.2)) is only valid for this contribution below about 3 K.

The best fit obtained is shown in Figure (5.3.20),

where :- $\Theta_1 = 23.0\,K, \qquad N_1 = 0.096/fu$

$\Theta_2 = 9.6\,K, \qquad N_2 = 0.018/fu$

and Figure (5.2.21) shows the low temperature part on an expanded scale.

Although fits could be obtained well within the estimated error on C' with a range of 19 to 24 K for Θ_1, 7 to 10 K for Θ_2, the choice of the above values as the most likely is felt to be well justified as Θ_1 is well known from previous data.

This contribution from the gallium atoms shows a strongly preferential occupancy of the loose atom sites by gallium.

The specific heat data for all six samples is tabulated in Appendix 2.

(FIG 5.2.2.) $\frac{C}{T}$ VERSUS T^2 SAMPLE Nº 7

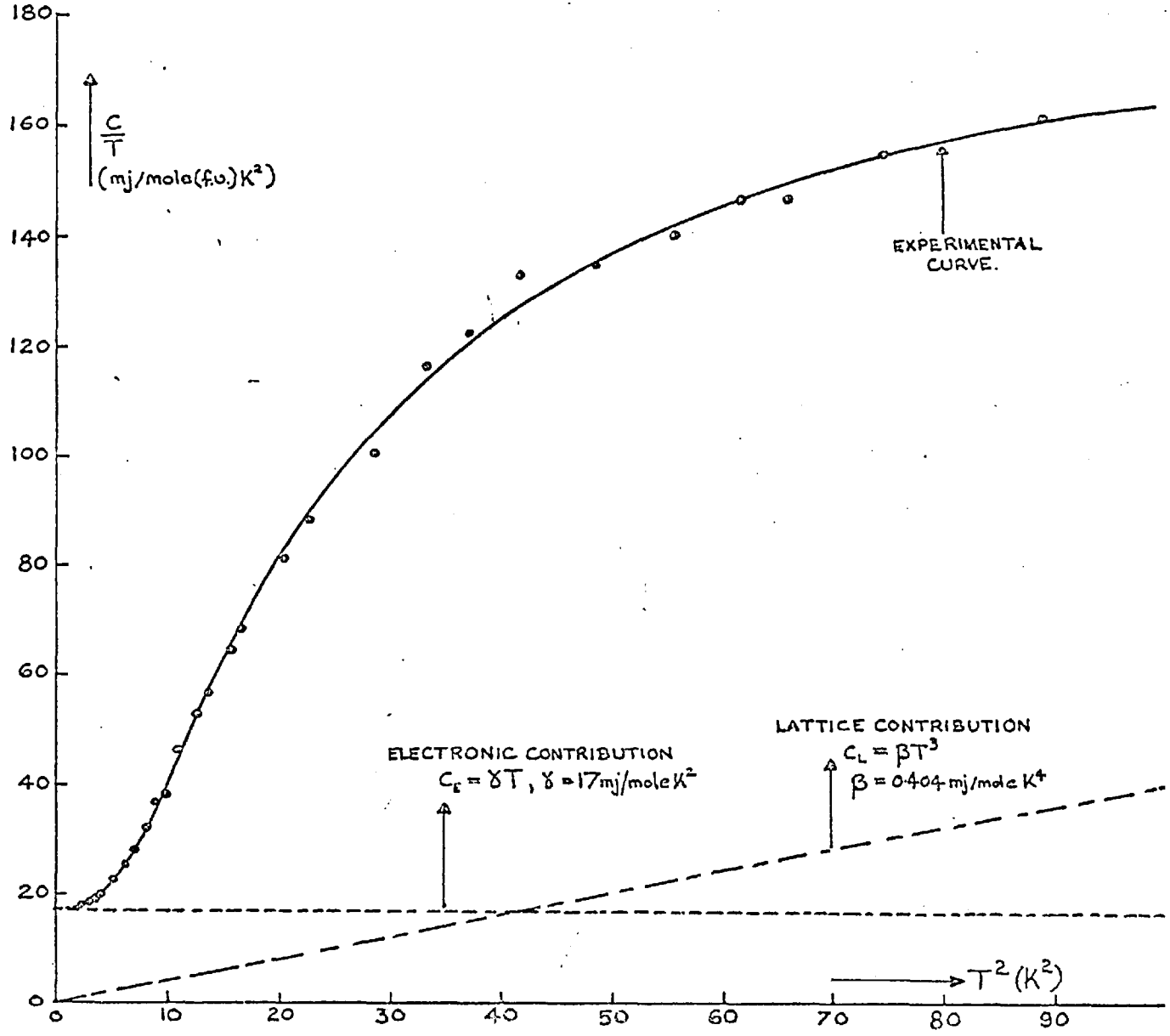
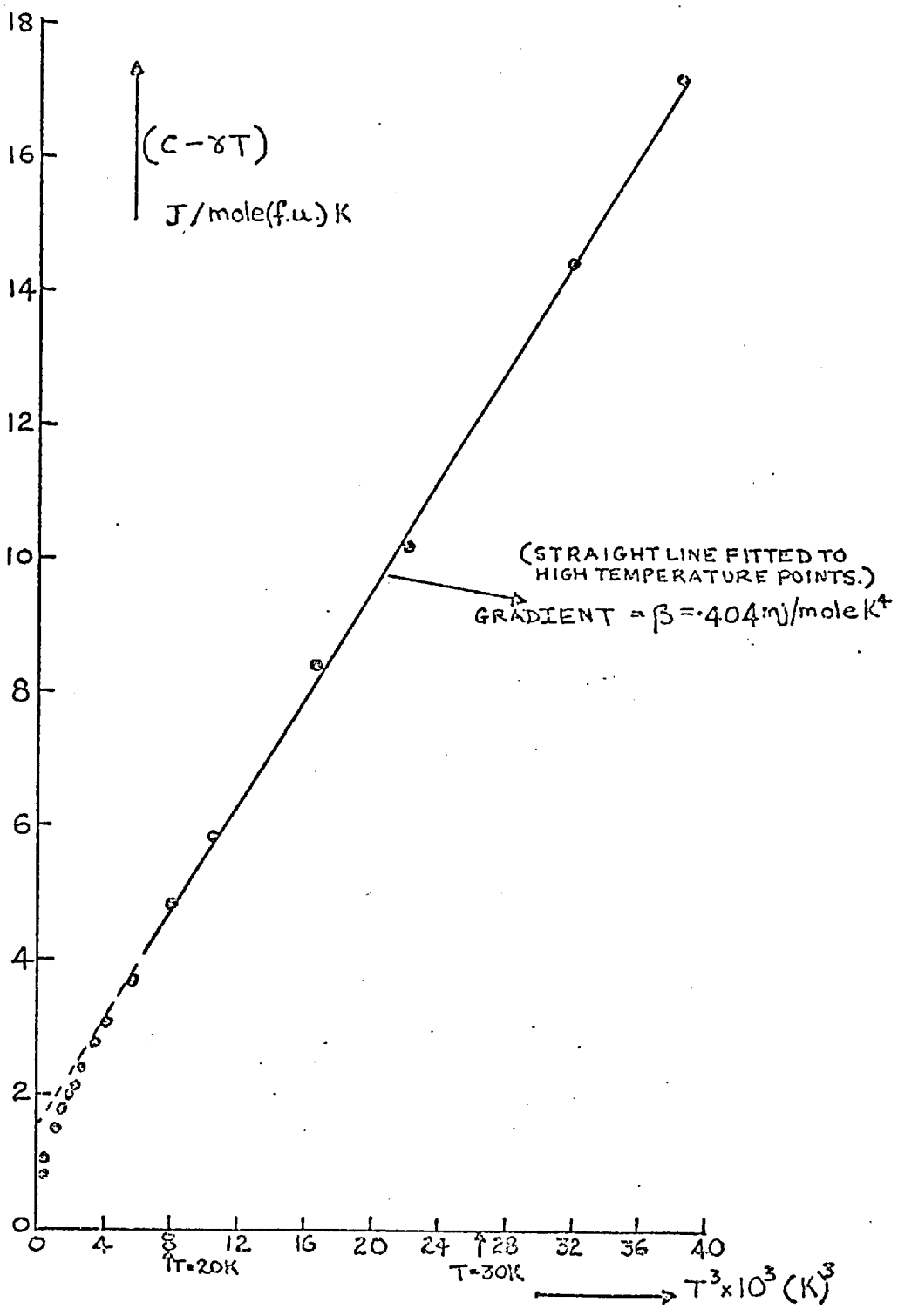
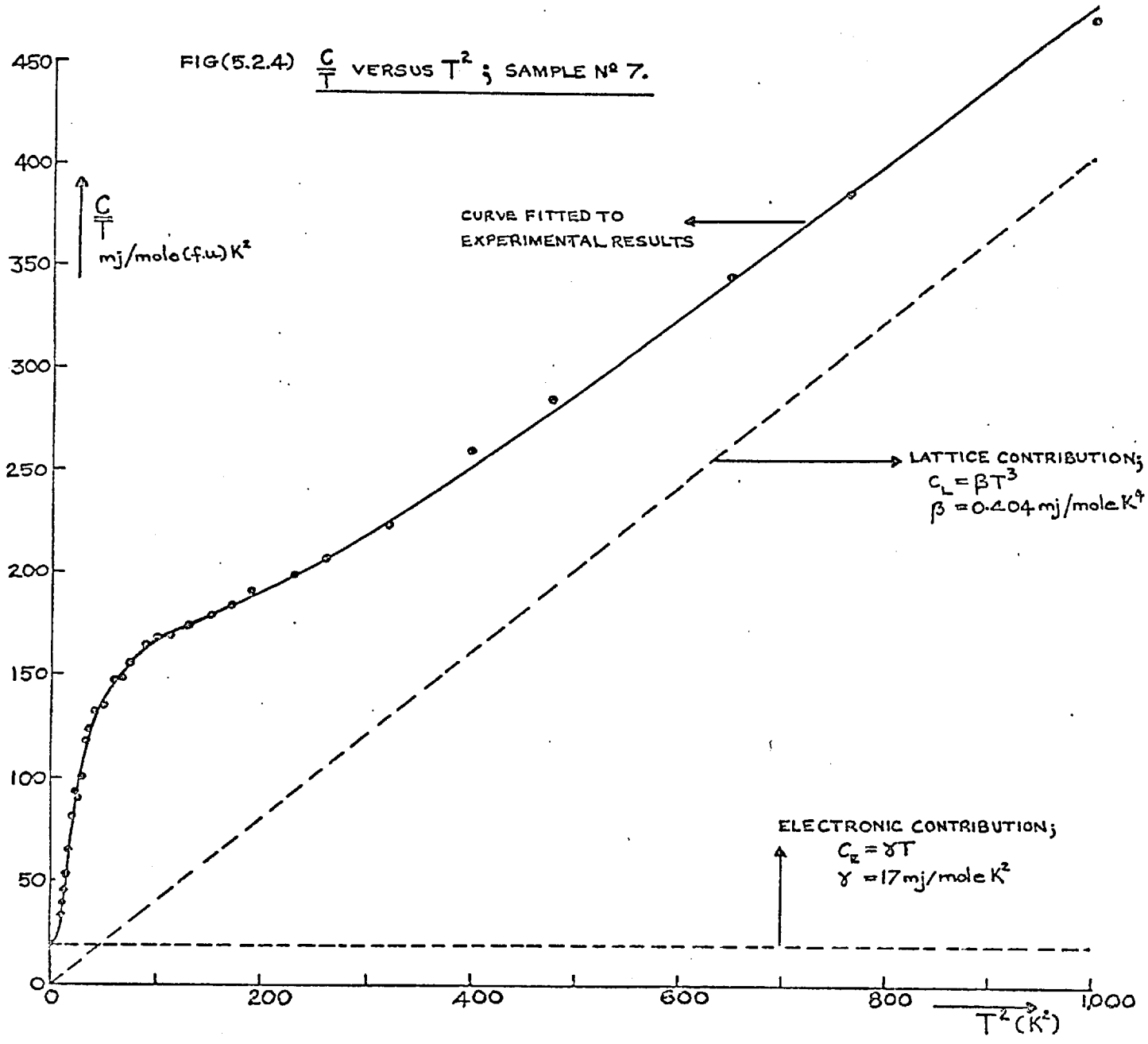


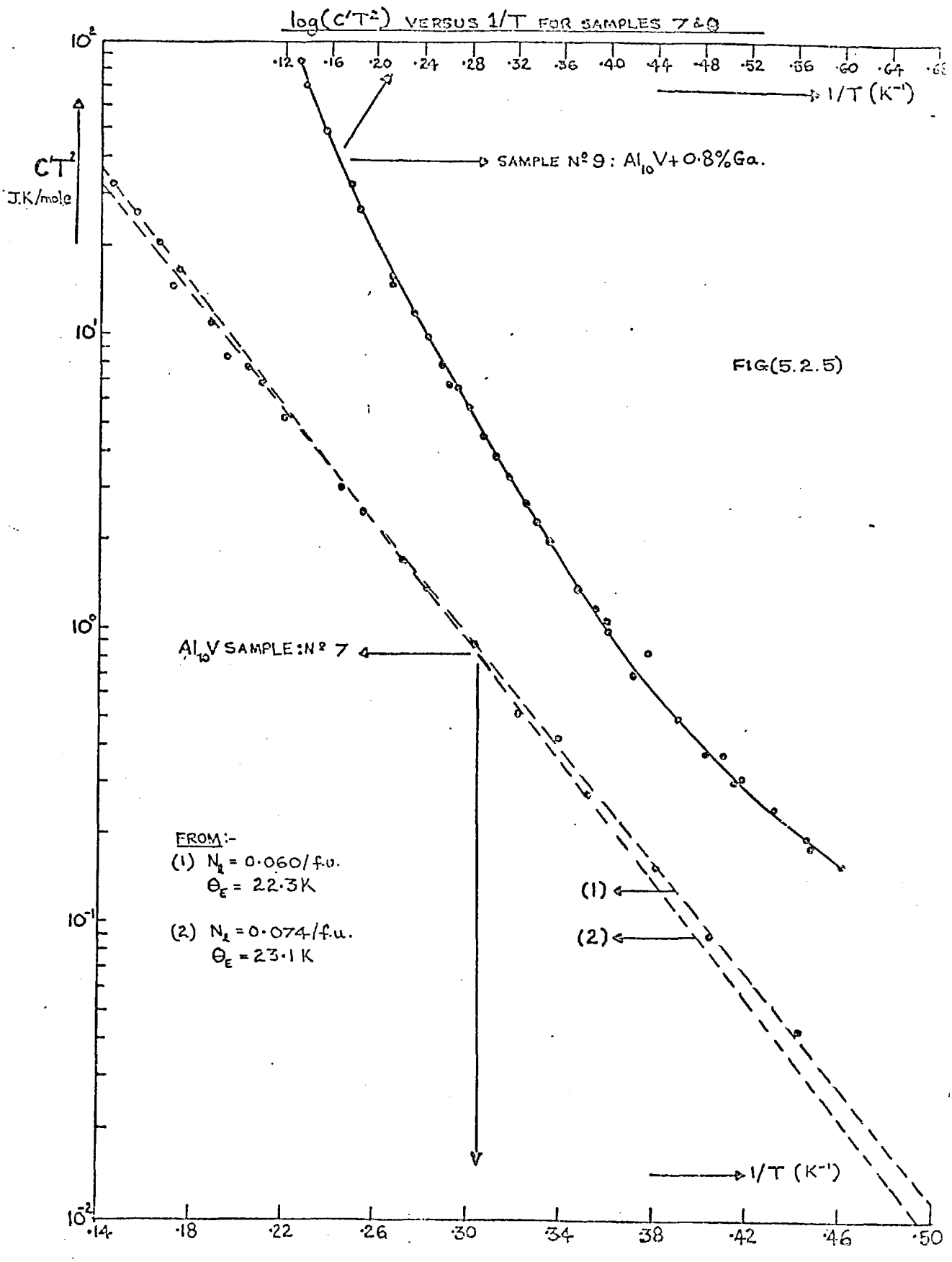
FIG (5.2.3.)

(C − γT) VERSUS T^3 FOR SAMPLE Nº 7

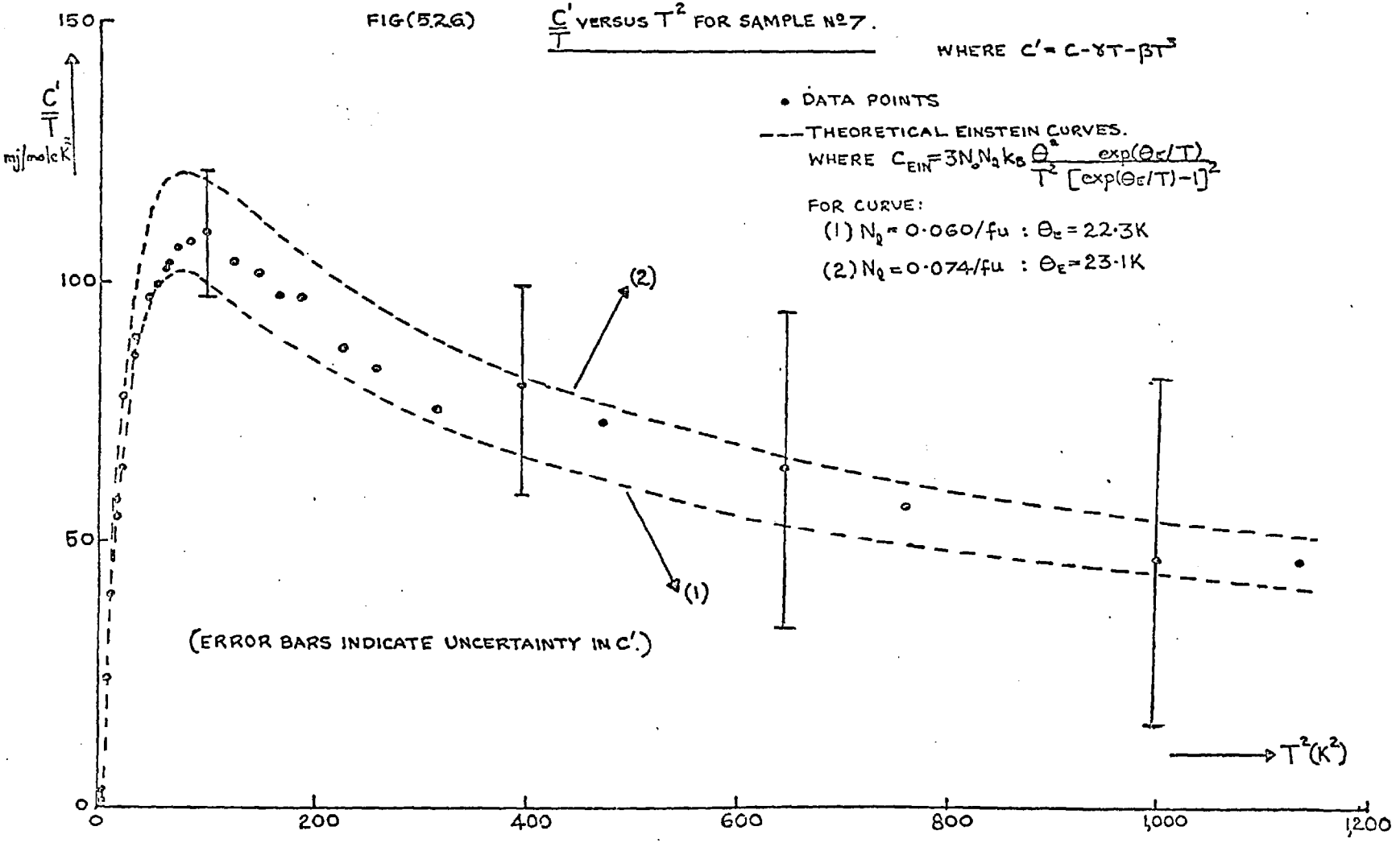


FIG(5.2.4) $\frac{C}{T}$ VERSUS T^2 ; SAMPLE Nº 7.



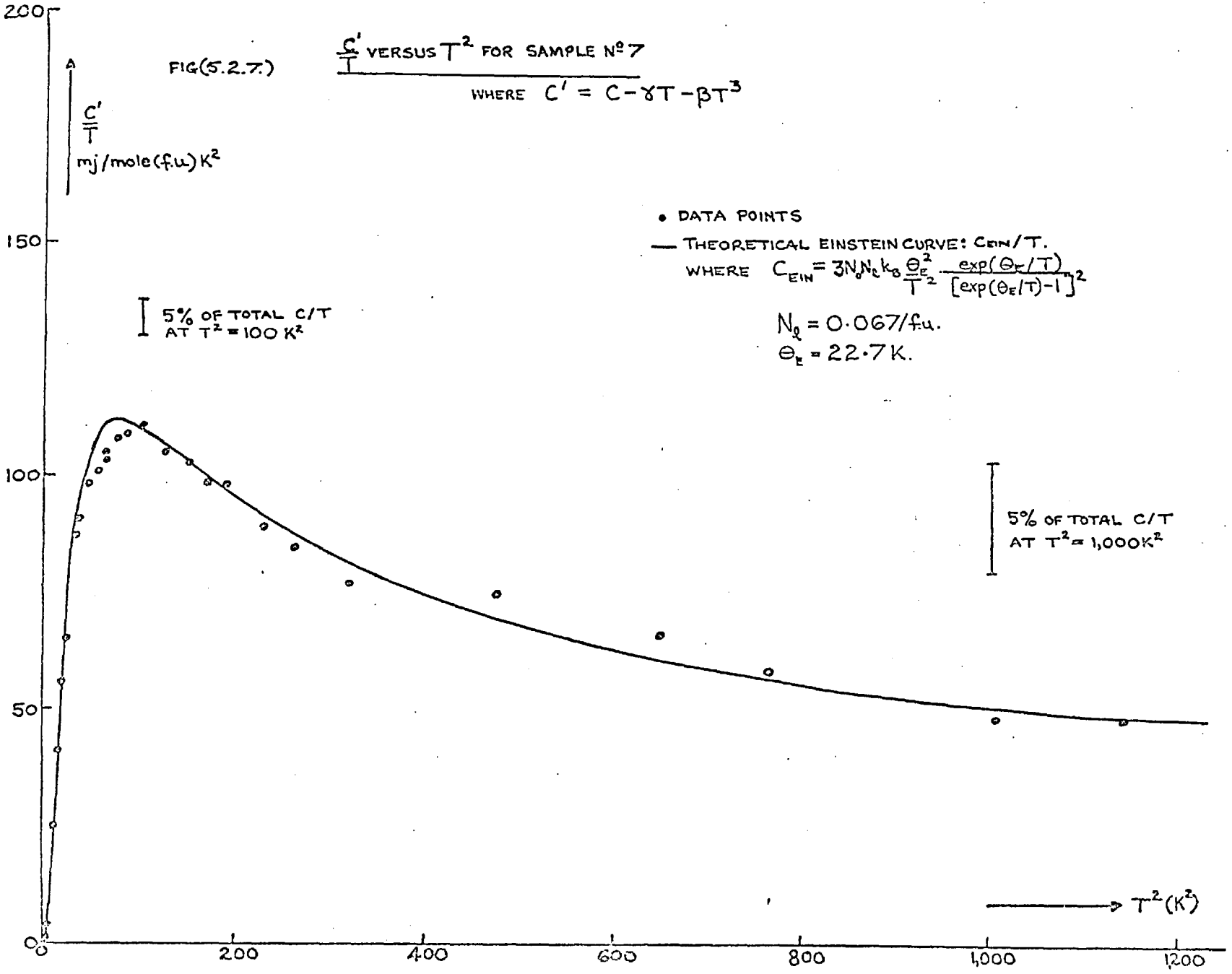

log(C'T²) VERSUS 1/T FOR SAMPLES 7 & 9
C'T²
J.K/mole
1/T (K⁻¹)
SAMPLE Nº 9 : Al10V + 0·8%Ga.
Al10V SAMPLE: Nº 7
FROM:-
(1) N = 0·060/f.u.
θE = 22·3K
(2) N = 0·074/f.u.
θE = 23·1 K
(1)
(2)
V
1/T (K⁻¹)

FIG(5.2.5)

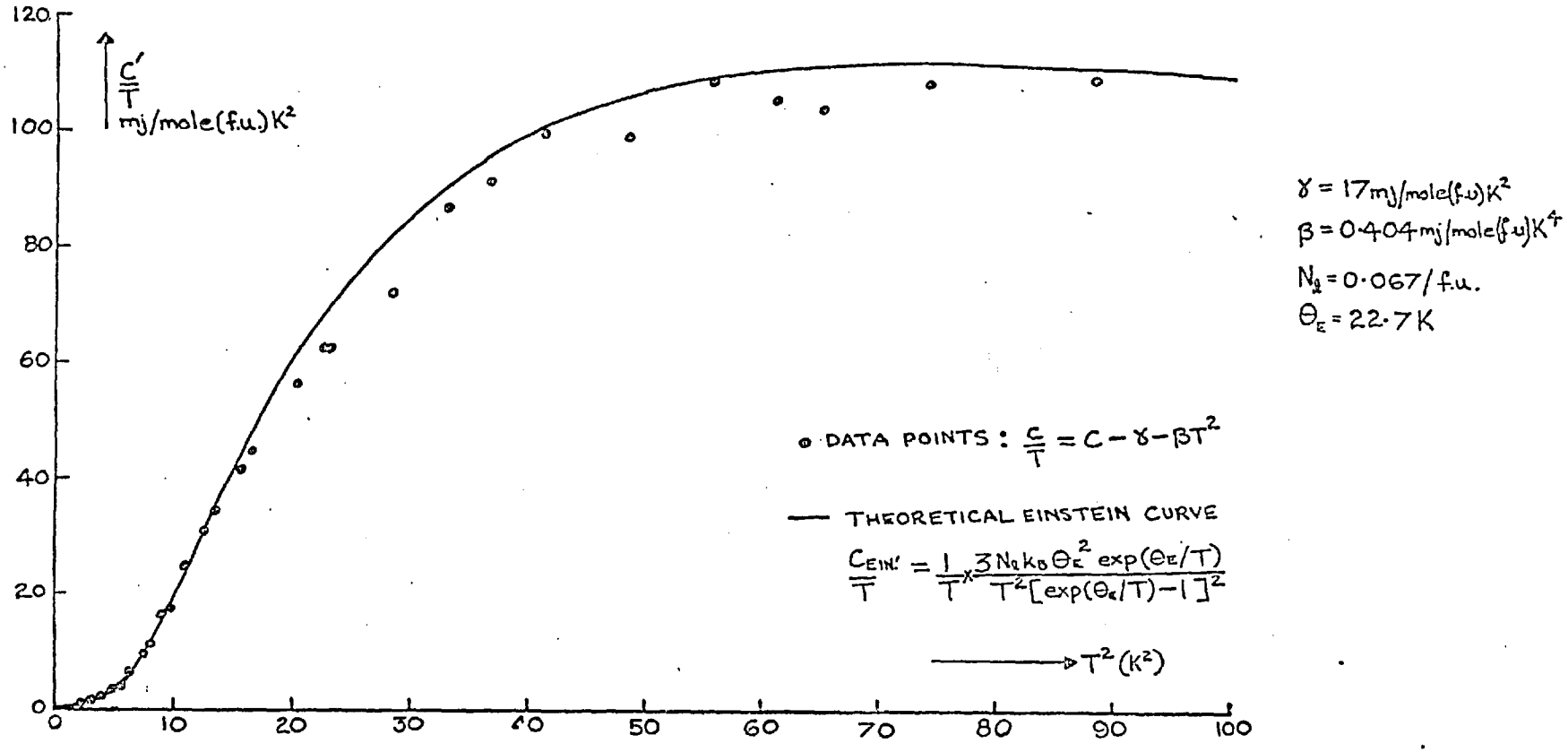

FIG(5.26) C'/T VERSUS T² FOR SAMPLE Nº7.
WHERE C' = C-γT-βT³
• DATA POINTS
---THEORETICAL EINSTEIN CURVES.
WHERE $C_{EIN}=3N_0N_Ak_B\frac{\theta_E^2}{T^2}\frac{\exp(\theta_E/T)}{[\exp(\theta_E/T)-1]^2}$
FOR CURVE:
(1) N_A = 0·060/fu : θ_E = 22·3K
(2) N_A = 0·074/fu : θ_E = 23·1K
(2)
(1)
(ERROR BARS INDICATE UNCERTAINTY IN C'.)
C'/T mj/mole K²
150
100
50
0
0
200
400
600
800
1,000
1,200
T²(K²)

FIG(5.2.7.) $\frac{C'}{T}$ VERSUS T^2 FOR SAMPLE Nº 7

WHERE $C' = C - \gamma T - \beta T^3$



FIG(5.2.8) GRAPH TO SHOW COMPARISON BETWEEN THEORETICAL EINSTEIN CURVE AND EXPERIMENTAL DATA FOR SAMPLE Nº 7 AT LOW TEMPERATURES.

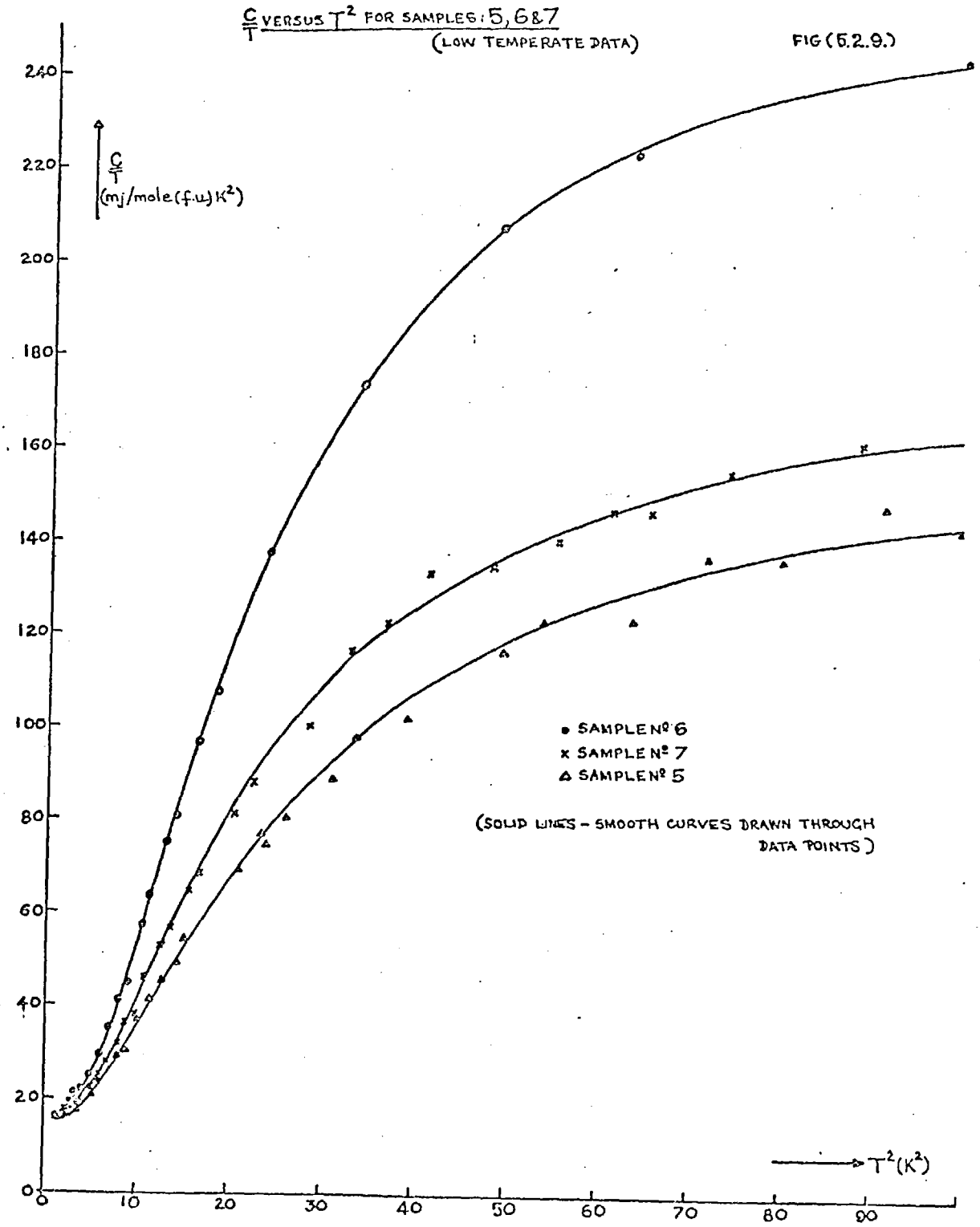


$\gamma = 17 mj/mole(f.u)K^2$

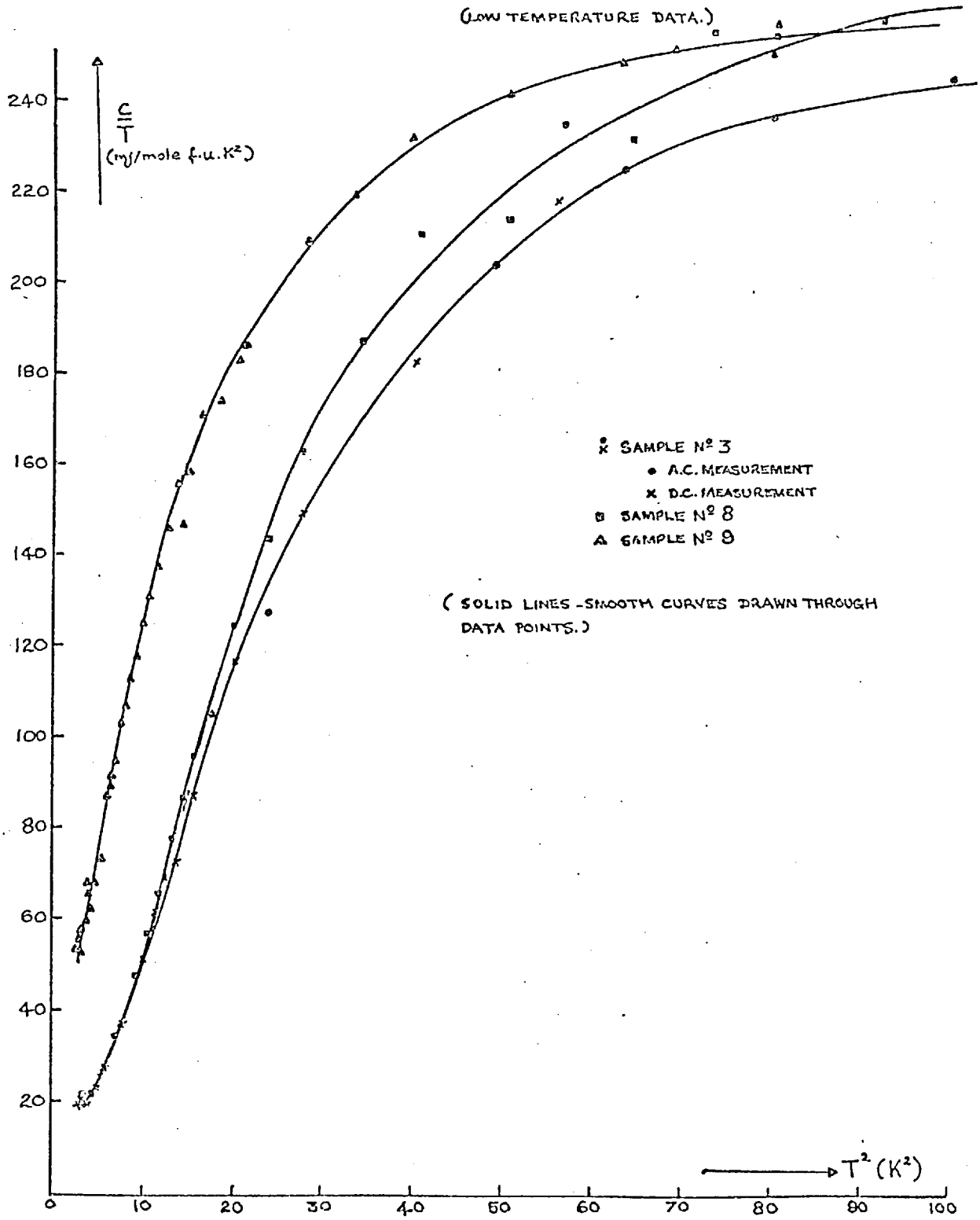
$\beta = 0.404 mj/mole(f.u)K^4$

$N_a = 0.067/f.u.$

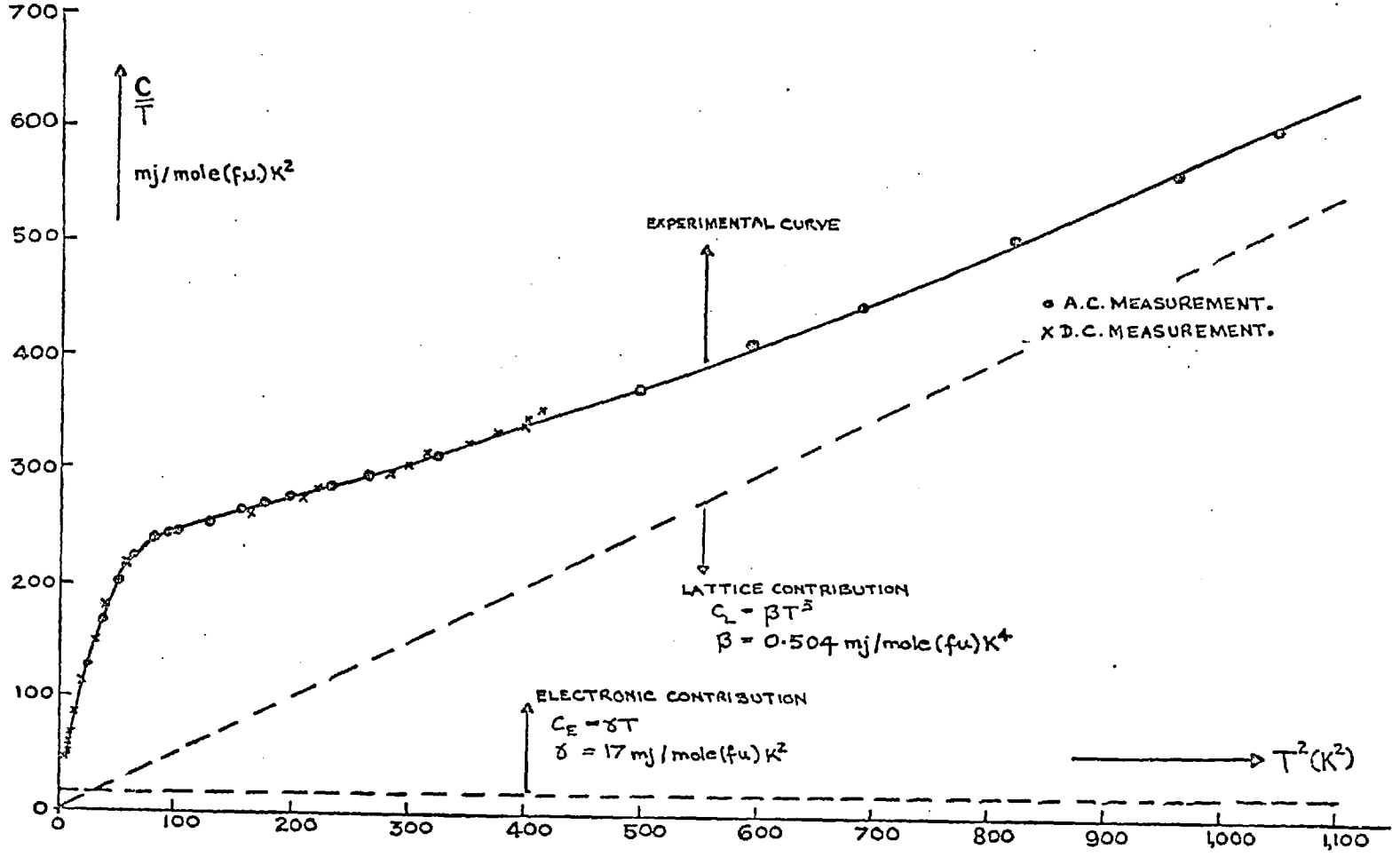
$\theta_E = 22.7 K$


C/T VERSUS T² FOR SAMPLES: 5, 6 & 7
(LOW TEMPERATE DATA)
FIG (5.2.9.)
C/T (mj/mole(f.u)K²)
240
220
200
180
160
140
120
100
80
60
40
20
0
0
10
20
30
40
50
60
70
80
90
T²(K²)
• SAMPLE Nº 6
× SAMPLE Nº 7
△ SAMPLE Nº 5
(SOLID LINES – SMOOTH CURVES DRAWN THROUGH DATA POINTS)

FIG(5.2.10) C/T VERSUS T^2 FOR SAMPLES 3,8&9.



FIG(5 2.11.) C/T VERSUS T^2 FOR SAMPLE Nº3



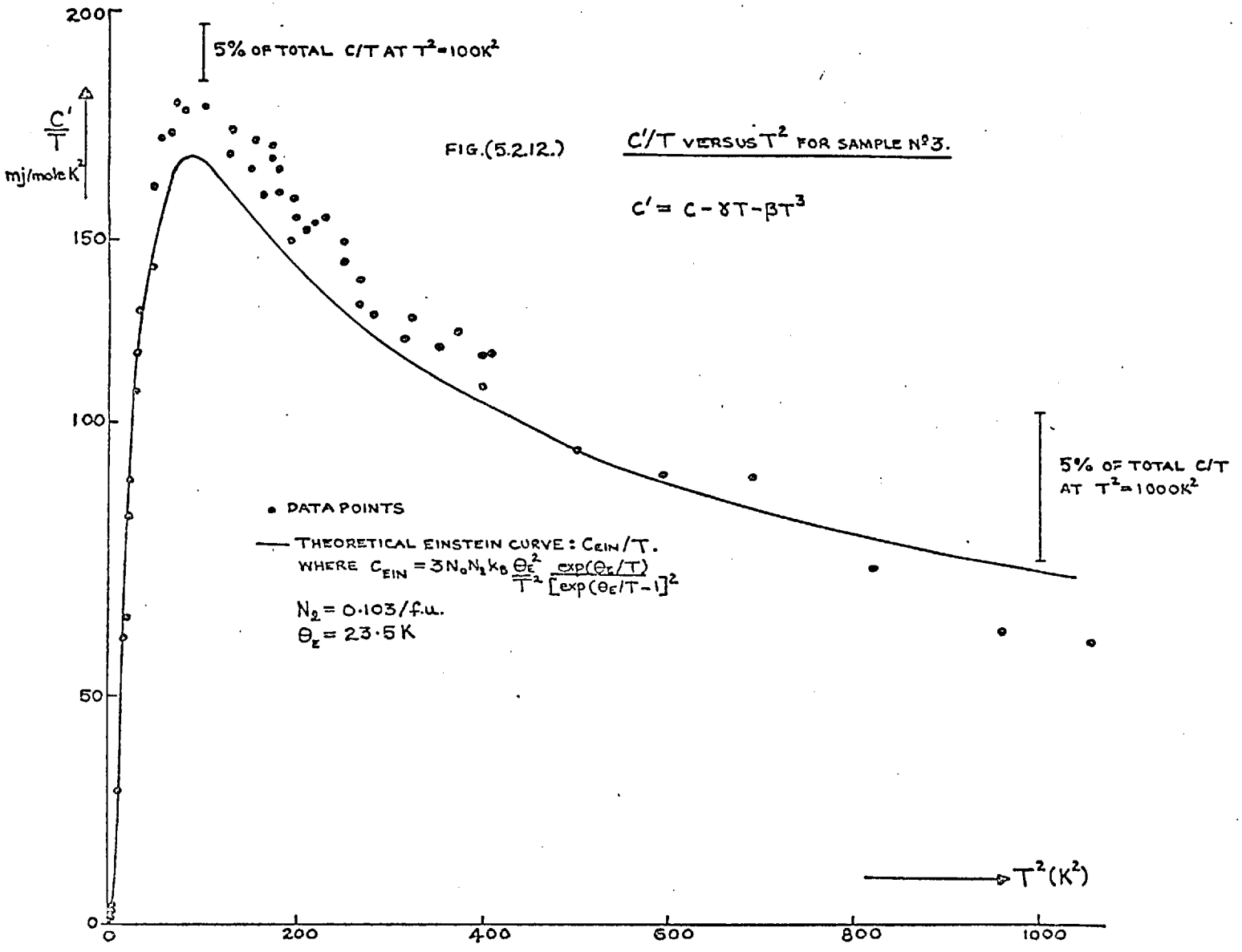


FIG.(5.2.12.) C'/T VERSUS T² FOR SAMPLE Nº3.

$C' = C - \gamma T - \beta T^3$

FIG (5.2.13.) $\frac{C}{T}$ VERSUS T^2 FOR SAMPLE Nº 5.

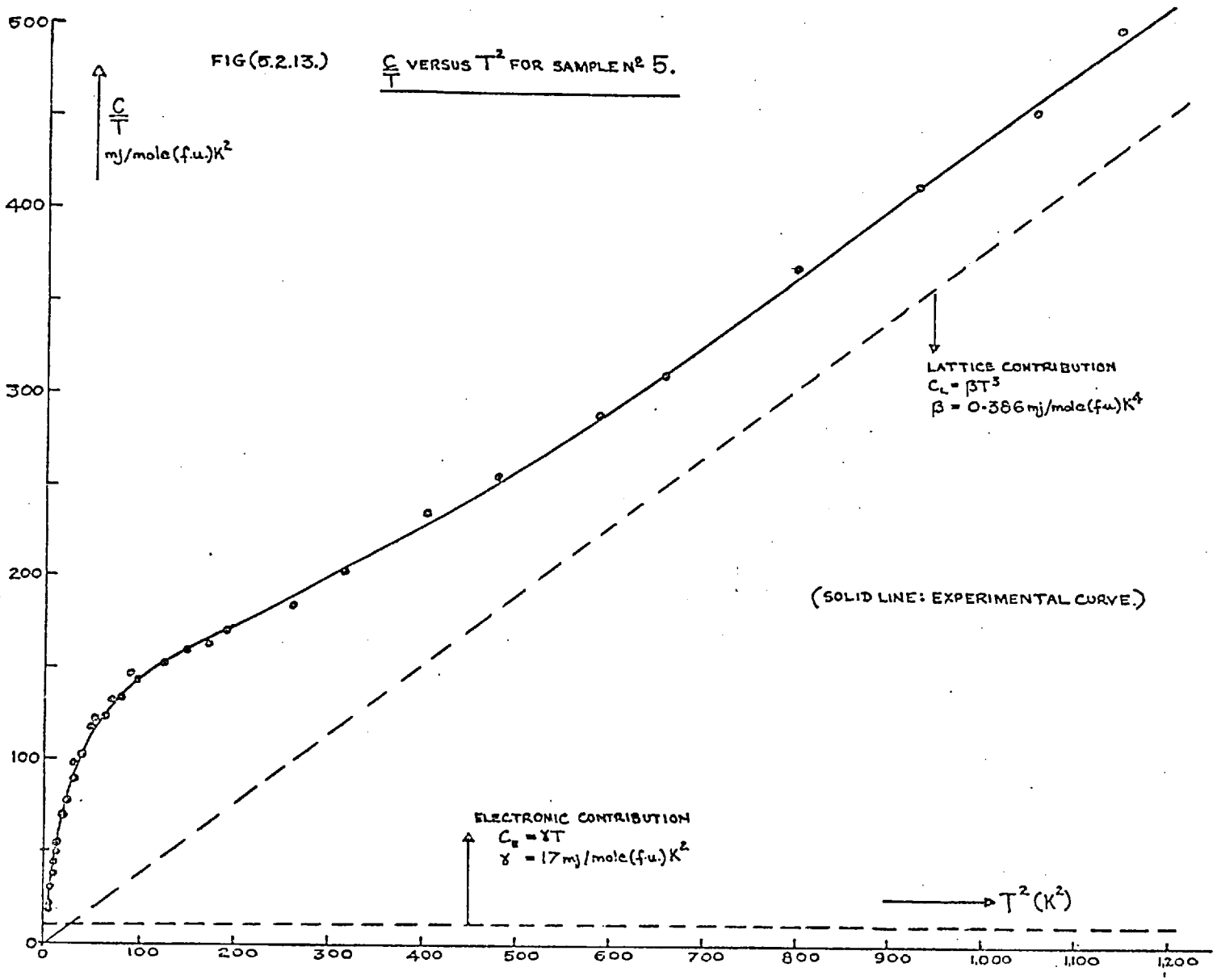
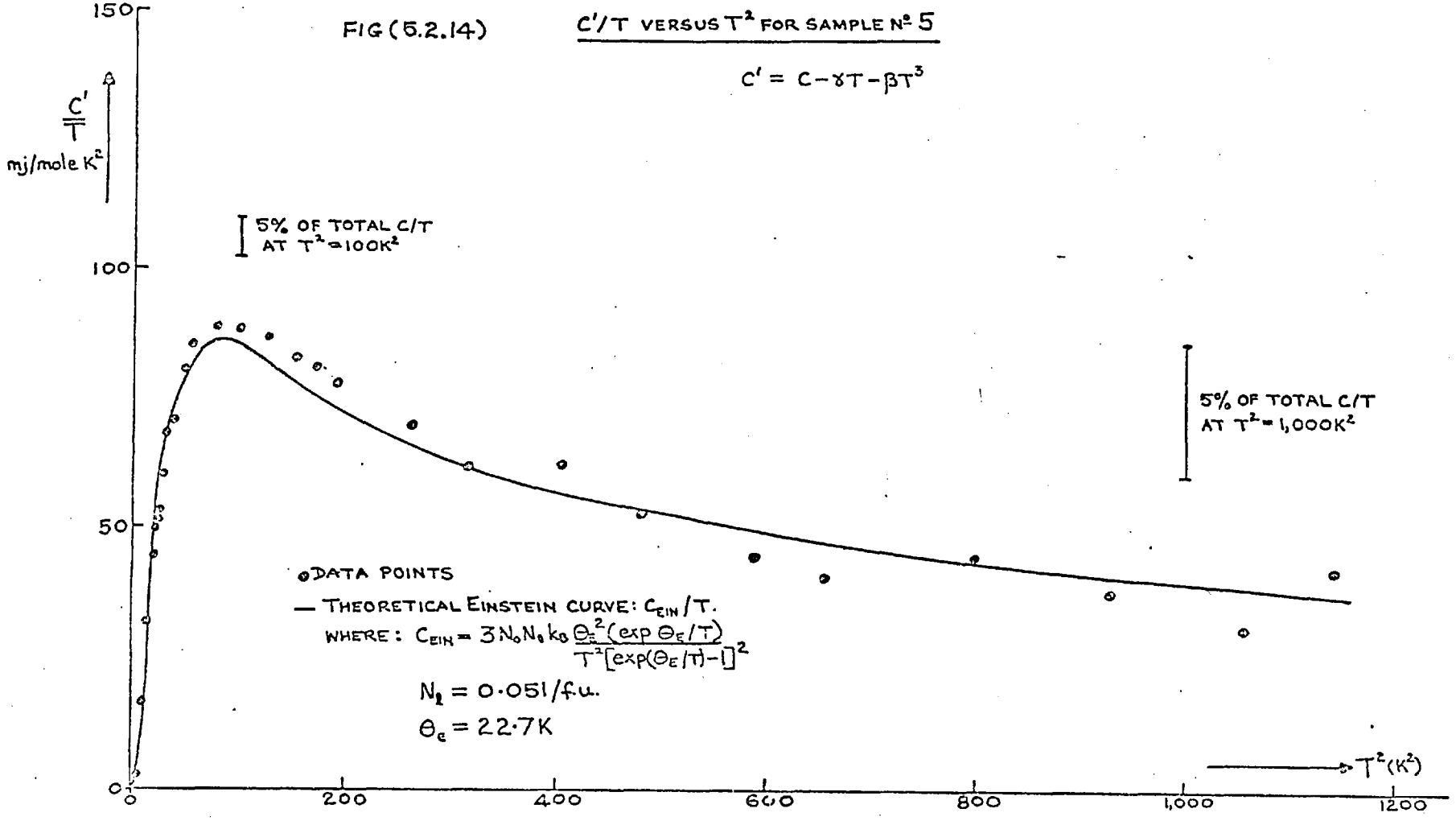
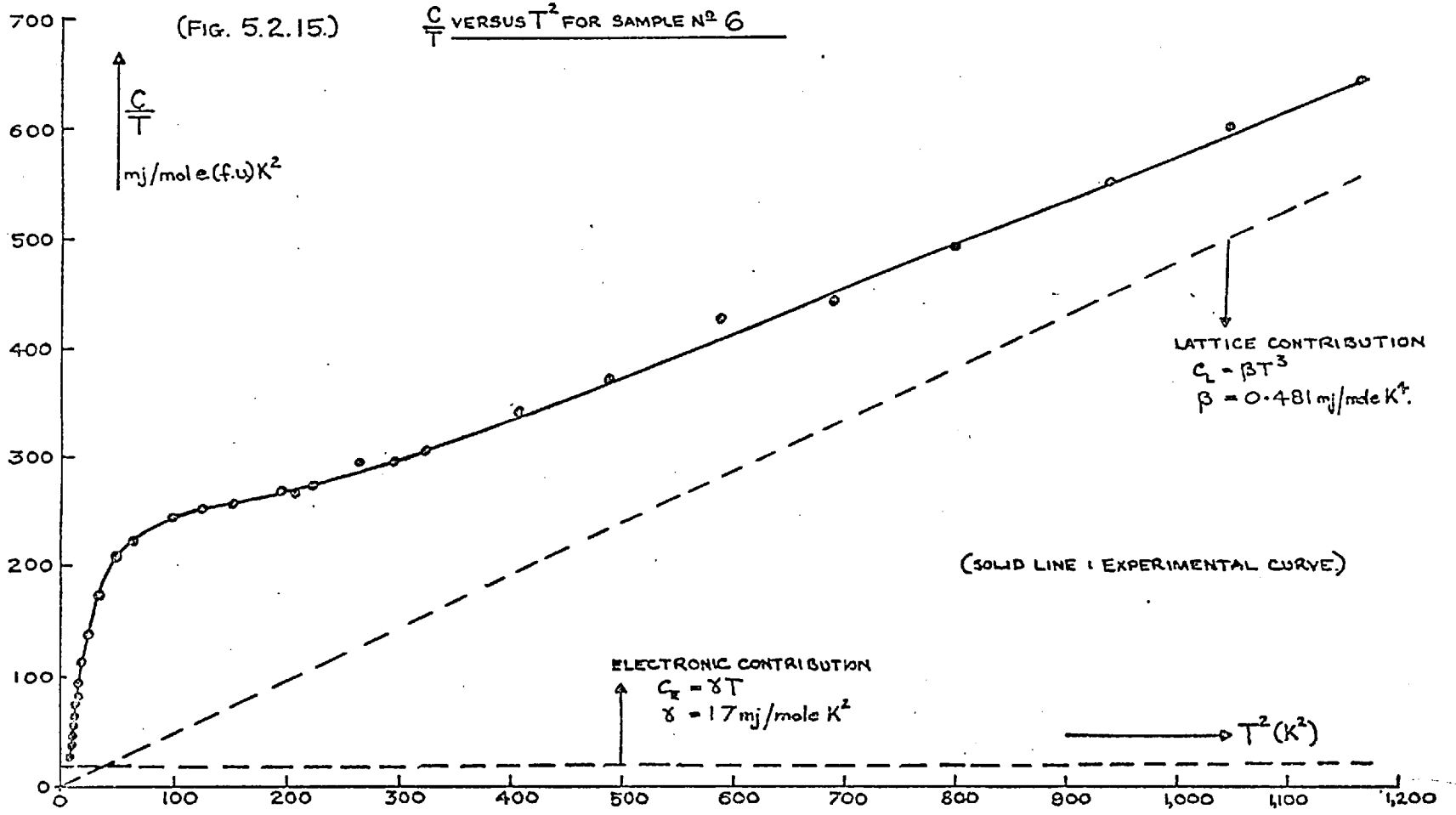


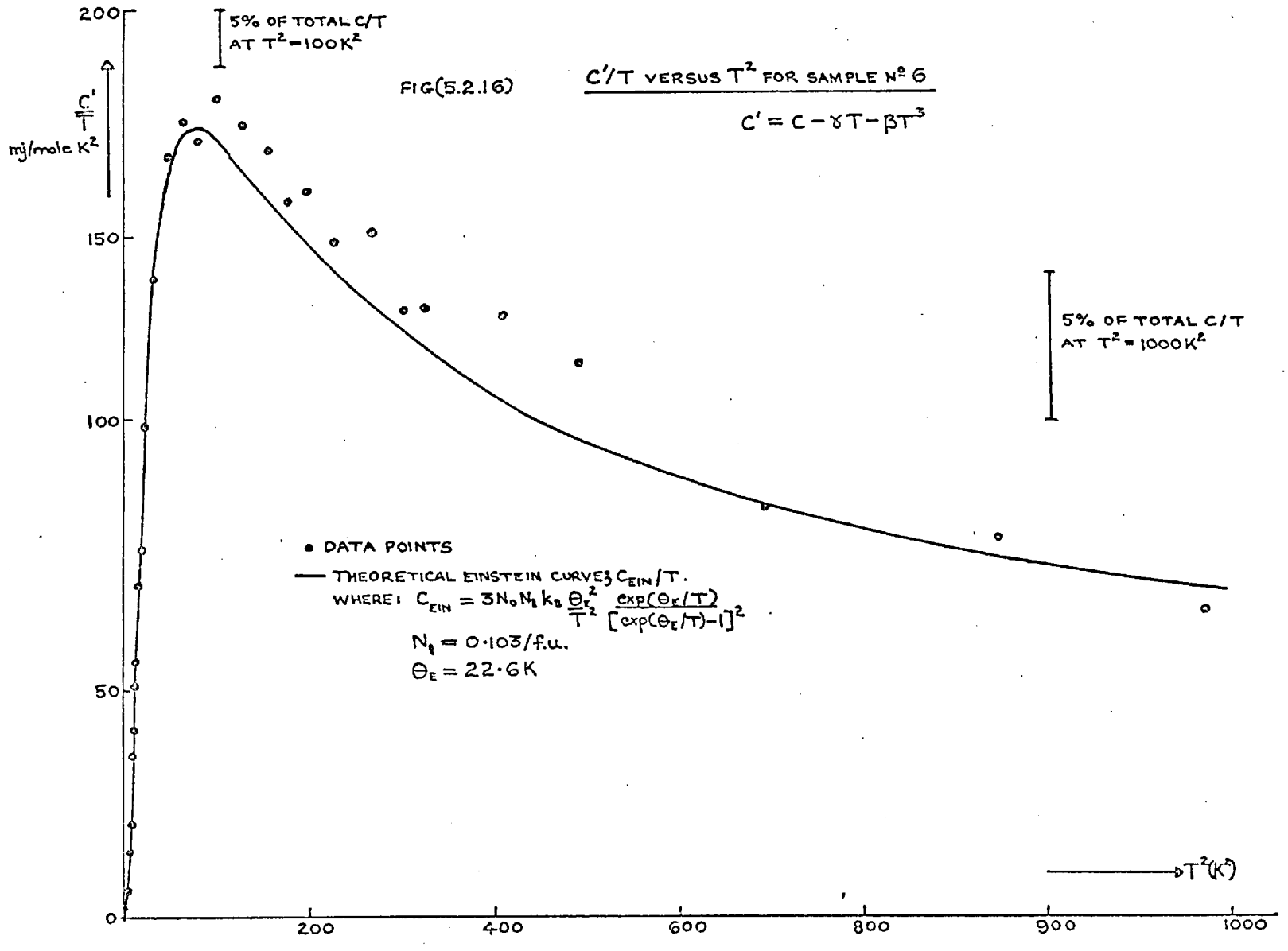
FIG (5.2.14) C'/T VERSUS T^2 FOR SAMPLE Nº 5

$C' = C - \gamma T - \beta T^3$



(FIG. 5.2.15.) $\frac{C}{T}$ VERSUS T^2 FOR SAMPLE Nº 6

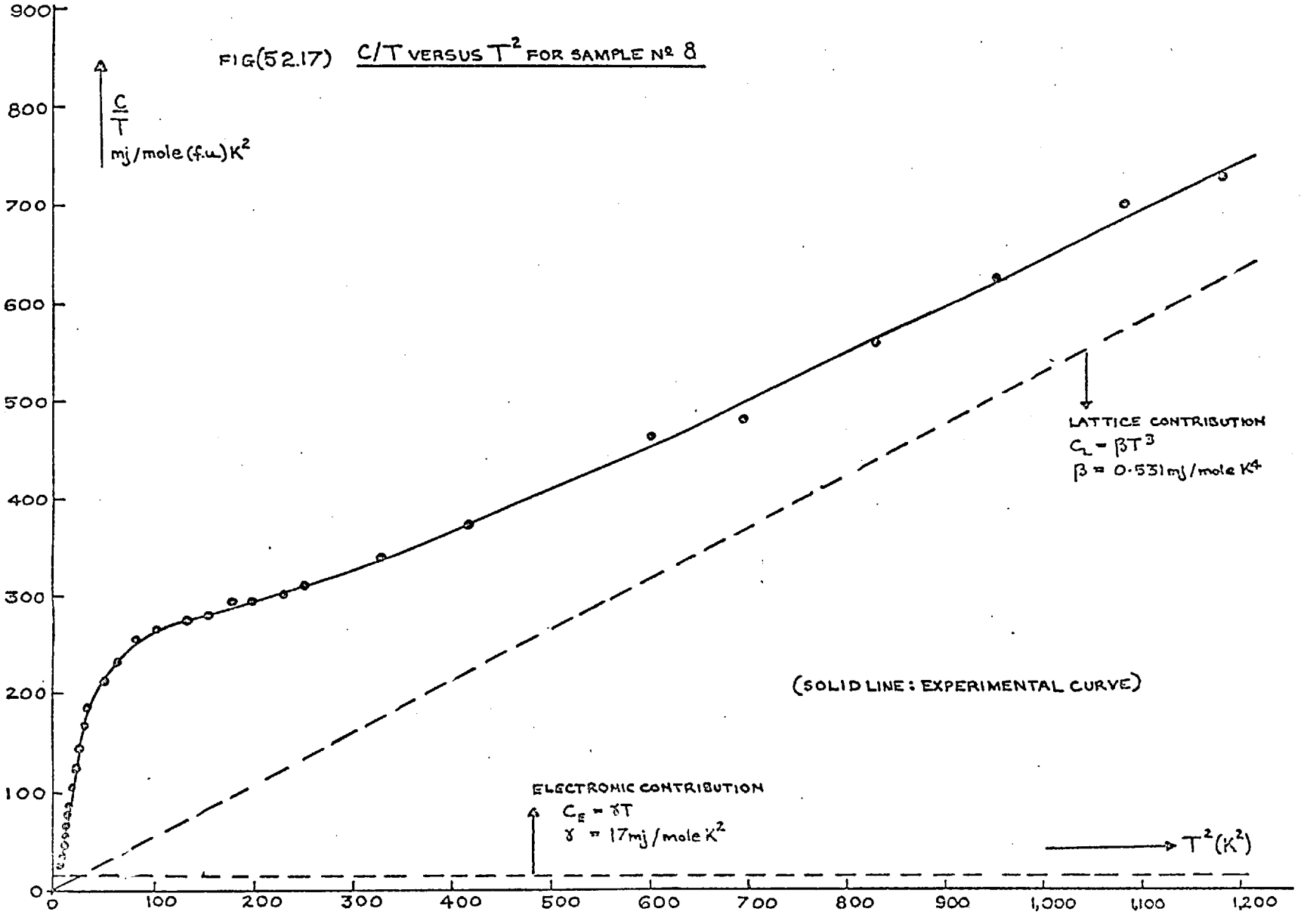


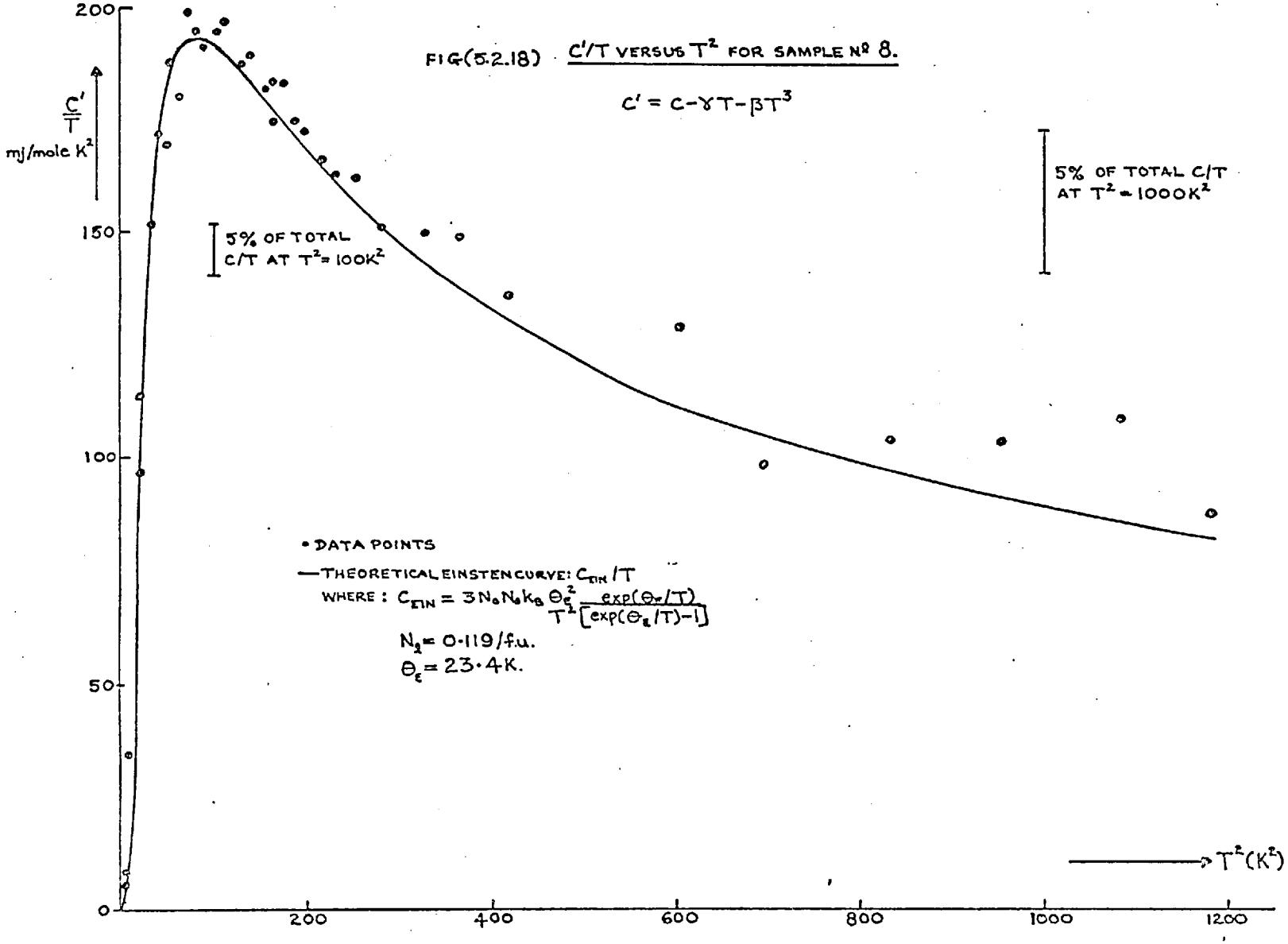


FIG(5.2.16) C'/T VERSUS T^2 FOR SAMPLE Nº 6

$C' = C - \gamma T - \beta T^3$

FIG(52.17) C/T VERSUS T^2 FOR SAMPLE Nº 8

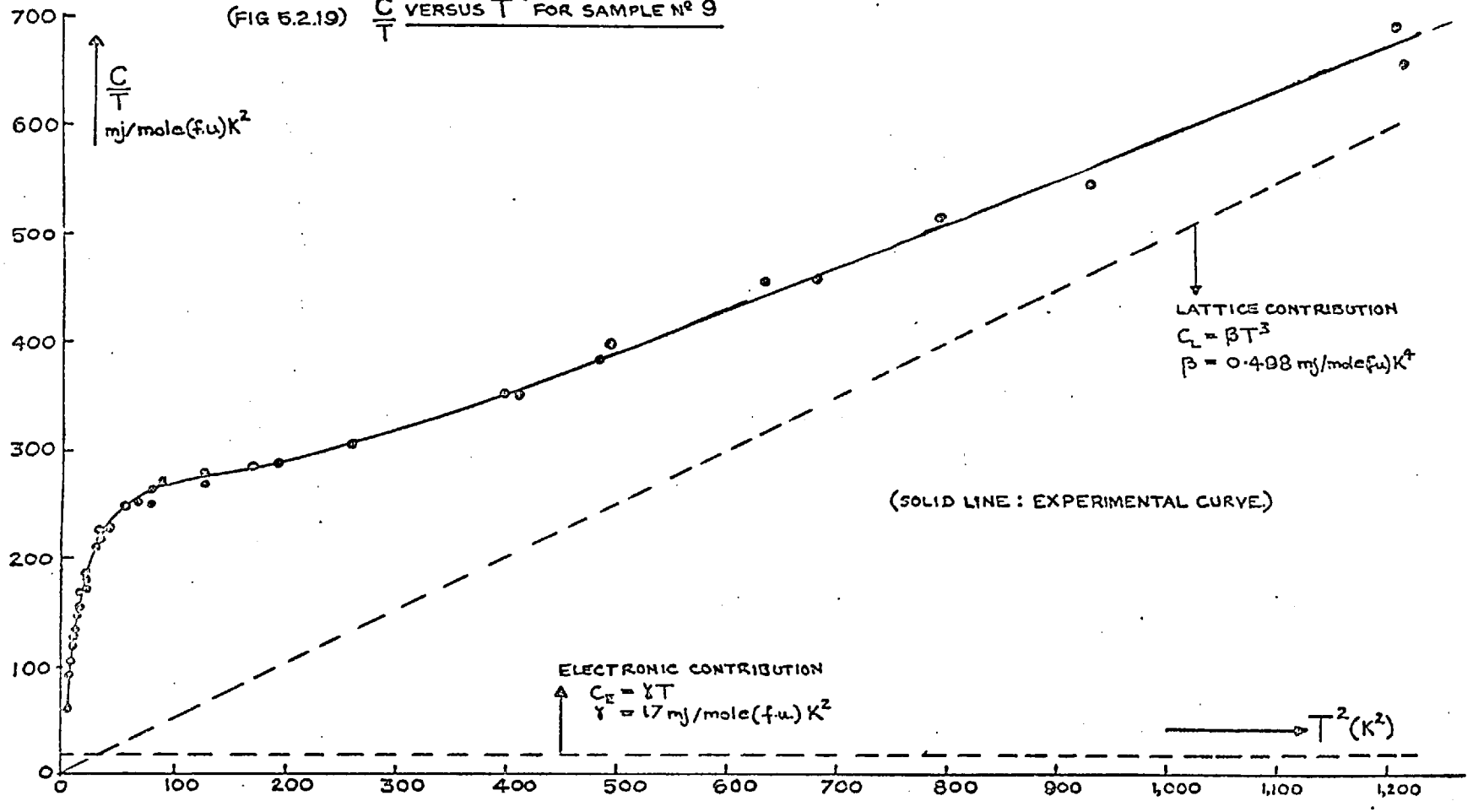




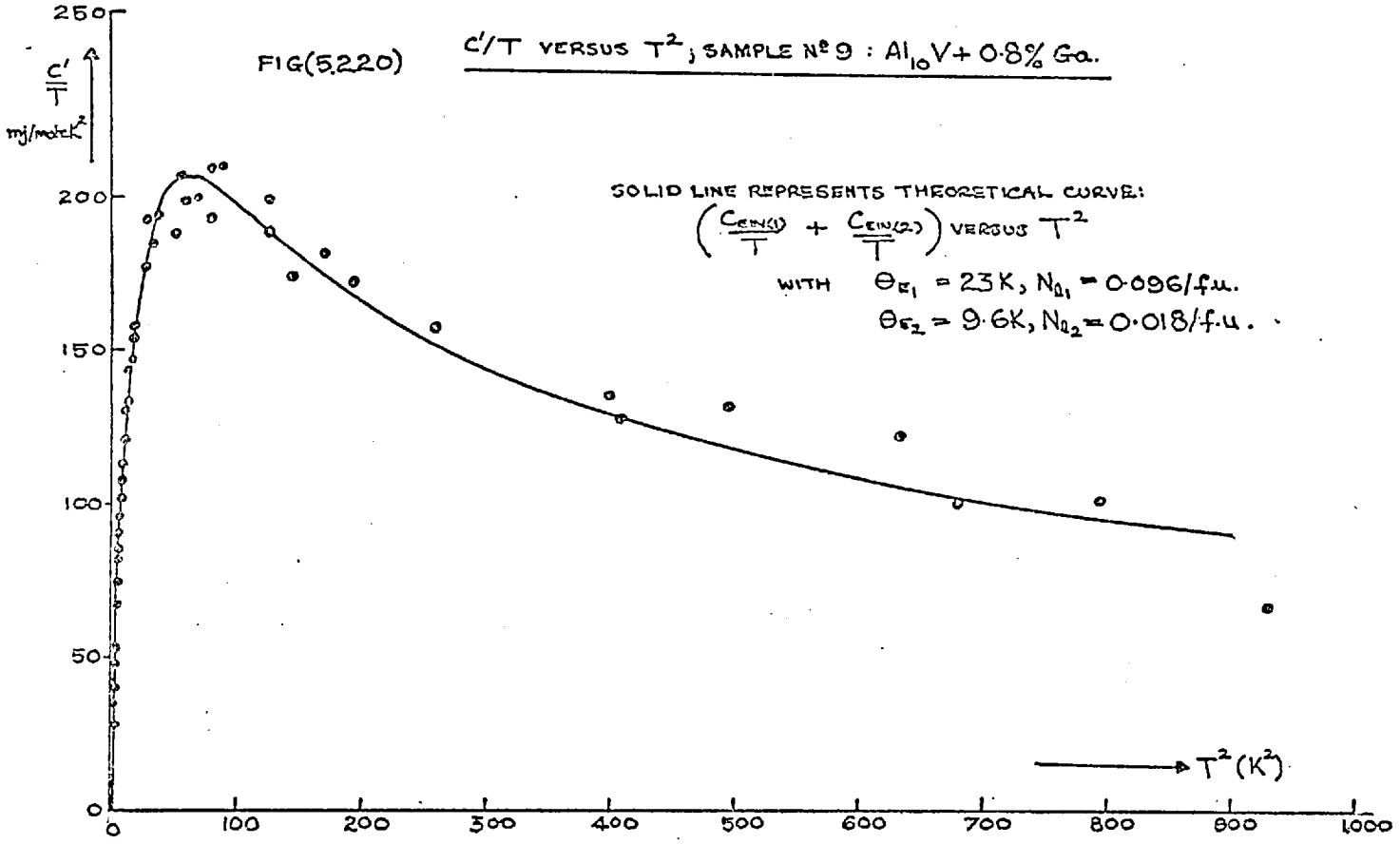
FIG(5.2.18) C'/T VERSUS T^2 FOR SAMPLE Nº 8.

$C' = C - \gamma T - \beta T^3$

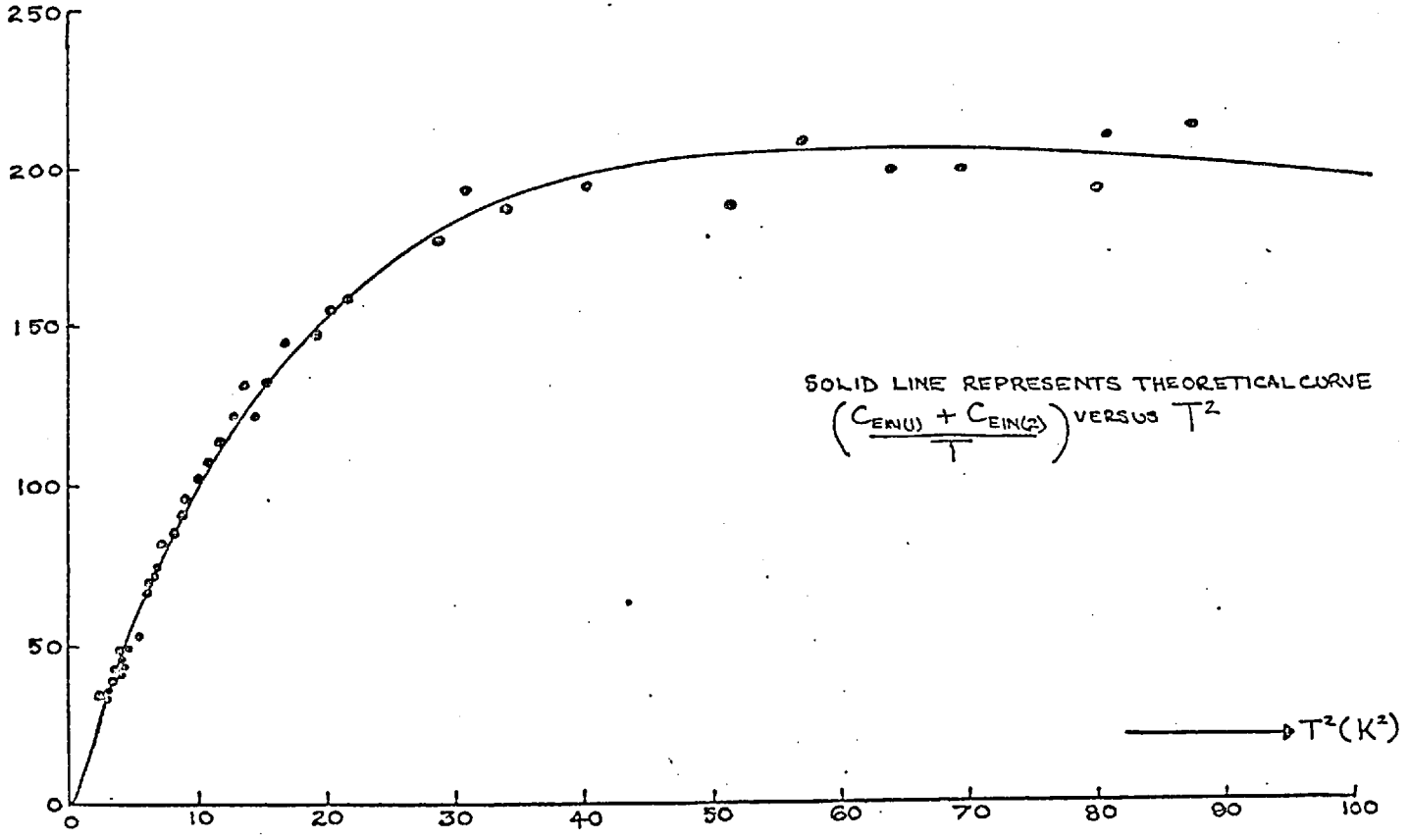
(FIG 5.2.19) $\frac{C}{T}$ VERSUS T^2 FOR SAMPLE Nº 9



FIG(5.220) C'/T VERSUS T^2; SAMPLE Nº 9 : $Al_{10}V$ + 0·8% Ga.



FIG(5.22) C'/T VERSUS T^2, FOR LOW TEMPERATURE ($T<10K$) DATA : SAMPLE Nº 9
$Al_{10}V + 0{\cdot}8\%$ Ga.

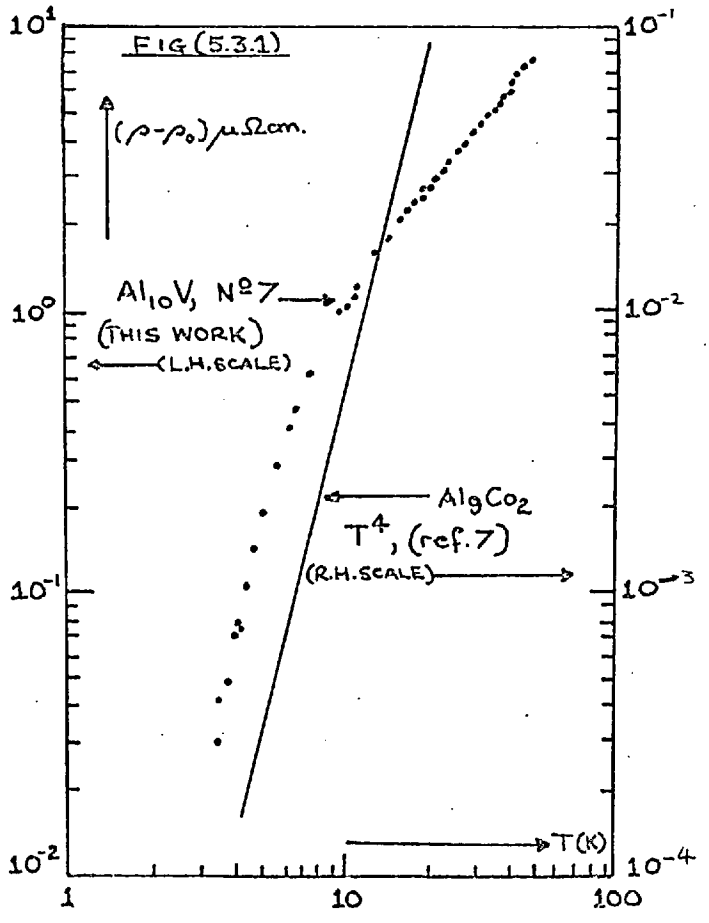


5.3 ELECTRICAL RESISTIVITY

INTRODUCTION

The electrical resistivity of four of the samples used in the specific heat work was measured in the temperature range 4 K to 50 K. Although there is large uncertainty in the absolute values due to the poor geometrical factor of the samples, the general form of the results show the resistivity to be highly anomalous and to fit well the expression given for the low temperature resistivity of an Einstein oscillator (see Chapter IV, 2(ii)b).

In Figure (5.3.1) the anomalous behaviour of the temperature dependent part of the electrical resistivity of $Al_{10}V$ is shown by comparing the results for sample No.7 with those for Al_9Co_2 (after Ref.7).



5.3.(i) METHOD OF MEASUREMENT

The standard four probe technique was employed using a conventional glass double dewar system. The sample current was supplied by a Tinsley

Current Stabiliser of stability of order one part in 10^6, and the potential readings taken using a Tinsley Galvanometer Amplifier and a secondary galvanometer. This arrangement is able to read voltages to 1 nV.

Details of the apparatus and experimental procedure may be found in reference (47).

Attachment of Leads

To achieve uniform current distribution throughout the samples, (which are of the order of 1 cm in diameter), the current leads were attached to copper plates soldered over the ends of the samples. The potential leads (27 gauge Eureka) were spot welded to the sides of the samples a few millimetres from the ends. Eureka was used as this was the only material found that could be successfully spotwelded to the samples.

The Geometrical Factor

The geometrical factor is given by A/ℓ, where A is the mean cross-sectional area and ℓ the distance between the potential leads.

To evaluate A/ℓ, the density (d) of the samples was measured using Archimedes principle and A then calculated from :-

$$A = m/dL$$

where m = sample mass

L = sample length.

ℓ was measured using Vernier calipers.

The geometrical factors for the four samples measured are listed below together with their resistance ratios ($R_{300}/R_{4.2}$ = Room Temperature Resistance / 4.2 K Resistance) and residual resistivities.

TABLE 5.3.1

Sample No.	A/ℓ cm	$\frac{R_{300}}{R_{4.2}}$	ρ_o $\mu\Omega$.cm
6	1.04	12.02	5.83
7	1.33	11.60	6.09
8	3.57	4.94	44.80
9	2.08	4.58	15.76

5.3.(ii) ANALYSIS OF DATA

As stated in Chapter IV, the low temperature, temperature dependent part of the resistivity for an Einstein oscillator is given by :-

$$\rho(T) = \frac{KTC_E}{M\Theta_E^2 k_B} = ATC_E \qquad (5.4)$$

At low temperatures this term will dominate and so ignoring the phonon contribution the measured resistivity may be expressed as :-

$$\rho = \rho_o + ATC_E \qquad (5.5)$$

To evaluate the residual resistivity, ρ_o , therefore, $C_E T$ is plotted against ρ to give a straight line of gradient A and intercept ρ_o . C_E is calculated using the parameters N_ℓ , and Θ_E as evaluated from the specific heat data.

To estimate the residual resistivity of the gallium doped sample (No.9) it is assumed that the scattering strengths of the loosely bound aluminium and gallium atoms are the same. The resistivity may then be expressed as

$$\rho = \rho_o + B\left(C_{E(1)}T + C_{E(2)}T\right). \qquad (5.6)$$

The temperature dependent part of the resistivities are shown in Figures (5.3.2) to (5.3.5) together with the theoretical curves.

5.3.(iii) ESTIMATED ACCURACY OF RESISTIVITY DATA

Due to the bad geometrical factor the resistance of the samples is very small (of the order of 10 $\mu\Omega$ at 4K), with a measuring current of 500 mA,

and reading the voltage to 10 nV there is an uncertainty of the order 4 in 10^3 in the measured resistance R. The large uncertainties in the values of ρ_o evaluated from the $C_E T$ against ρ plots are quoted below in Table (5.3.2).

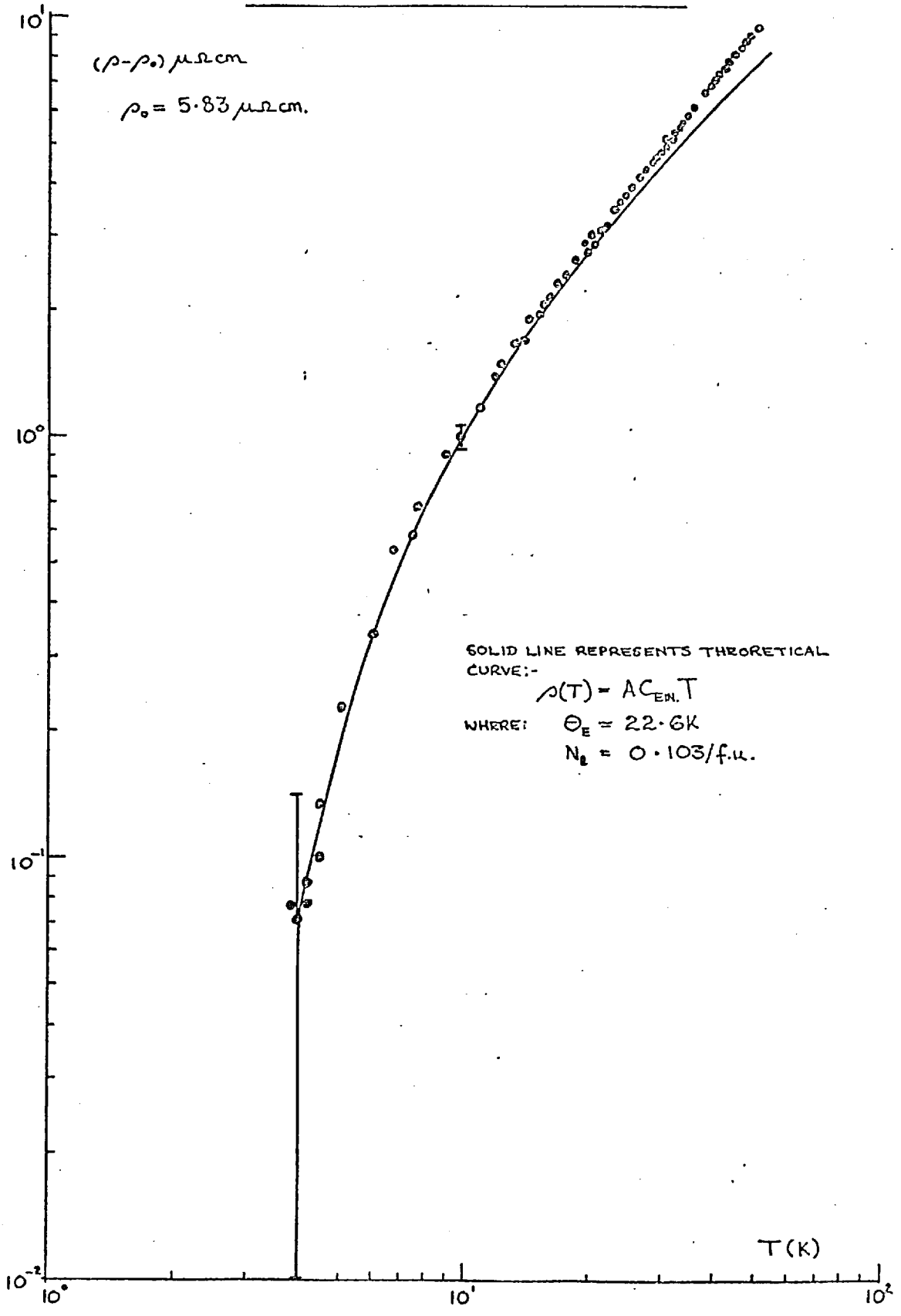
TABLE 5.3.2

Sample No.	6	7	8	9
ρ_o ($\mu\Omega$cm)	5.83 $\pm$ .05	6.09 $\pm$ .06	44.8 $\pm$ .40	15.76 $\pm$ .21

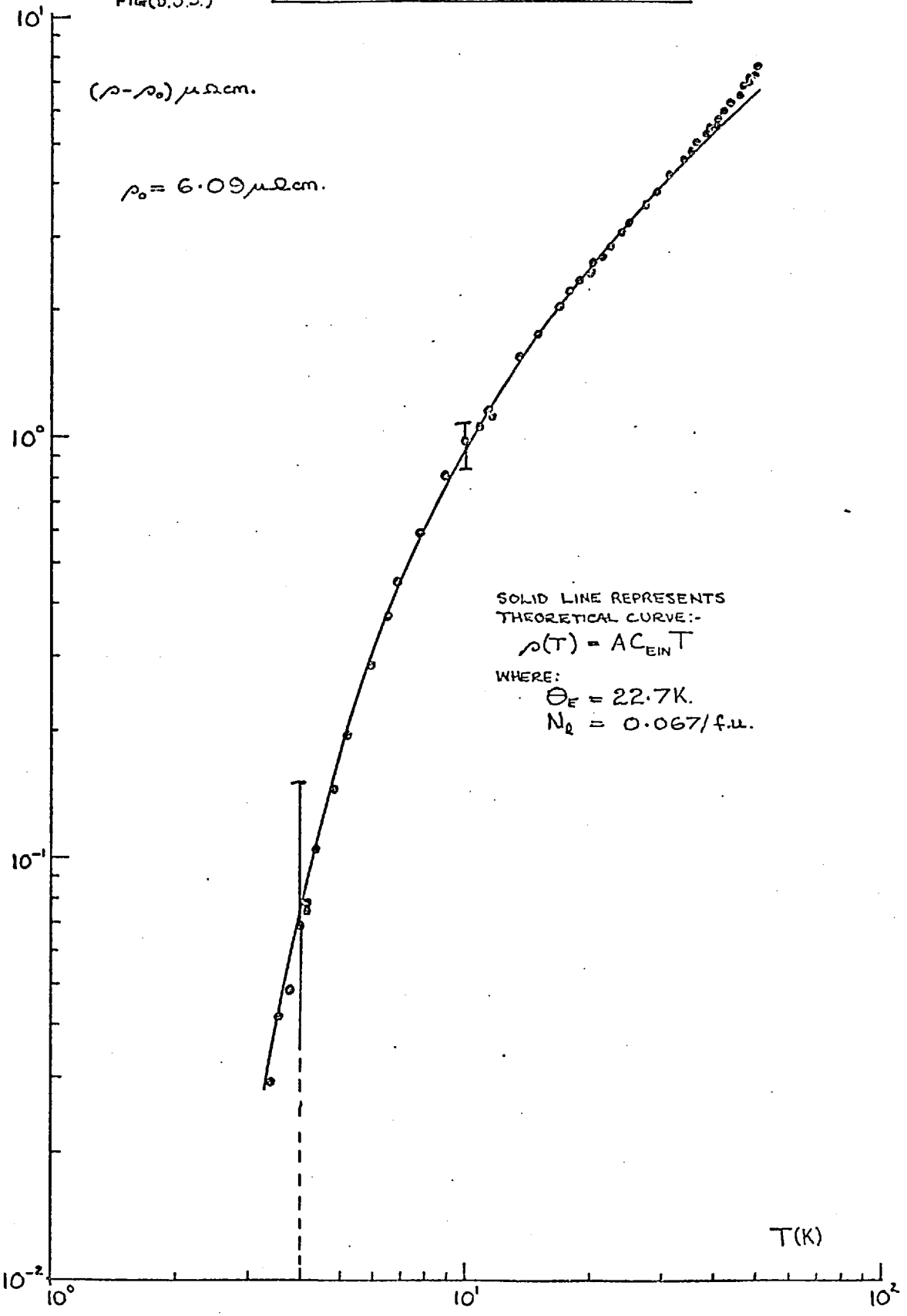
The error bars shown in Figures (5.3.2. to 5.) show the resultant large uncertainty in ρ (T) at low temperatures.

The absolute resistivity is highly uncertain as is indicated by the apparently spurious results from Sample No.8, (where the results are higher than those for the other samples by a factor of at least 3). The suspected cause of this is bad current distribution due to poor contact between the copper plates and sample ends.

FIG(5.32.) ELECTRICAL RESISTIVITY OF SAMPLE Nº 6



FIG(5.33.) ELECTRICAL RESISTIVITY OF SAMPLE Nº 7.



FIG(5.3.4) ELECTRICAL RESISTIVITY OF SAMPLE Nº 8

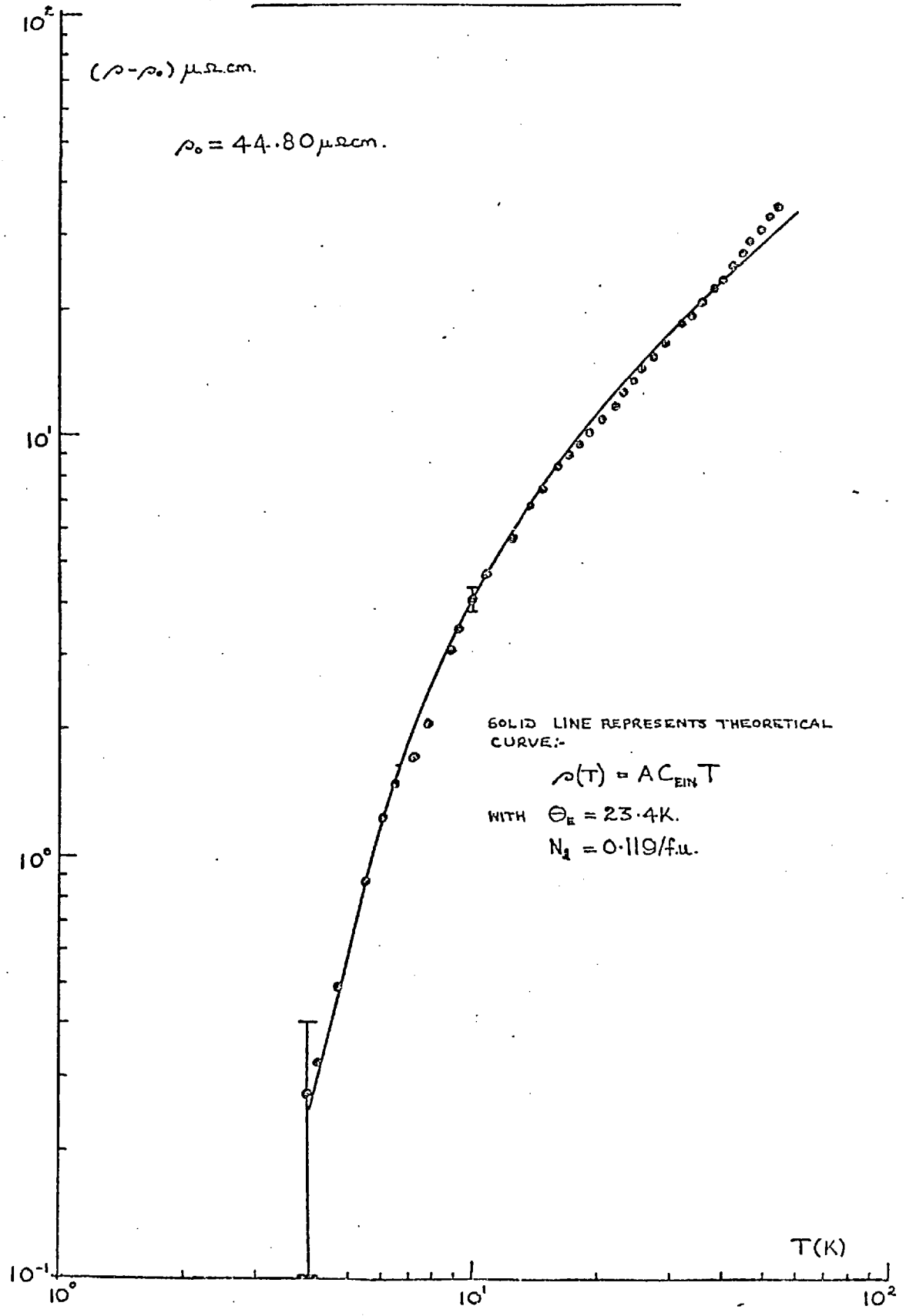
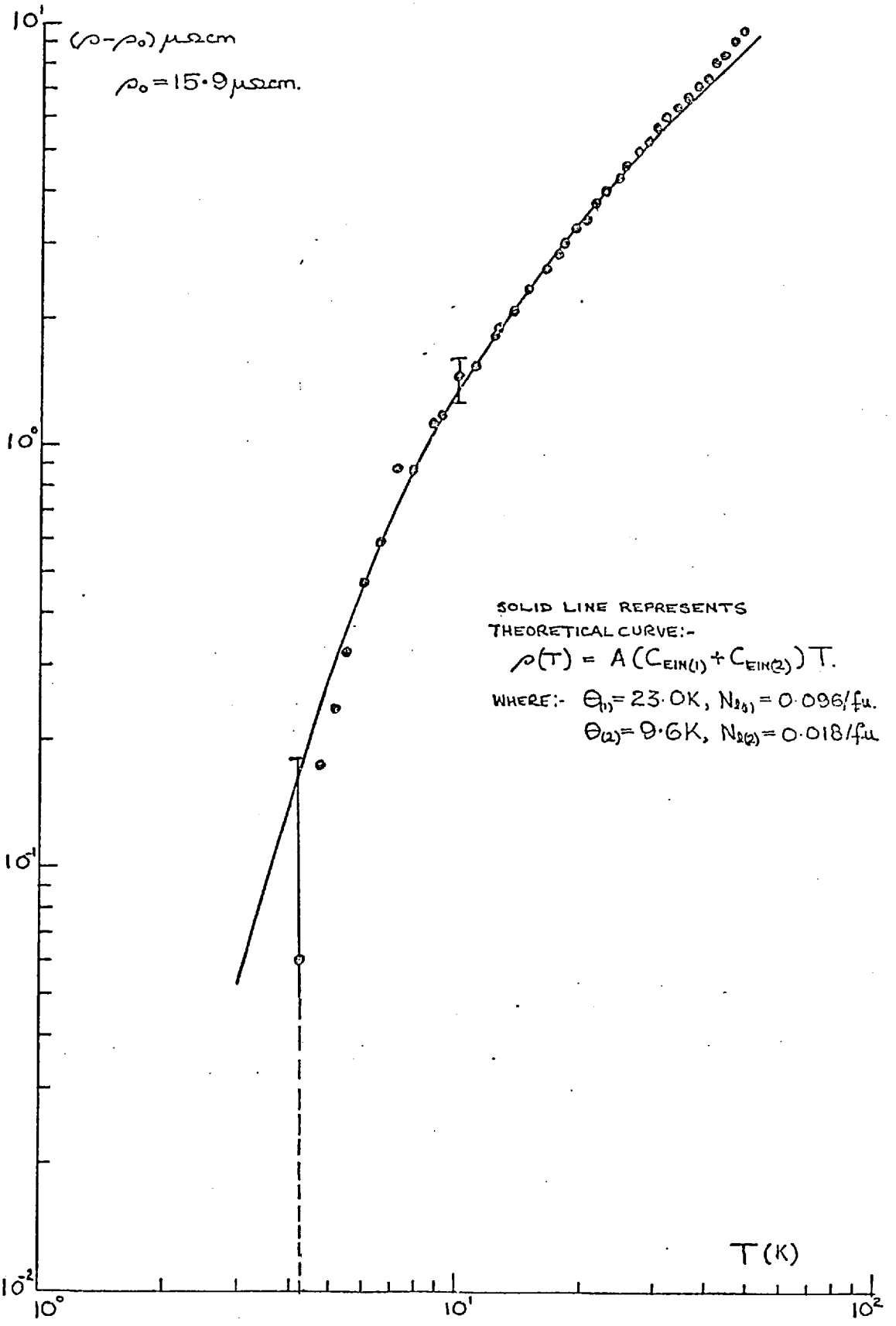


FIG (5.3.5) ELECTRICAL RESISTIVITY OF SAMPLE Nº 9: $Al_{10}V$+0·8% Ga.



5.4 INELASTIC NEUTRON SCATTERING FROM $Al_{10}V$

INTRODUCTION

Neutron experiments are the most valuable sources of data available on phonon energies. Neutrons may be collimated into beams having both momentum and energy comparable with the corresponding phonon values. This is in contrast with photons; in the infra-red region the photon energies are comparable with phonon energies but their momenta are negligible compared to that of phonons, whereas X-rays carry momenta comparable to phonon momenta but have energies six orders of magnitude larger.

In the case of $Al_{10}V$ the local mode energy (2 meV) is of the order of thermal neutron energies, and therefore the energy change on scattering should be relatively large and easily detectable. A high flux reactor was required for the investigation of $Al_{10}V$ as the concentration of loose atoms in the compound is low (of the order of 1% of the total), aluminium has a small scattering cross-section and the size of the sample available was small (approximately 5 cm^3).

The condition for energy conservation to be satisfied for the scattering process (considering energy loss since we are working at low temperature) is given by :-

$$E_i - E_f = \frac{\hbar^2 k_i^2}{2m} - \frac{\hbar^2 k_f^2}{2m} = \hbar\omega_{osc}$$

where E_i and k_i are the incident neutron energy and wave vector respectively, and, E_f and k_f the final energy and wave vector. ω_{osc} is the local mode frequency, and from the specific heat data $\hbar\omega_{osc}$ = 2 meV. For this work an incident neutron energy of 10 meV was used.

Although aluminium is primarily a coherent scatterer the loose aluminium atoms giving rise to the local excitations are "randomly" distributed, which gives a scattering cross-section effectively like an incoherent one, i.e. no momentum conservation.

5.4.(i) ROTATING CRYSTAL TIME OF FLIGHT SPECTROMETER, IN4.

The neutron work on $Al_{10}V$ was carried out on the high flux reactor at ILL, Grenoble, using IN4, a rotating crystal time-of-flight (TOF) spectrometer which is shown in Fig.(5.4.1). The variable temperature, He^4 cryostat used for low temperature measurements is not shown in the diagram. This apparatus is useful for scattering measurements over a large range of energy and momentum transfers, with typical values of 2 and 4% for the momentum and energy resolution respectively.

The use of the double monochromator (primary spectrometer) reduces the background of epithermal neutrons to give a good peak to background ratio. When used with both the single crystals (pyrolytic graphite) rotating, order contamination is eliminated. The resultant monochromatic beam, which is pulsed in time, thus determines the incident energy (E_i) and wave vector (k_i). The monochromator frequency is variable and was set at 120 Hz for this work, giving a time interval between consecutive pulses of 4.2 msecs.

The secondary spectrometer consists of an aluminium housing of radius 4m, at the end of which there are 67 positions for the detector boxes. The 35 detector boxes (each of which contains six He^3 detectors, six pre-amplifiers, and a high voltage supply) may be distributed as required over the periphery of the aluminium housing. The smallest scattering angle measured in these experiments was 52^o and the largest 158^o.

The TOF distribution of the scattered neutrons is measured with a TOF analyser with 128 input channels. Data is collected and summed by the data acquisition system Nicole (Telefunken TR 86) in order to obtain the TOF distribution.

Five samples (numbers 3,5,6,7 and 8) were used giving a total sample mass of 9 grammes and volume approximately 5 cm^3. The samples

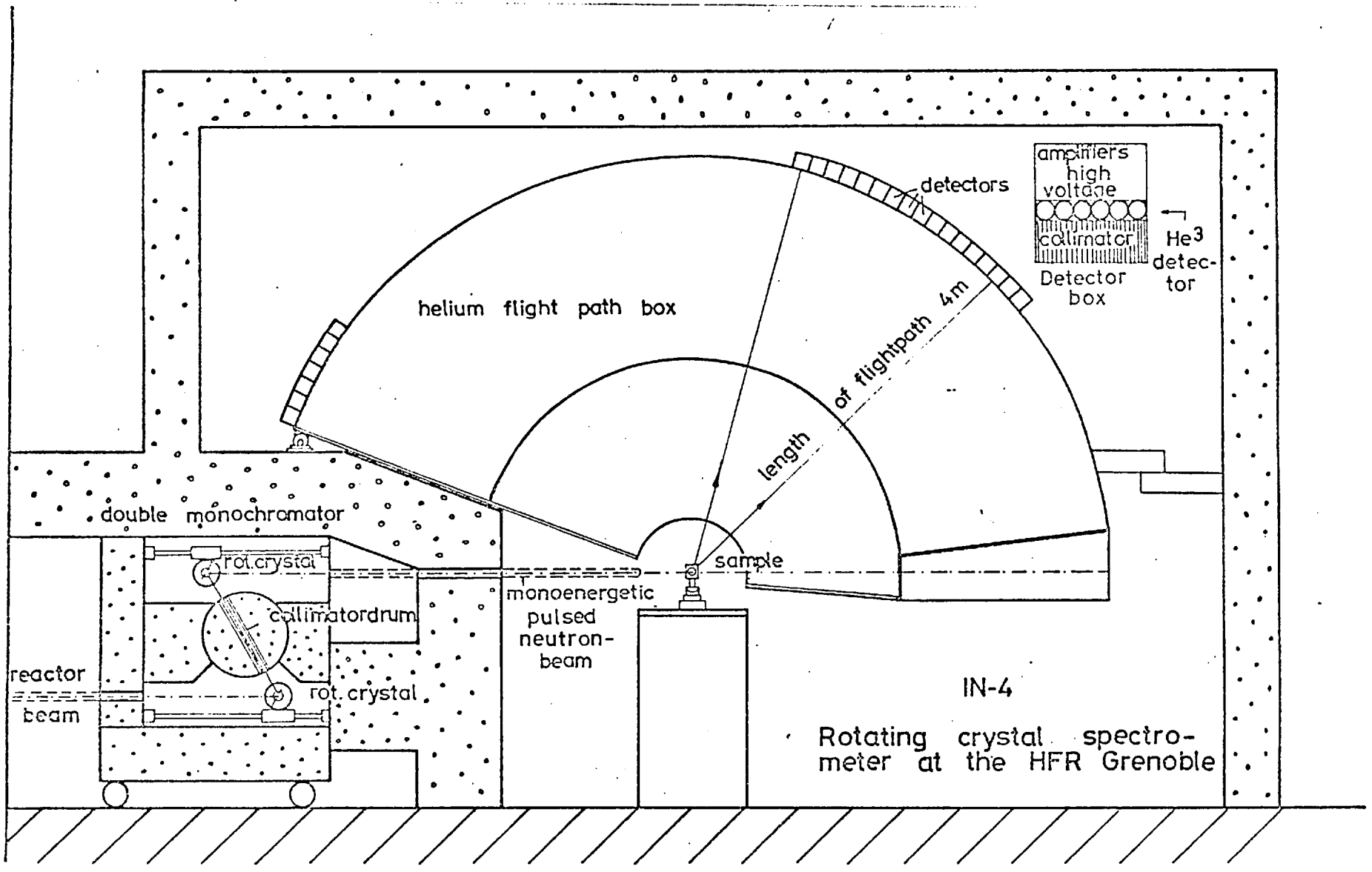


FIG (5.4.1) ROTATING CRYSTAL TIME OF FLIGHT SPECTROMETER.

were secured in an aluminium sample holder and the neutron beam was masked down to sample size using cadmium sheeting.

5.4.(ii) RESULTS

Experiments were carried out at 4.8K, 31K, and 49K for an average counting time of about 24 hours. Figure (5.4.2) shows the corrected neutron counts (Y_C) against energy transfer for these three temperatures, at the mean scattering angles (Θ) indicated on the diagram. Y_C are the neutron counts normalised for instrumental effects to an absolute scale using vanadium. The units of Y_C are those of $1/\Delta\tau$ where $\Delta\tau$ is the channel width in μsec/m.

The 4.8K data shows a well defined peak at 2.05 meV $\equiv$ 23.8K, in good agreement with the characteristic temperature (23 ± 1K) of the first excited state for the local mode as evaluated from the specific heat data. There is some indication also of a second leval at an energy of 4 meV. At 31K the first level is much less well defined and at 49K no peak is visible.

The differential scattering cross-section per loose aluminium atom has been estimated from the 4.8K data, from the expression :-

$$\frac{d\sigma}{d\Omega} = \frac{N_{osc.}}{N_s}\frac{\sigma_s}{4\pi}.\Delta\tau.\sum_{peak} Y_c \quad . \tag{5.7}$$

where N_{osc}, N_s, and σ_s are : the number of oscillators, the total number of atoms and the scattering cross-section for the sample respectively.

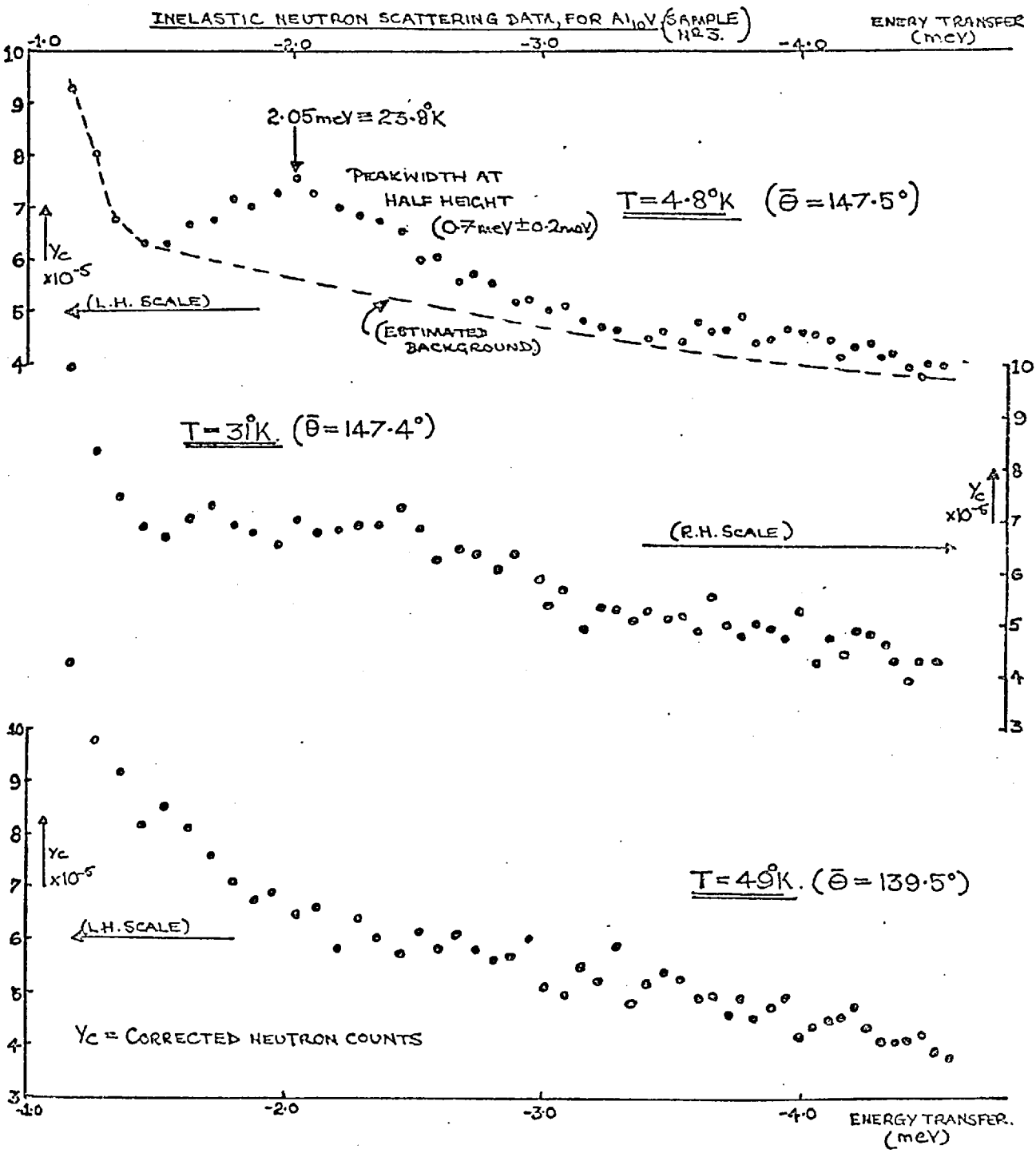
The estimated background subtracted before summing the counts over the peaks is indicated by the dashed line in Fig.(5.4.1), and is only good to about 25%.

The following values of $d\sigma/d\Omega$ have been determined from the 4.8K data :-

1st peak $d\sigma/d\Omega \simeq 10^{-2}$ barns steradian^{-1} per oscillator.

2nd peak $d\sigma/d\Omega \simeq .2 \times 10^{-2}$ barns steradian^{-1} per oscillator.

FIG(5.4.2.)



N.B. ELASTIC PEAK WIDTH AT HALF HEIGHT = 0·5meV.

5.5 THERMAL EXPANSION

The thermal expansion of sample number 3 has been measured by Dr. P. Lanchester of Southampton University. Figure (5.5.1) shows the linear coefficient of thermal expansion ($\alpha = \frac{1}{l}\frac{dl}{dT}$) against temperature, as compared to that of aluminium. The expansion is seen to be anomalously large.

The Gruneisen parameter, γ_G , is given by :-

$$\gamma_G = \frac{3\alpha BV}{C_v} \tag{5.8}$$

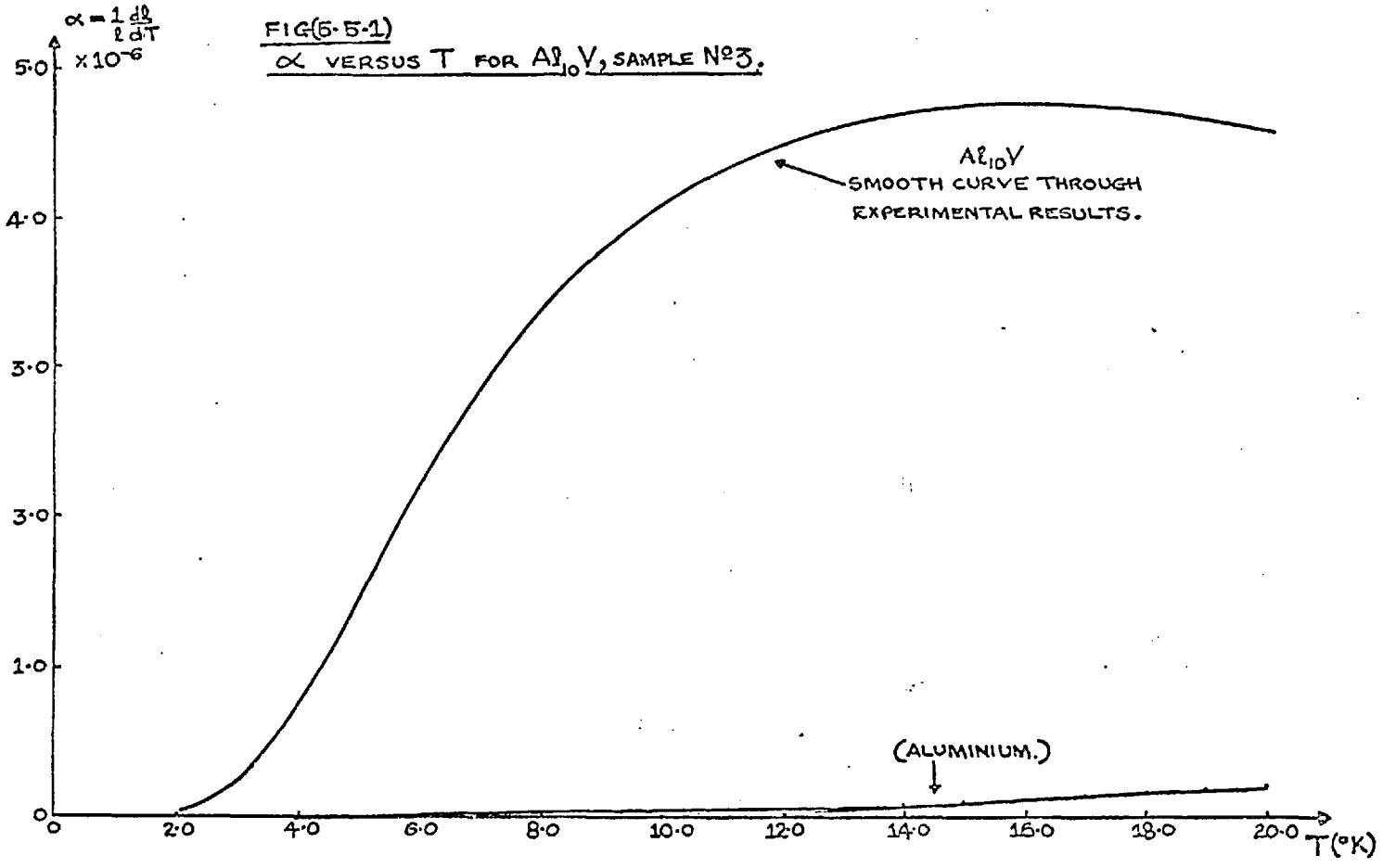
where B is the bulk modulus (which is unknown for $Al_{10}V$) and V the volume. In Figure (5.5.2), (γ_G/B) is shown as a function of temperature, as evaluated from the smoothed thermal expansion and specific heat data. The scale on the right-hand side of this graph indicates γ_G evaluated using the bulk modulus for aluminium of 0.79×10^{12} dynes cm^{-3}. For comparison γ_G for aluminium is also shown; this was evaluated from the lattice (γ_l) and electronic (γ_e) contributions given on the diagram; from the equation :-

$$\gamma_G C_{Total} = \gamma_e C_e + \gamma_l C_l \tag{5.9}$$

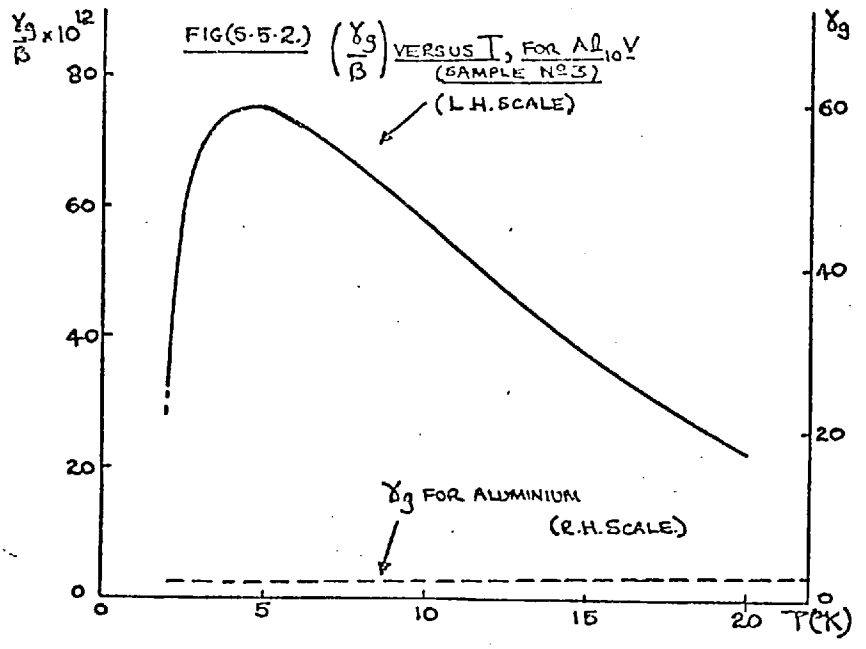
Up to about 10 K the lattice and electronic contributions to the expansion of $Al_{10}V$, if taken as those of aluminium, are negligible. On this basis the local mode contribution to γ_G, γ_{lm}, may be expressed as :-

$$\gamma_{lm} = \alpha 3BV/C_{EIN.} \tag{5.10}$$

and is found to be constant up to about 8 K. Figure (5.5.3) shows α plotted against C_{EIN}, in the linear region γ_{lm} is found to be 84.



FIG(6·5·1)
α VERSUS T FOR $Al_{10}V$, SAMPLE Nº3.

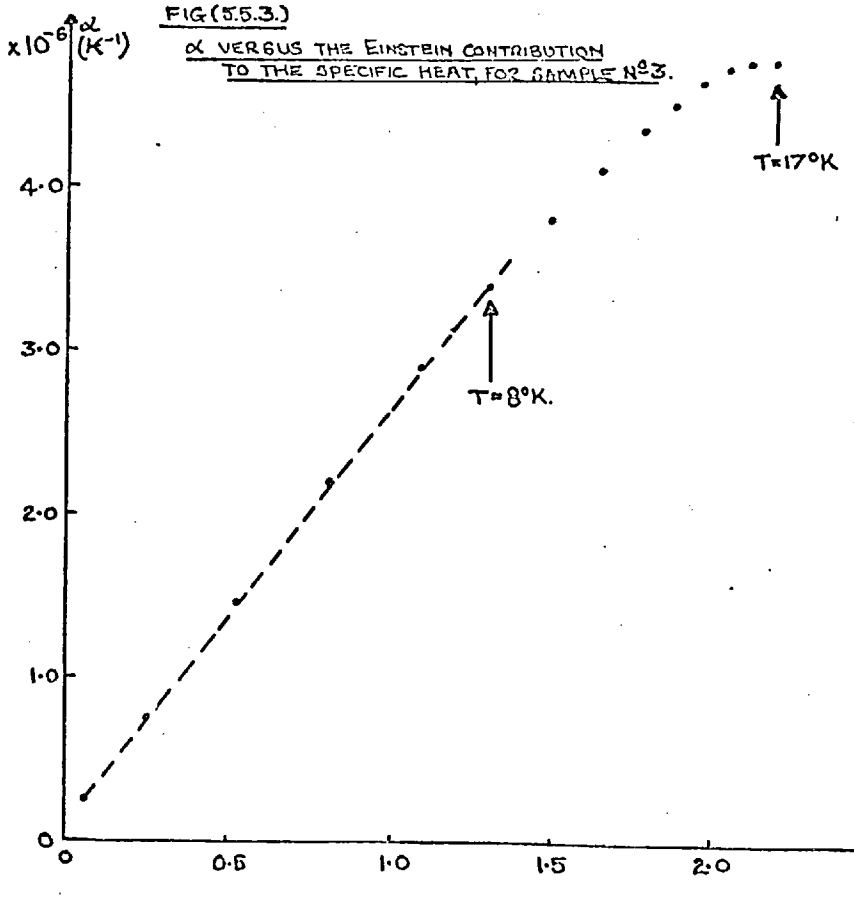


FIG(5·5·2.) $\left(\frac{\gamma_g}{\beta}\right)$ VERSUS T, FOR $Al_{10}V$ (SAMPLE Nº3)

FOR ALUMINIUM:

$\gamma_{electronic} = 1.8 \pm .1$

$\gamma_{lattice} = 2.65 \pm .15$



FIG(5.5.3.)

α VERSUS THE EINSTEIN CONTRIBUTION TO THE SPECIFIC HEAT, FOR SAMPLE Nº3.

CHAPTER VI

DISCUSSION AND CONCLUSIONS

INTRODUCTION

As stated in an earlier chapter the low temperature heat capacity and electrical resistivity measurements of Caplin et al (38) indicate the presence of a very low frequency local mode, of Einstein character, in $Al_{10}V$. The aim of this work was to further investigate this local mode. In this chapter the implications of the experimental results presented in Chapter V will be discussed and the results of calculations of the interatomic pseudo-potential seen by the low frequency oscillator are presented. One section of the chapter is devoted to a consideration of certain local mode systems which exhibit some similar characteristics to those of $Al_{10}V$, although no truly analogous system has been found.

6.1 DISCUSSION OF EXPERIMENTAL RESULTS

6.1.(i) Specific Heat Data

The coefficient of the electronic contribution to the heat capacity, for all the samples of $Al_{10}V$ measured, was found to be (17.0 ± 1.4) mj/mole(fu)K^2, which gives a value of (1.55) mj.K^{-2} per mole of average atom. Although this is high compared to the values reported (7) for the other aluminium-rich Al-T3 compounds (where γ lies in the range 0.96 to 1.3 mj.K^{-2} per mole of average atom) it is consistent with the values for the other Al-V compounds of 1.5 mj.K^{-2} for Al_3V and 1.6 mj.K^{-2} for Al_7V. (See Fig.(4.1.2)).

The vibrational contribution to the heat capacity is highly anomalous. The excess heat capacity over the "normal" lattice term (βT^3) is seen to fit the Einstein expression very well. The Einstein temperature, Θ_E , is found to be 23.0 ± 1.3 ^oK for all the $Al_{10}V$ samples measured, whereas

the number of oscillators (N_ℓ / formula unit) varies from sample to sample; ranging from 0.051/fu (approximately 10% filling of the vacant sites, assuming three dimensional oscillators) in sample No.5 to 0.119/fu (approximately 24% filling) in sample No.8. There appears to be a correlation between the "normal" lattice contribution to the specific heat and the number of oscillators present in a given sample. Even accounting for the large uncertainty in β, there is a significant trend as N_ℓ increases for β to increase (see Table (6.1.1)).

TABLE (6.1.1)

Comparison of the coefficient of the lattice contribution (β) to specific heat and number of oscillators per formula unit (N_ℓ) for each sample

Sample No.	β ± 10%	N_ℓ ± 1%
5	.386	.051
7	.404	.067
6	.481	.103
3	.504	.103
8	.531	.119

The increase in β with N_ℓ is thought to be explicable in terms of hybridization of the local modes with the band phonon modes. Fig.(6.1.1a) shows the dispersion curve for a system having Einstein modes at ω_E and $2\omega_E$, and lattice modes represented by the Debye approximation. Fig.(6.1.1b) shows the proposed dispersion curve for $Al_{10}V$ with some hybridization between the local and band modes. This effectively increases the number of modes at frequencies just greater than ω_E ($\equiv$ 23 K), which corresponds to the temperature region in which β is evaluated.

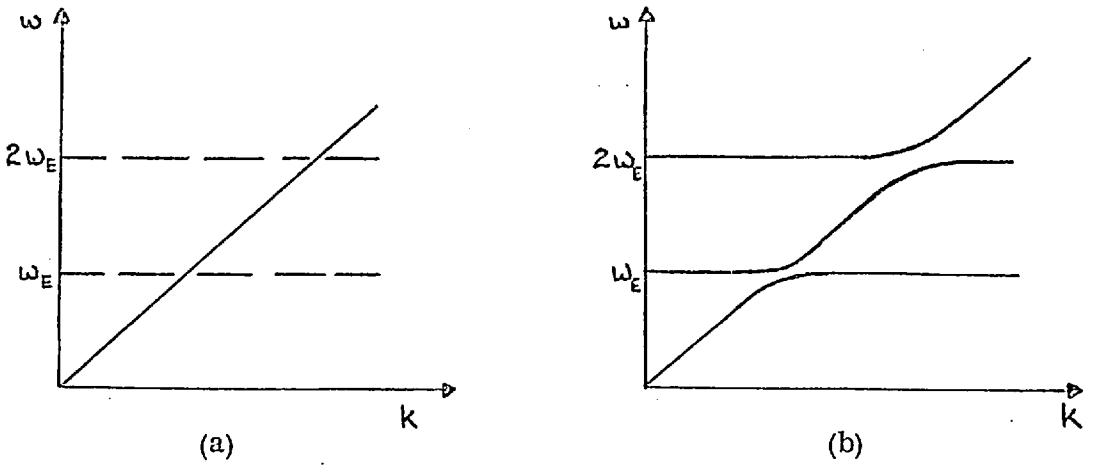


FIGURE (6.1.1)

6.1.(ii) ELECTRICAL RESISTIVITY

As shown in the previous chapter the electrical resistivity of $Al_{10}V$ is highly anomalous both in magnitude and in the form of its temperature dependence (see Chapter V, Figure (5.2.1)). Although as stated, the uncertainty in the absolute value of the resistivity is large, the values for samples 6, 7 and 9 are in reasonable agreement with the results of Caplin, Grüner and Dunlop (38). The poor quality of the samples used for these resistivity measurements is reflected in Table (5.3.1) where their geometrical factors, resistance ratios and residual resistivities are given.

For all four samples measured the temperature dependent part of the resistivity is well fitted (up to about 40K) by the expression given by Cooper (43) for the low temperature behaviour of an Einstein oscillator (see Chapter IV, (4.2(ii)). These results thus further substantiate the evidence for Einstein type oscillators in $Al_{10}V$, and the fact that the Einstein contribution is well pronounced up to at least 40 ^{o}K suggests the mode to have at least three levels above the ground state.

A convenient measure of the scattering strength of the transition metal atoms in the Al-T3 compounds is the high temperature gradient of the

temperature dependent part of the electrical resistivity ($d\rho/dT$) divided by the fraction, f , of T3 atoms in the compound. Figure (6.1.2) below shows this quantity across the series of aluminium-rich Al-T3 compounds. It is seen that the value for $Al_{10}V$ obtained from this work agrees in general magnitude with the results for Al_3V reported by Dunlop et al (7).

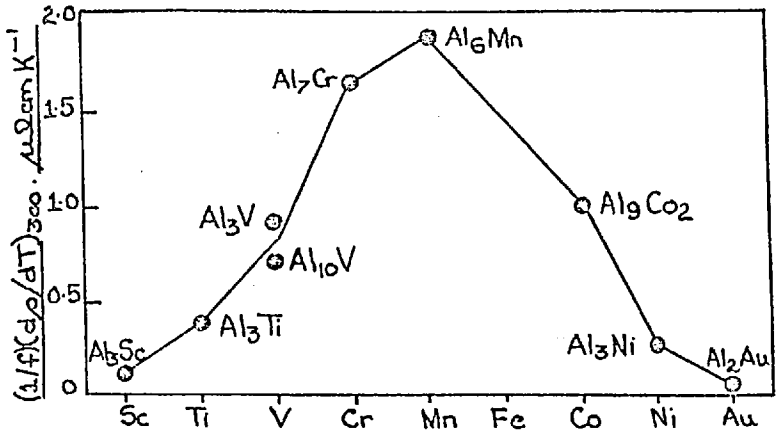


FIGURE (6.1.2)

This is indicative that at high temperature the local mode is no longer well defined. If there was still a well defined local mode then there would be a large contribution to $\frac{1}{f}\left(\frac{d\rho}{dT}\right)$ from the loose atoms, given by the high temperature limit of Equation (4.3).

i.e. for $T \gg \Theta_E$:- $\rho_{EIN}(T) = KNT/M\Theta_E^2$

To give :-

$$\frac{1}{f}\left(\frac{d\rho}{dT}\right) = \frac{1}{f}\frac{KN}{M\Theta_E^2} \simeq \cdot 5\,\mu\Omega cm/K$$

Hence if present, this additional contribution would nearly double the value expected on the basis of the reported results for Al_3V.

6.1.(iii) NEUTRON DATA

Although the scattering cross-section for the loose atoms is small, there is definite evidence from the low temperature (4.8K) data of a local mode at 2 meV and possibly some indication of a second level at twice this energy. The first level is no longer visible by 50 K.

The magnitude of the scattering cross-section for the second level (although highly uncertain) gives an indication that the local mode is behaving more like a harmonic oscillator than a rigid rotator. The experimental values of the low temperature differential scattering cross-section for the two levels have been compared with calculations of $(d\sigma/d\Omega)$ for (a) a harmonic oscillator and (b) a rigid rotator.

(a) $(d\sigma/d\Omega)$ for a harmonic oscillator

Marshall and Lovesey (48) give an expression for $(d\sigma/d\Omega)$ of a gas of isotropic harmonic oscillators, which simplifies for the case of the loose aluminium atom in $Al_{10}V$ (considering two levels) to :-

$$\frac{d^2\sigma}{d\Omega dE} = A^2 \frac{k_f}{k_i} \exp\left(-\frac{\hbar K^2}{2M\omega_o}\right)^2 \sum_{n=1}^{2} \frac{1}{n!} \left(\frac{\hbar K^2}{2M\omega_o}\right) \delta(\hbar\omega - \hbar\omega_o)$$

where :-

A = Coherent scattering length

K = Scattering vector

k_i and k_f are the initial and final wavevectors respectively

M = Oscillator mass

$\hbar\omega_o$ = Oscillator energy.

(b) $(d\sigma/d\Omega)$ for a rigid rotator

Zemach et al (49) derive an expression for $(d\sigma/d\Omega)$ for the scattering of neutrons by a single point scatterer constrained to move on the surface of a sphere. The energy loss part of Zemach et al's expression simplifies to give :-

$$\frac{d\sigma}{d\Omega} \simeq \frac{2}{3} A^2 (k_i b)^2 \frac{k_f}{k_i} (1 - \cos\theta)^{1/2}$$

where b is the radius of the sphere.

Marshall and Lovesey (48) derive an expression for the ratio of the differential scattering cross sections for the first and second excited

states of a rigid rotator. For the case of the loose aluminium atom in $Al_{10}V$ the expression reduces to :-

$$\frac{(d\sigma/d\Omega)_{1ST\ level}}{(d\sigma/d\Omega)_{2ND\ level}} \simeq \left(\frac{5!\,2!}{3!\,Kb}\right)^2 \simeq 400$$

The calculated cross sections for the local mode in $Al_{10}V$ are listed in Table (6.1.1) below together with the experimentally determined values. It is seen that the magnitude of $(d\sigma/d\Omega)$ for the second level, as evaluated from the experimental results, is indicative that the local mode is not a rotator.

TABLE (6.1.1)

Approximate Scattering Cross-Sections for the Loose Al atoms in $Al_{10}V$, in units of barns steradian^{-1} per loose atom

	$(d\sigma/d\Omega)$ (1st Level)	$(d\sigma/d\Omega)$ (2nd Level)
Experimental :-	10^{-2}	$\simeq 0.2 \times 10^{-2}$
Theoretical :-		
(a) Harmonic Oscillator -	3×10^{-2}	0.3×10^{-2}
(b) Rigid Rotator -	10^{-2}	$.003 \times 10^{-2}$

6.1.(iv) THERMAL EXPANSION DATA

The results of measurement of the thermal expansion presented in Chapter V, show an anomalously large contribution at low temperatures. Thermal expansion data are often presented in terms of the Gruneisen approximation, which can be written as :-

$$\beta = \Sigma_i \beta_i = (BV)^{-1} \Sigma_i \gamma_i C_{vi}$$

assuming that independent contributions to the thermal expansion ($\beta = 3\alpha$)

and to the heat capacity can be identified. In the simplest case the thermodynamic properties of each contribution depend only on a volume dependent characteristic energy ($k_B\Theta_i$) and then; $\gamma_i = -\frac{d\ln\Theta_i}{d\ln V}$. γ_i is typically 1 to 5 for most thermal properties, whereas in the case of $Al_{10}V$, we have a value of 84 for γ local mode; ($k_B\Theta_i$ here corresponds to the oscillator energy $k_B\Theta_{EIN}$).

This anomalously large contribution to the thermal expansion is hence taken to be indicative of a strong volume dependence of the structure of the local mode energy levels.

6.1.(v) DISCUSSION OF RESULTS ON DOPED SAMPLES OF $Al_{10}V$

The results of low temperature specific heat and electrical resistivity measurements on one doped sample of $Al_{10}V$ are presented in the previous chapter (sample No.9, $Al_{10}V$ + ·8% gallium).

The specific heat data shows two Einstein terms contributing to the excess specific heat, consistent with a 19% filling of vacant sites by aluminium atoms and a 4% filling by gallium atoms. This shows a preferential occupancy of the vacant sites by the gallium atoms. The contribution from the gallium atoms gives an Einstein temperature of about 9.6K, distinctly lower than for the aluminium atoms, as would be expected from the larger atomic mass of gallium.

Further investigations are being carried out, by Miss J. Turner at Imperial College, into samples doped with other elements and preliminary data on the electrical resistivity of a thallium doped sample ($Al_{10}V$ + ·8% thallium) is indicative of a second Einstein term of characteristic temperature obviously lower than that for gallium and probably around 6K.

6.2 INTERATOMIC PSEUDOPOTENTIAL FOR THE "LOOSE" Al ATOM IN $Al_{10}V$

The low frequency local mode in $Al_{10}V$, identified from the specific heat data, is attributed to the occupancy of some of the 8(b) sites by aluminium atoms, which are very loosely bound and may be envisaged as being situated in cages of aluminium atoms. These loose atoms are well spaced from the surrounding atoms, having twelve neighbours at 3.18 Å and four at 3.14 Å (compared to the nearest neighbour distance in metallic aluminium of 2.86 Å).

The interatomic pseudopotential has been calculated* in three crystallographic directions for the "loose" atom in its cage of aluminium atoms, using two different values for the Fermi wavevector (k_F).

The values used were :-

(1) k_F = 0.9256 a.u. = k_F for metallic aluminium.

(2) k_F = 0.8723 a.u. = 0.94 k_F for metallic aluminium.

The values of k_F were chosen by estimating the possible electron density of the relevant neighbouring Al atoms (16(d) and 96(g)) with respect to their neighbours.

Both calculations gave the same form for the pseudopotential, i.e. steep sided with a high central maximum having minima approximately 0.4 Å off-centre. The validity of the model may be further checked by estimating the Debye temperature for aluminium from the second derivative of the potential (d^2U/dz^2) at the nearest neighbour distance for metallic aluminium (2.86 Å),

* The pseudopotential calculations were carried out by Dr. M.W. Finnis of A.E.R.E. Harwell. For details of the model used see reference (50), the model potential parameters used were those of Appapillai, reference (51).

i.e. by evaluating the harmonic oscillator frequency :-

Let; $\alpha = \frac{1}{2}\frac{d^2U}{dz^2}$

then the total energy, E, is given by :-

$$E = \frac{1}{2} M\dot{z}^2 + \alpha z^2$$

where M is the mass of an aluminium atom.

Hence $M\ddot{z} = -\alpha z$, and $\omega = (\alpha/M)^{1/2}$

Evaluated using (d^2U/dz^2) for the calculated pseudopotential at $z \simeq 2.8$ Å, this gives a value of $\Theta_D = 330$ K; which is in reasonable agreement with Θ_D (0°K) for aluminium (430 K).

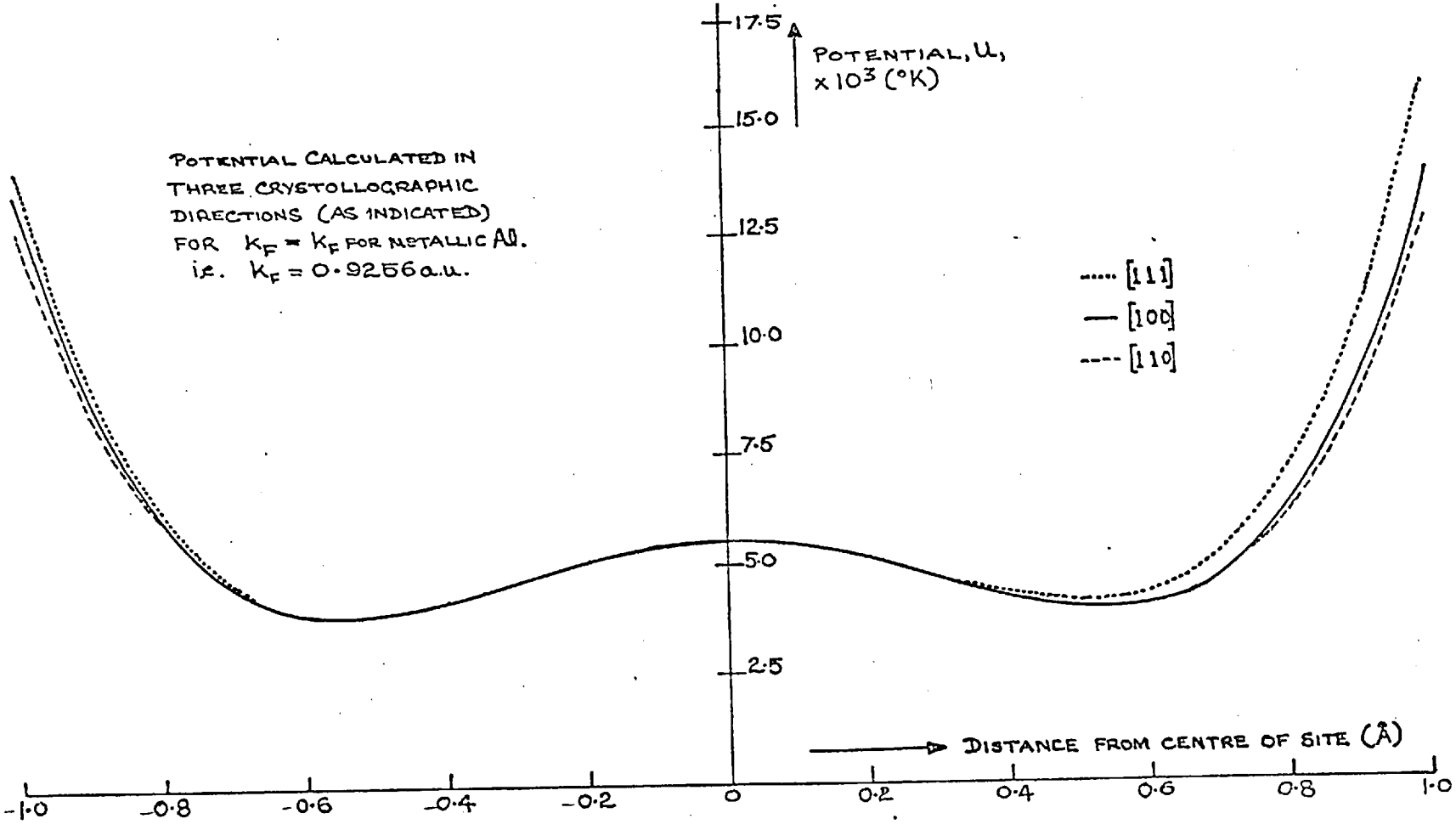
Figure (6.2.1) depicts the interatomic pseudopotential for $k_F = (k_F$ for metallic aluminium,) in three crystallographic directions, as a function of distance from the centre of the site.

The central maximum is of the order of 1600K high and the off-centre minima are at a distance of about 2.8 Å from the surrounding atoms, which is approximately the nearest neighbour distance in metallic aluminium. The potential is not quite spherically symmetrical, variations occurring around the sphere of the order of a few tens of degrees Kelvin.

On this model the aluminium atom is considered to be moving, in some way, on the surface of this nearly spherical central region. If the potential were isotropic the motion would be that of a rigid rotator. The experimental evidence however, is indicative of the atom behaving as a harmonic oscillator. This atom is therefore visualised as being trapped by depressions on the sphere and executing one or two dimensional harmonic motion. (Three dimensional motion is thought to be improbable as calculations show radial motion of the atom to be unfavourable).

FIG (6.2.1)

INTERATOMIC PSEUDOPOTENTIAL FOR LOOSE ALUMINIUM ATOM.



6.3 OTHER LOCAL MODE SYSTEMS

INTRODUCTION

There are numerous different local mode systems which have received much attention in recent years.

The literature on local modes is exhaustive and only a few examples will be discussed in this section. The first part will be concerned with localised modes associated with off-centre atoms. Specifically one of the doped alkali halides, K-Cl : Li is described where the behaviour of impurity ions sited in 1-D double potential wells is explained in terms of a tunneling model. Similar tunneling states have been found in amorphous materials; in this case however the tunneling states appear to be an inherent property of the material, rather than being associated with impurities.

Materials of the cubic β -tungsten structure are described, where soft phonons give rise to second order phase transitions to a structure of lower symmetry.

The last part of this section deals with certain hexagonal-tungsten-bronzes and the argon quinol clathrates; in both these classes of material local modes give rise to an excess specific heat of Einstein character.

6.3.(i) TUNNELING MODES

Various localised excitations (tunnel, rotation, and inband resonant modes) have been identified in many doped alkali-halide crystals, (e.g. see reference (52)). In this section one example, the case of potassium chloride doped with lithium (K-Cl : Li) will be described, which gives rise to a tunneling mode.

It has been established that small impurity ions such as Li^+ incorporated into K-Cl do not simply substitute for K^+ but occupy off-centre

positions (53), and that this is a direct consequence of a potential well with a shallow maximum at the conventional lattice site, together with the small size of the Li^+ ion. The low frequency impurity mode has been observed in K-Cl : Li through phonon resonance scattering in thermal conductivity measurements (52), and by low temperature specific heat measurement (54), in which a Schottky anomaly is observed. The mode is explained through tunneling states associated with a quasi-rotational motion of the small Li^+ ion between its eight equilibrium positions located in the [111] crystallographic directions, (55). A tunneling model using a simple one-dimensional double harmonic potential indicated a potential barrier of 96 cm^{-1} (138°K) and a tunnel splitting of 9 cm^{-1} for the first excited state of the harmonic oscillator.

The pseudopotential calculations for the oscillators in $Al_{10}V$ indicate that the three-dimensional potential seen by a loose aluminium atom has a central maximum of approximate height (1600K). The potential minimum is at about 0.4 Å from the centre of the site, and the loose atom is visualised as moving in a harmonic fashion on this central region. The first excited state is at 23 K above the ground state.

The tunnel-split ground state has been used, as mentioned above, to explain anomalies in the thermal conductivity and heat capacity of the doped alkali-halides. These phenomena depend on the magnitude of the splitting whereas the thermal expansion involves the volume dependance of the splitting [thermal expansion coefficient, β , is given by :-

$$\beta = \left(\frac{\partial \ln V}{\partial T}\right)_P \propto \left(\frac{\partial S}{\partial V}\right)_T \quad]$$

Measurements of β (T) for K-Cl : Li (and other doped alkali-halides) have been made (56) and show low temperature anomalies which are ascribed to

tunnel splitting of the impurity ground states. The barrier height is expected to vary with volume in a "normal" fashion, whereas the tunnel splitting (and hence the entropy associated with it) is relatively sensitive to volume change. Expressed in terms of Gruneisen parameters the effect corresponds to a value of 300 for γ_G in K-Cl : Li.

The low temperature thermal expansion data so far obtained on $Al_{10}V$, indicates a very large contribution from the local mode. γ local mode is approximately 84 at low temperatures and is similarly attributed to high sensitivity of the structure of the local mode energy levels to volume change.

The tunneling states described above in the doped alkali-halide K-Cl : Li are due to the presence of impurity atoms; in amorphous crystals however, tunneling states are suggested to be an inherent property of the material.

The specific heat of vitreous silica and of silica and germania based glasses has been measured in the temperature range 70 mK to 1 K (57). The results confirmed earlier studies (58 and 59) indicating a linear term in the specific heat, of the order of 10^{-6} T J/gm K. for all three materials. Phillips (60) and Anderson et al (61) proposed models in which the glasses are described as containing a statistical distribution of localised tunneling states each of which may be represented by a particle in an assymetric one-dimensional double well. Each tunneling state gives rise to a Schottky anomaly in the specific heat, and the observed linear temperature dependence arises from the uniform energy distribution of these states.

These tunneling states are not identified with any specific molecular vibration in the amorphous materials as their low frequency modes are not well characterized. These materials differ fundamentally from perfect crystals in that finite displacements do not necessarily increase the internal

energy. It is considered that tunneling states corresponding to two neighbouring positions could occur naturally in some amorphous solids.

6.3.(ii) COMPOUNDS OF THE CUBIC β-TUNGSTEN STRUCTURE

In the search for high temperature superconductors interest arose in many transition metal compounds and alloys, and in particular in superconducting materials having the cubic β-tungsten structure, e.g. V_3Si and Nb_3Sn, which have superconducting transition temperature, T_c, of 17·1 and 18·0 K respectively. It became apparent that high T_c materials are often unstable and that possibly this instability is actually necessary in some way to maintain high temperature superconductivity.

Low temperature X-ray investigations (62) revealed that both V_3Si and Nb_3Sn undergo structural transformation to tetragonal symmetry above T_c. Testardi (63) observed marked relaxations involving the $(C_{11} - C_{12})$ elastic constants giving further evidence of an overall softening of the structure.

The β-tungsten structure is unusual in that the atoms of the transition elements are arranged along three mutually perpendicular systems of chains, whilst the non-transition elements are contained in icosehedral cages that are relatively too large for them (see Fig.(6.3) below). This might well account for the intrinsic hydrostatic instability of the structure, as is indicated by the low temperature anharmonicity found by Shier and Taylor (64) in their Mössbauer investigations on Nb_3Sn.

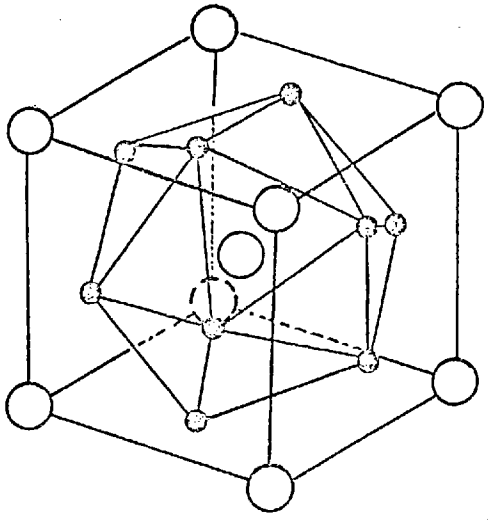


FIGURE (6.3)

The Nb_3Sn Structure.

Investigations by Kunzler et al (65) showed a pronounced decrease in the low temperature heat capacity of V_3Si with stress at temperatures below T_c and a large increase of the heat capacity above 25 K. The effect appeared not to be directly related to structural transformation as it was observed in samples that transformed and in those that did not. They suggested that the effect could be a consequence of the "softness" of the crystal with respect to shear (which in turn provides conditions leading to structural changes). The changes in heat capacity appeared too large however to be attributable to changes in lattice heat capacity alone and Kunzler et al concluded that a large change in the density of states at the Fermi surface may be involved.

Measurements have been made by Smith et al (66) of the thermal expansion and heat capacity of two transforming and one non-transforming sample of Nb_3Sn. An anomalous positive contribution to the expansion of the two transforming samples was found ($\gamma_G \simeq 5$ at 20 K in these, as opposed to a value of $\gamma_G \simeq 1.7$ in the non-transforming compounds). There was no sign of any extra contribution to the heat capacity due to the lattice contribution in these measurements, although earlier data on two high purity single crystals of Nb_3Sn (67) had exhibited small anomalies at about T_m.

The extent to which the presence of the soft mode is a decisive factor in the production of the high T_c in Nb_3Sn is still under debate. Allen (68) has estimated that the total contribution from electron coupling to the soft modes is only effective in raising T_c from 16 K to 18 K. It appears that there is no appreciable dependence of T_c upon lattice instability.

Smith et al (66) concluded that the anomalous expansion behaviour

is not associated with the soft mode but is electronic in origin, and possibly related to changes in the density of states at the Fermi level due to interband charge transfer (as suggested for the V_3Si compounds). In $Al_{10}V$ the anomalous expansion behaviour is thought to be attributable to the local mode.

6.3.(iii) OTHER EXAMPLES OF EINSTEIN MODES

(a) Hexagonal-Tungsten-Bronzes

Bevola et al (69) have measured the heat capacity of four tungsten bronzes K_xWO_3, Rb_xWO_3, Cs_xWO_3 and Tl_xWO_3, which are non-stoichiometric superconducting compounds with the general formula M_xWO_3, where M is a metal and $0 < x < 1$. In all cases an excess heat capacity of Einstein form was observed.

The structure of these bronzes comprises cornerbonded WO_6 octehedra with metal ions occupying the interstitial sites. It has been shown by Magnali (70), that if M is an alkali metal, the hexagonal structure consists of six member rings forming channels. The Einstein mode observed by Bevola is attributed to the metal ions vibrating in these channels.

The Einstein temperatures (Θ_E) of three of the compounds are listed in Table (6.3.1) below together with their atomic masses, ionic radii and the force constants (k) associated with the restoring forces on the M^+ ions.

TABLE (6.3.1)

	Rb_xWO_3	Cs_xWO_3	Tl_xWO_3
Θ_E(K)	58 ± 2	70 ± 2	38 ± 2
Atomic Mass (amu)	86	133	204
Ionic Radius (Å)	1.49	1.65	1.49
k (N/m)	8	19	8

The respective Einstein temperatures are explained semi-quantatively in terms of the masses (m), and ionic radii of the metal ions. Considering simple harmonic motion of the ion M^+, the Einstein frequency ν_E is given by :

$$\nu_E = \frac{k_B \Theta_E}{h} = \left(\frac{k}{m}\right)^{1/2} \Big/ 2\pi$$

Hence the force constant, k, may be evaluated from ;

$$\Theta_E = \frac{\hbar}{k_B}\left(\frac{k}{m}\right)^{1/2}$$

The volume of the channel site containing the metal ions does not change appreciably from one bronze to another, and hence the overlap of the M^+ ion orbitals, which presumably produces the restoring force, will depend primarily on the ionic radius. This conclusion helps to account for the quoted values of the force constants, e.g. Rb^+ and Tl^+ have the same ionic radius and the calculated values of k are the same. Considering Θ_E for Rb_xWO_3 and Cs_xWO_3 it may be seen that the heavier Cs^+ ion has the greater Θ_E which is explicable in terms of its larger ionic radius, and, hence, k.

Using the same semi-quantitative argument to compare the doped and undoped $Al_{10}V$ samples one obtains the values given in Table (6.3.2) for k. In the cases so far investigated Θ_E decreases with increasing mass. The force constants are much lower than those found in the tungsten-bronzes.

TABLE (6.3.2)

Oscillator	Al	Ga	Tl
Mass (a.m.u.)	27	70	204
Radius (Å)	1.26	1.26	1.49
Θ_E(K)	23	9.6	6
k(N/m)	.4	.2	.2

(b) Inert Gas Clathrates

The weakest kind of bonding is that involving inert gases and soft local modes have been found in inert gas clathrates, e.g. in the argon β -quinol clathrate.

The existance of the β -quinol clathrates depends on the occurrance in pure β -quinol of regularly spaced cavities. These cavities are approximately spherical and of 3.9 Å radius, this permits them to accommodate a variety of small molecules.

Parsonage and Staveley (71) report the results of measurements of the heat capacity from 13 K to 273 K on five clathrates of argon and β -quinol, $(3C_6H_4(OH)_2 . \alpha A)$, of different compositions, the argon content ranging from 20% to about 80% of the maximum possible amount.

The argon atoms (radius 1.7 Å) trapped in the cavities of the β -quinol give rise to an excess low temperature heat capacity. Regarding the low temperature motion as three dimensional simple-harmonic motion, the vibrational frequency corresponds to an Einstein temperature of about 48°K. The very weak bonding of the inert gas atoms trapped in these cavities is evidently still stronger than that of the "loose" atoms in the anomalous sites in $Al_{10}V$, as indicated by the Einstein temperatures recorded so far ranging from about 6 K for thallium to 23 K for aluminium.

CONCLUSION

The low temperature specific heat, electrical resistivity and inelastic neutron scattering data presented in this work, substantiate the earlier evidence (38) for a well defined local mode in $Al_{10}V$. All the results indicate a characteristic energy of 2 meV for the first excited state. From the neutron data there is an indication of a second level at 4 meV. and the well pronounced Einstein contribution to the electrical resistivity up to at least 40°K is

indicative of at least three levels above the ground state.

The identification of the low frequency "oscillator" with very loosely bound aluminium atoms on some of the vacant 8(b) is well justified in terms of earlier crystallographic evidence (40). The $Al_{10}V$ structure may be visualised as a strongly bonded Al_3V framework, the voids of which are filled by aluminium atoms (72). Al_7V is found to be based on the same body centred tetragonal Al_3V framework, but there are no vacant sites and no such anomalous behaviour is seen in the heat capacity. In these Al-V compounds (Al_3V, Al_7V and $Al_{10}V$) not only are the Al-V distances anomalously short, but simultaneously there are unusually long Al-Al distances elsewhere in the unit cell. It has been suggested by Brown (40) that it is a strong Al-V interaction giving rise to the framework of linked icosehedra which is important in the formation of this structure, and that aluminium atoms that are not in contact with vanadium can take little part in this interaction. These atoms are either not present or show an anomalously large radius. The bonding of the loose aluminium atoms is surprisingly weak, weaker even than that involving the inert gases in the inert gas clathrates which exhibit local modes. The local modes found in the doped alkali halides (e.g. K-Cl : Li) are due to Li^+ ions sited in double potential wells with shallow maxima giving rise to tunneling. In the case of $Al_{10}V$ the experimental results indicate the loose atoms to be behaving as harmonic oscillators, presumably trapped in some way on the minimum energy surface of the potential. The thermal expansion data reported on $Al_{10}V$ indicates the structure of the energy levels of the local mode to be highly sensitive to changes in volume as is thought to be the case in the doped alkali-halides.

There is no indication of any structural transformation in this compound as is found in the A15 compounds Nb_3Sn and V_3Si; nor is $Al_{10}V$ a high temperature superconductor.

The work presented here has led to a better understanding of this unusual compound but there is still much to be clarified. It is not clear why the local mode is so weakly coupled to the bulk phonon modes, nor why covalent bonding should apparently play such an important role in the $Al_{10}V$ compounds. Further experimental work into the electrical resistivity and thermal expansion of some more doped samples is being carried out. Investigations planned by other workers on the elastic constants and pressure dependent resistivity and specific heat should prove informative.

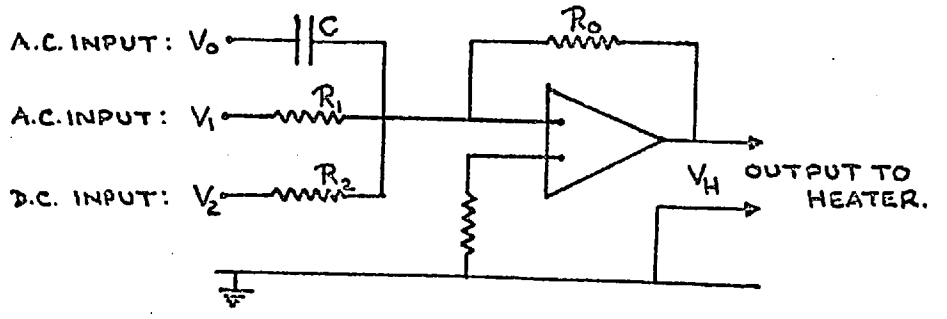
APPENDIX I

Derivation of the temperature response of the sample for the four possible input heater signals

As shown in Chapter III (Section 2), the heater supply circuit enables the a.c. input voltages to be either resistively or capacitively coupled to the operational amplifier, and accordingly the amplitude of the output voltage to the heater will be either frequency independent or frequency dependent.

For simplicity we shall consider the heater as supplying heat to a totally isolated system, i.e. $\tau_1 = \infty$, $\tau_2 = 0$. The derivation of the form of the temperature response of such a system is explained for the four possible signals input to the simplified circuit shown below in Fig.A.1.

FIGURE A.1.



With this arrangement the four possible input signals are :-

(1) a capacitively coupled a.c. signal : $V_o = V_{AC} \cos \omega t$

(2) a resistively coupled a.c. signal : $V_1 = V_{AC} \cos \omega t$

(3) a capacitively coupled a.c. signal plus a resistively coupled d.c. signal : $V_o + V_2 = V_{AC} \cos \omega t + V_{DC}$

(4) a resistively coupled a.c. and d.c. signal : $V_1 + V_2 = V_{AC} \cos \omega t + V_{DC}$

If the heater voltage is V_H and the heater resistance is R_H, then the temperature response is given by :

$$T(t) = \int \frac{V_H^2}{R_H C_S}\, dt$$

where C_S is the heat capacity of the system. Hence for case :-

(1) the heater voltage is given by,

$$V_H = R_o C \frac{dV_o}{dt} = -R_o C \omega V_{AC} \sin \omega t.$$

and the temperature response is :

$$T(t) = \int \frac{R_o^2 C^2 \omega^2 V_{AC}^2}{2 C_S R_H} (1 - \cos 2\omega t)\, dt$$

$$= \frac{R_o^2 C^2 \omega^2 V_{AC}^2}{2 C_S R_H} \left(t - \frac{1}{2\omega} \sin 2\omega t\right) \qquad \text{(A.1.1}$$

and in (2) for the resistively coupled a.c. signal,

$$V_H = \frac{R_o}{R_1} V_1 = \frac{R_o}{R_1} V_{AC} \cos \omega t$$

and

$$T(t) = \int \frac{1}{2} \frac{R_o^2}{R_1^2} \frac{V_{AC}^2}{R_H C_S} (1 - \cos 2\omega t)\, dt$$

$$= \frac{R_o^2 V_{AC}^2}{2 R_1^2 R_H C_S} \left(t + \frac{1}{2\omega} \sin 2\omega t\right) \qquad \text{(A.1.2}$$

Hence for an a.c. signal only, the a.c. part of the temperature response is at twice the applied frequency and its amplitude is frequency dependent.

For case (3) where the a.c. part is capacitively coupled, the heater voltage is given by :

$$V_H = R_o C \frac{d(V_o)}{dt} + \frac{R_o}{R_2} V_2 = \frac{R_o}{R_2} V_{DC} - R_o C \omega V_{AC} \sin \omega t$$

and the temperature response is :

$$T(t) = \frac{1}{R_H C_s}\int\left(\frac{R_o}{R_2}V_{DC} - R_o C\omega V_{AC}\sin\omega t\right)^2 dt$$

$$= \frac{1}{R_H C_s}\int\left(\frac{R_o^2 V_{DC}^2}{R_2^2} - \frac{2R_o^2 C\omega V_{DC}}{R_2}V_{AC}\sin\omega t + R_o^2 C^2\omega^2 V_{AC}^2\sin^2\omega t\right)dt$$

$$= \frac{1}{R_H C_s}\left(\frac{R_o^2 V_{DC}^2}{R_2^2}t + \frac{2R_o^2 C V_{DC}}{R_2}V_{AC}\cos\omega t + R_o^2 C^2\omega^2 V_{AC}^2\left[\frac{t}{2} - \frac{\sin 2\omega t}{2\omega}\right]\right) \quad (A.1.3$$

and in case (4) the heater voltage is ;

$$V_H = \frac{R_o}{R_1}V_{AC}\cos\omega t + \frac{R_o}{R_2}V_{DC}$$

and :

$$T(t) = \frac{1}{R_H C_s}\left(\frac{R_o^2}{R_2^2}V_{DC}^2 t + \frac{2R_o^2 V_{DC}V_{AC}}{R_1 R_2\omega}\sin\omega t + \frac{R_o^2 V_{AC}^2}{2R_1^2}\left[t + \frac{1}{2\omega}\sin 2\omega t\right]\right) \quad (A.1.4$$

As may be seen by equations (A.1.3) and (A.1.4) the temperature response for an (a.c. + d.c.) input signal comprises both first and second harmonic components, the relative magnitudes of which depend on R_1, R_2, C, V_{AC} and V_{DC}. For case (3) the first harmonic term is independent of frequency, which is the condition used in the determination of τ_2 as explained in Chapter II, Section (3.b).

APPENDIX 2

TABULATION OF SPECIFIC HEAT DATA

The specific heat, C, of the six samples measured is tabulated at 0.5 K intervals for the temperature range 2 K to 10 K and at 2 K intervals for the range 10 K to 30 K. The coefficient of the electronic contribution (γ), the lattic contribution (β), and the sample mass are quoted for each sample. The values given for the Einstein contribution, C_{EIN}, are the theoretical values evaluated from the following equation :

$$C_{EIN} = 3RN_{\ell}\left(\frac{\Theta_E}{T}\right)^2 \frac{\exp(\Theta_E/T)}{(\exp(\Theta_E/T)-1)^2}$$

where N_{ℓ} and Θ_E are the number of oscillators per formula unit and the Einstein temperature respectively. N_{ℓ} and Θ_E have been evaluated for each sample from the experimental results as explained in Chapter V.

TABULATION OF THE SPECIFIC HEAT FOR SAMPLE NO. 3

γ = (17.0 $\pm$ 1.4) mj / mole (fu) K^2
β = (0.504 $\pm$ .050) mj / mole(fu) K^4
N_ℓ = (0.103 $\pm$ .001) / fu
Θ_E = (23.50 $\pm$ .71) K
Sample mass = 1.650 gms.

T(K)	C(J/mole(fu)K)	C_{EIN}(J/mole(fu)K)	T(K)	C(J/mole(fu)K)	C_{EIN}(J/mole(fu)K)
2.0	.042	.003	8.5	1.970	1.412
2.5	.071	.019	9.0	2.133	1.502
3.0	.129	.063	9.5	2.296	1.584
3.5	.219	.141	10.0	2.450	1.657
4.0	.340	.251	12.0	3.156	1.889
4.5	.504	.383	14.0	3.850	2.047
5.0	.680	.527	16.0	4.672	2.158
5.5	.861	.674	18.0	5.652	2.238
6.0	1.044	.819	20.0	6.760	2.298
6.5	1.231	.956	22.0	8.118	2.344
7.0	1.414	1.085	24.0	9.720	2.379
7.5	1.601	1.204	26.0	11.622	2.407
8.0	1.766	1.313	28.0	13.776	2.429
8.5	1.970	1.412	30.0	16.350	2.447

TABULATION OF THE SPECIFIC HEAT FOR SAMPLE NO. 5

γ = (17.0 ± 1.4) mj / mole(fu) K^2
β = (0.386 ± .039) mj / mole(fu) K^4
N_β = (0.051 ± .005) / fu
Θ_E = (22.67 ± .71) K
Sample mass = 2.324 gms.

T(K)	C(J/mole(fu)K)	C_{EIN}(J/mole(fu)K)	T(K)	C(J/mole(fu)K)	C_{EIN}(J/mole(fu)K)
2.0	.039	.002	8.5	1.132	.727
2.5	.063	.012	9.0	1.245	.771
3.0	.098	.038	9.5	1.366	.810
3.5	.151	.083	10.0	1.490	.845
4.0	.221	.143	12.0	1.908	.955
4.5	.304	.213	14.0	2.308	1.029
5.0	.395	.288	16.0	2.960	1.082
5.5	.495	.363	18.0	3.672	1.119
6.0	.599	.436	20.0	4.540	1.147
6.5	.706	.505	22.0	5.566	1.168
7.0	.811	.568	24.0	6.816	1.184
7.5	.916	.626	26.0	8.268	1.197
8.0	1.022	.679	28.0	9.996	1.207
8.5	1.132	.727	30.0	12.000	1.216

TABULATION OF THE SPECIFIC HEAT FOR SAMPLE NO. 6

γ = (17.0 ± 1.4) mj / mole(fu) K^2
β = (0.481 ± .048) mj / mole(fu) K^4
N_Ω = (0.103 ± .001) / fu
Θ_E = (22.57 ± .71) K
Sample mass = 2.544 gms.

T(K)	C(J/mole(fu)K)	C_{EIN}(J/mole(fu)K)	T(K)	C(J/mole(fu)K)	C_{EIN}(J/mole(fu)K)
2.0	.045	.004	8.5	1.996	1.476
2.5	.076	.025	9.0	2.151	1.563
3.0	.138	.079	9.5	2.299	1.642
3.5	.238	.170	10.0	2.450	1.713
4.0	.378	.293	12.0	3.060	1.933
4.5	.539	.436	14.0	3.752	2.083
5.0	.718	.588	16.0	4.560	2.187
5.5	.897	.740	18.0	5.562	2.263
6.0	1.065	.888	20.0	6.760	2.318
6.5	1.258	1.027	22.0	8.096	2.361
7.0	1.449	1.155	24.0	9.456	2.393
7.5	1.643	1.273	26.0	11.492	2.419
8.0	1.824	1.380	28.0	13.580	2.440
8.5	1.996	1.476	30.0	15.960	2.457

TABULATION OF THE SPECIFIC HEAT FOR SAMPLE NO. 7

γ = (17.0 ± 1.4) mj / mole (fu) K^2
β = (0.404 ± .040) mj / mole (fu) K^4
N_ℓ = (0.067 ± .001) / fu
Θ_E = (22.69 ± 0.71) K
Sample mass = 2.395 gms.

T(K)	C(J/mole(fu)K)	C_{EIN}(J/mole(fu)K)	T(K)	C(J/mole(fu)K)	C_{EIN}(J/mole(fu)K)
2.0	.040	.003	8.5	1.309	.955
2.5	.065	.016	9.0	1.422	1.012
3.0	.111	.049	9.5	1.539	1.063
3.5	.177	.108	10.0	1.665	1.109
4.0	.264	.187	12.0	2.148	1.254
4.5	.365	.279	14.0	2.688	1.352
5.0	.480	.377	16.0	3.312	1.420
5.5	.605	.476	18.0	4.068	1.470
6.0	.732	.572	20.0	5.000	1.506
6.5	.852	.662	22.0	6.138	1.534
7.0	.968	.745	24.0	7.512	1.556
7.5	1.082	.822	26.0	9.100	1.573
8.0	1.194	.892	28.0	10.920	1.586
8.5	1.309	.955	30.0	13.050	1.597

TABULATION OF THE SPECIFIC HEAT FOR SAMPLE NO. 8

γ = (17.0 $\pm$ 1.4) mj / mole(fu) K^2
β = (0.531 $\pm$ .053) mj / mole (fu) K^4
N_γ = (0.119 $\pm$ .001) / fu
Θ_E = (23.38 $\pm$ 0.71) K
Sample mass = 2.485 gms.

T(K)	C(J/mole(fu)K)	C_{EIN}(J/mole(fu)K)	T(K)	C(J/mole(fu)K)	C_{EIN}(J/mole(fu)K)
2.0	.042	.003	8.5	2.098	1.641
2.5	.075	.023	9.0	2.273	1.745
3.0	.138	.075	9.5	2.470	1.838
3.5	.249	.167	10.0	2.650	1.923
4.0	.391	.296	12.0	3.456	2.189
4.5	.554	.450	14.0	4.116	2.370
5.0	.744	.618	16.0	4.992	2.498
5.5	.960	.789	18.0	5.994	2.590
6.0	1.171	.956	20.0	7.240	2.658
6.5	1.368	1.115	22.0	8.756	2.710
7.0	1.554	1.264	24.0	10.536	2.751
7.5	1.738	1.401	26.0	12.558	2.782
8.0	1.920	1.527	28.0	15.120	2.808
8.5	2.098	1.641	30.0	17.940	2.829

TABULATION OF THE SPECIFIC HEAT FOR SAMPLE NO. 9

γ = 17.0 mj / mole (fu) K^2
β = 0.498 mj / mole (fu) K^4
$N_{\ell(1)}$ = (0.096)/ fu $N_{\ell(2)}$ = (0.018) / fu
$\Theta_{E(1)}$ = (23.0) K $\Theta_{E(2)}$ = (9.6) K
Sample mass = 2.636 gms.

T(K)	C(J/mole(fu)K)	C_{EIN}(J/mole(fu)K)	T(K)	C(J/mole(fu)K)	C_{EIN}(J/mole(fu)K)
2.0	.127	.090	8.5	2.140	1.753
2.5	.213	.169	9.0	2.288	1.840
3.0	.344	.270	9.5	2.437	1.919
3.5	.503	.395	10.0	2.600	1.989
4.0	.662	.539	12.0	3.384	2.210
4.5	.824	.695	14.0	4.158	2.359
5.0	.992	.855	16.0	5.024	2.463
5.5	1.166	1.012	18.0	6.012	2.538
6.0	1.344	1.162	20.0	7.160	2.594
6.5	1.515	1.303	22.0	8.536	2.636
7.0	1.681	1.432	24.0	10.152	2.686
7.5	1.839	1.550	26.0	11.960	2.695
8.0	1.990	1.657	28.0	14.000	2.715
8.5	2.140	1.753	30.0	16.260	2.732

REFERENCES

Ref. No.

1. Zemansky, M.W., Heat and Thermodynamics (4th ed.) McGraw and Hill, New York. (1957).
2. Bardeen, J., Cooper, L.N. and Schrieffer, J.R., Phys.Rev. 108, 1175. (1957).
3. McMillan, W.L., Phys.Rev. 167, 331. (1968).
4. Friedel, J., Can.J.Phys., 34, 1190. (1956).
5. Anderson, P.W., Phys.Rev., 124, 41. (1961).
6. Caplin, A.D., Dunlop, J.B., J.Phys.F. 3, (1973).
7. Dunlop, J.B., Grüner, G. and Caplin, A.D., J.Phys.F., 4 (1974).
8. Kondo, J., S.S.Phys. (Seitz, F. and Turnbull, D., and Ehrenreich, H. Eds.) Academic Press, New York, 23, 183 (1969).
9. Heeger, A.J., S.S.Phys. (Seitz, F., Turnbull, D. and Ehrenreich, H. Eds.) Academic Press, New York, 23, 283 (1969).
10. Heiniger, F., Bucher, E. and Muller, J., Phys.Kondens Materie, 5, 243 (1966).
11. Lounasamaa, O.V., Hyperfine Interactions, (Freem, A.J. and Franker, R.B., Eds.), Academic Press, New York, 467, (1967).
12. Phillips, N.E., C.R.C. Critical Reviews in Solid State Sciences, 467, (1971).
13. Blackman, M., Proc.Roy.Soc.(London), A148, 384 (1935); A159, 416 (1937); Proc.Camb.Phil.Soc., 33, 94, (1937).
14. Kellerman, E.W., Phil.Trans. A238, 513 (1940); Proc.Roy.Soc. (London), A178, 17, (1941).
15. Maradudin, A.A., S.S.Phys.(Seitz, F. and Turnbull, D. Eds.), Academic Press, New York, 18, (1960).

Ref. No.

16. Kagan, Yu. and Iosilenskii, Y.A., Soviet Phys.J.E.T.P., 18, 562 (1964).

17. Cape, J.A., Lehman, G.W., Johnston, W.V. and De Wames, R.E., Phys.Rev.Lett. 16, 892 (1966).

18. Hartmann, W.M., Culbert, H.V. and Huebener, R.P., Phys.Rev., B.1., 1486 (1970).

19. Stoner, E.C., Proc.Roy.Soc.(London), A154, 646 (1936).

20. Cohen, M.L. and Heine, V., S.S.Phys. (Seitz, F., Turnbull, D. and Ehrenreich, H., Eds.), Academic Press, New York, 24, 37 (1970).

21. Snow, E.C. and Waber, J.T., Acta.Met., 17, 623 (1969).

22. Gopal, E.S.R., Specific heats at low temperatures, Plenum Press, New York, (1966).

23. Partington, J.R., An Advanced Treatise on Physical Chemistry, Longmans-Green, London, Vol.3., (1952).

24. Ramanathan, K.G. and Srinivasan, T.M., Phil.Mag., 46, 338 (1955).

25. Luengo, C., Ph.D.Thesis, University of California, La Jolla, (1971).

26. Morin, F.J. and Maita, J.P., Phys.Rev., 129, 3, (1964).

27. Kunzler, J.E., Walker, L.R. and Galt, J.K., Phys.Rev., 119, 5, (1960).

28. Dunlop, J.B., Ph.D.Thesis, University of London, (1972).

29. Bachmann, R., et al., Rev.Sci.Inst., 43, 205, (1972).

30. Sullivan, P.F. and Seidel, G., Phys.Rev., 173, 3, (1968).

31. Clement, J.R. and Quinnell, E.H., Rev.Sci.Inst., 23, 213, (1952).

32. Holste, J.C., Cetas, T.C. and Swenson, C.A., Rev.Sci.Inst., 43, 670, (1972).

33. Raynor, G.V., Prog.Metal Phys., 1, 1, (1949).

34. Taylor, M.A., Proc.Phys.Soc., 78, 1244, (1961).

35. Pauling, L., Proc.Roy.Soc., A196, 343, (1949).

Ref.No.

36. Wenger, A., Bürri, G. and Steinemann, S., S.S.Comm., 9,1255,(1971).

37. Mott, N.F., Adv. in Phys., 13, 325, (1964).

38. Caplin, A.D., Grüner, G. and Dunlop, J.B., Phys.Rev.Lett., 30, 22, (1973).

39. Carlson, O.N., Kenney, D.J. and Wilhelm, H.A., Trans.A.S.M., 47, 520, (1955).

40. Brown, P.J., Acta.Cryst., 10, 133, (1957).

41. Ray, A.E. and Smith, J.F., Acta.Cryst., 10,604, (1957).

42. Einstein, A., Ann-Phys., (Leipzig), 22, 180, (1907).

43. Cooper, J.R., Phys.Rev., B9, 6, (1974).

44. Mott, N.F. and Jones, H., Theory and Properties of Metals and Alloys, Oxford University Press, Chapter 7, (1936).

45. Ziman, J., Electrons and Phonons, Oxford University Press, Chapter 9, (1960).

46. Elliot, R.P. and Mondolfo, L.F., Trans.A.S.M., (Discussion on (39)), 47, 538, (1955).

47. Barber, A.J., Ph.D.Thesis, University of London, (1974).

48. Marshall, W. and Lovesey, S.W., Theory of Thermal Neutron Scattering, Oxford University Press, Chapter 12, (1970).

49. Zemach, A.C. and Glauber, R.J., Phys.Rev., 101, 1, (1956).

50. Finnis, M.W., J.Phys.F., 4, 1645, (1974).

51. Appapillai, M., Ph.D.Thesis, University of Cambridge, (1972).

52. Pohl, R.O., Proc. 1st Int.Conf. on Localised Excitations in Solids, (Wallis, R.F., Ed.), Plenum, New York, 434, (1967).

53. Lombardo, G. and Pohl, R.O., Phys.Rev.Lett., 15, 291, (1965).

54. Harrison, J.P., Peressini, P.P. and Pohl, R.O., Proc.1st Int.Conf. on Localised Excitations in Solids, 474, (1967).

Ref.No.

55. Baumann, F.C., Harrison, J.P., Pohl, R.O. and Seward, W.D., Phys.Rev., 159, 691, (1967).

56. Case, C.R. and Swenson, C.A., Phys.Rev., B9, 10, (1974).

57. Zeller, R.C. and Pohl, R.O., Phys.Rev., B4, 2029, (1971).

58. Choy, C.L., Hunt, R.G. and Salinger, G.L., J.Chem.Phys., 52, 3629, (1970).

59. Antoniou, A.A. and Morrison, J.A., J.App.Phys., 36, 1873, (1965).

60. Phillips, W.A., J.Low Temp.Phys., 7, 351, (1972).

61. Anderson, P.W., Halpern, B.I., Varma, C.M., Phil.Mag., 25, (1972).

62. Batterman, B.W. and Barrett, C.S., Phys.Rev.Lett., 13, 390, (1964).

63. Testardi, L.R., Phys.Rev., B5, 4342, (1972).

64. Shier, J.S. and Taylor, R.D., Phys.Rev., 174, 346, (1968).

65. Kunzler, J.E., Maita, J.P., Levinstein, H.J. and Ryder, E.J., Phys.Rev., 143, 2, (1966).

66. Smith, T.F., Finlayson, T.R. and Taft, A. To be published (1976).

67. Vieland, L.J. and Wicklund, A.W., Solid St.Comm., 7, 37, (1969).

68. Allen, P.B., Solid St.Comm., 14, 937, (1974).

69. Bevola, A.J., Shanks, H.P., Sidles, P.H. and Danielson, G.C., Phys.Rev., B9, 8, (1974).

70. Magnali, A., Nature, 169, 791, (1952).

71. Parsonage, N.G. and Staveley, L.A.K., Mol.Phys., 2, 212, (1959).

72. Laves, F., Intermetallic Compounds, (Westbrook, J.H., Ed.), Pub. John Wiley and Sons, Inc., New York, 140, (1967).